STRAIN ENERGY AND JOINTING

IN COAL AND ADJACENT SEDIMENTS

By

RONALD M. LINDEN

Submitted in Partial Fulfillment
of the Requirements for the Degree of
Master of Science in Geology

New Mexico Institute of Mining and Technology

Socorro, New Mexico

April 1987

Acknowledgments

Funding for this study was provided by a grant from the New Mexico State Mining and Mineral Resources Research Institute, which is gratefully acknowledged.

Special thanks are extended to Dr. Antonius J. Budding who served as thesis advisor and overall architect of this investigation. His knowledge, interest and guidance were instrumental in virtually all phases of this study, and added greatly to the project.

Thanks are also due to Drs. Alan Sanford and John Schlue who served as members of the thesis committee for their critical review of this manuscript. Their suggestions and inquiries were most helpful and have contributed to its quality and completeness.

Dr. David Johnson provided assistance is several forms, including, instruction on the use of thin-sectioning equipment, various types of rock saws, point-count analysis techniques, and photographic and dark room procedures, for which I am most grateful.

This manuscript was typed by my wife, Linda, who spent much time assisting in its refinement. Her willingness to help and continuous encouragement were a vital aid throughout the project, and I wish to thank her most of all.

I dedicate this work to my parents, Michael and Antonia Linden, for their love, understanding, patience, and support.

List of Symbols

Most symbols are defined each time they occur, but the following are commonly used.

b_n	bed number (n=1, 2, 3 ...)
C_o	uniaxial compressive strength
D	diameter
d	bed thickness
E	Young's modulus
E_{av}	average Young's modulus
e	strain
e_t	thermal strain
e_x, e_y	strain in x and y directions
e_1, e_2, e_3	principal strains
F	applied load
F_{max}	maximum load carried
G	shear modulus
G_n	shear modulus of neighboring bed
g	acceleration due to gravity
h	stress perturbation distance
j	joint density, joint frequency
K	spring constant
l	distance
L	characteristic jointing distance
m	Poisson's number
N	total number of joints
p	hydrostatic pressure
P_f	fluid pressure
P_j	fluid pressure in joint
P_u	fluid pressure in unfractured material
Q	temperature
R	radius of earth
r	length of sedimentary unit
S	shear strength
s	interjoint spacing
T	tensile strength
T_n	tensile strength of neighboring bed
t	thickness
V_p	compressional velocity
V_s	shear velocity
w	strain energy
x	distance from joint
z	depth below surface

α	angle of loading
α_l	linear coefficient of thermal expansion
δ	angle between sampling line and set normal
θ	angle subtended by sedimentary unit
λ, G	Lame's parameters
λ_f	fluid pressure ratio
μ_s	coefficient of static friction
ν	Poisson's ratio
π	constant = 3.1416
ρ	density
$\bar{\rho}$	average density
σ	stress
σ_e	stress due to horizontal extension
σ_G,	stress due to gravitational load
σ_m'	effective mean stress
σ_N	normal stress
σ_T	tensile stress
σ_t	thermal stress
σ_x, σ_y, σ_z	stress in x, y and z directions
σ_1, σ_2, σ_3	principal stresses
σ_1', σ_2', σ_3'	effective pricipal stresses
τ	shear stress
τ_h	additional shearing stress

Table of Contents

List of Figures

List of Tables

ABSTRACT

Tension joints in flat-lying sediments are produced during uplift by the release of strain energy imposed on the rocks during burial and compression. Theoretical studies show that the joint frequency is dependent on the bed thickness, the physical properties of both the rock bed and its surroundings, and the degree of tectonic deformation.

An integrated investigation into the relationship between strain energy and jointing involving field work, theory, and experiments in rock mechanics was conducted on three coal-bearing sedimentary sequences in New Mexico and Virginia. Data on the frequency, spacing, orientation, and surface characteristics of jointing in coals and adjacent sediments of the Cretaceous Fruitland and Crevasse Canyon formations (New Mexico) and the Pennsylvanian Lee formation (Virginia) were collected. Samples of the rocks were tested by a variety of experimental techniques to determine their physical properties. Methods included uniaxial compression, ultrasonic pulse velocity determinations, and diametral compression of circular disks and rectangular prisms. The elastic constants obtained through these procedures were used to calculate theoretical joint densities. The complex nature of the expressions by which the theoretical spacing is determined present some difficulties, however. Propagation of experimental error produces large uncertainties which render the otherwise good agreement between theory and observation extremely suspect. The conclusion is reached that the formulation of Hobbs (1967) cannot be used to obtain accurate theoretical joint spacings due to unattainable requirements of experimental precision.

INTRODUCTION

Joints are the most ubiquitous of rock structures, being found in all competent rocks at or near the surface of the earth. They are defined as cracks and fractures in rock along which there has been little or no displacement. It is commonly observed that adjacent sedimentary layers may display widely differing joint densities. This relationship between joint frequency and lithology is probably most striking in the case of coal beds and the surrounding sediments. Because coal is an organic substance and possesses elastic properties dissimilar to those of the sediments enclosing it, it will react differently to the application of stress. As the coal and adjacent sediments are subject to increasing amounts of tensional stress, each rock will fail at a stress level characteristic of the material.

The objective of this investigation is to see if the observed differences in the frequency of jointing found in adjacent sedimentary rocks can be explained on the basis of their mechanical properties. For the purpose of this study, we will be concerned with relatively horizontal, undeformed sediments, which are assumed to approximate elastic bodies, and the variations in stress that they experience due to burial, compaction, and uplift. To test this hypothesis, an integrated approach to the problem involving theory, field studies, and experimental rock mechanics was conducted. Theoretical investigations (Price, 1959; 1966) suggest that the mechanical origins of jointing are related to the loading history of rocks. The loading history is the record of applied forces, displacements, and temperature changes that produce the stress fields experienced by a body. It is generally

thought that joint formation is due to the release of tensile stresses generated during uplift and denudation. This uplift and denudation affects the preexisting state of stress in three ways: (1) by horizontal extension due to uplift, (2) expansion through the release of the gravitational load, and (3) contraction produced by cooling. These processes have a net effect of producing horizontal tension in most cases. The buildup of tensile stress will proceed until it eventually equals the tensile strength of the material, and jointing will occur. Theoretical studies show that the joint frequency is dependent upon the bed thickness, the physical properties of both the rock bed and its surroundings, and the degree of tectonic deformation (Hobbs, 1967).

Field studies were conducted at four locations to collect data on joint frequencies observed in neighboring sedimentary layers. The term joint frequency, j, will be used to indicate the number of times per unit distance (meter) a particular joint set is encountered during a linear traverse at right angles to the strike of the joint planes. Joint density is a term that is synonymous with joint frequency and will be used interchangeably. By comparing the theoretically expected joint frequencies with the actual values observed in the field, it is possible to evaluate the general validity of these hypotheses regarding strain energy and jointing.

In order to calculate the theoretical joint densities, it is necessary to know the values of some of the elastic constants of the rocks, particularly Young's modulus, the shear modulus, and the tensile strength. The values of these constants are determined by a variety of experimental techniques employed in rock mechanics. These include uniaxial compression, ultrasonic pulse velocity determinations, and the

Brazilian test. The theoretical joint densities may then be calculated by using the values obtained by these methods in equations which relate jointing to extensional strain (Hobbs, 1967).

Before we establish the theoretical basis for this investigation it is first necessary to consider some of the general characteristics of joints. We will then turn our attention to the physical conditions under which joint formation is possible.

General Characteristics of Joints

Joints are fracture planes along which there has been little or no displacement parallel to the fracture surface (Price, 1966). These fractures are usually planar and the joint surfaces are relatively smooth. In the case of sedimentary rocks which have undergone only slight deformation, the joint planes are often vertical and are generally uniform in direction over large areas; these structures are termed regional joints. They usually occur in systems composed of several joint sets oriented in different directions, the individual members of which are more or less parallel and regularly spaced. The morphology of joint surfaces provides some insight into the fracture mechanisms responsible for jointing. Joints formed in tension may display a hackly, abruptly uneven appearance and fresh, unweathered joint surfaces will exhibit delicate marks which are incompatible with frictional sliding (see section on fracture surface profiles, page 61). Structures characteristic of shear failure, such as scratches, grooves, gouge, or brecciation, will not be observed unless movement parallel to the joint surface has taken place. Many joints contain vein minerals which have formed in narrow open fissures, which suggests that these joints are probably tensile or transitional tensile fractures and did

not form with significant compressive normal stress acting across the fracture surface. Since movement along joint planes and deformation of the plane are rarely observed, joint formation early in the tectonic history of sediments is unlikely. No rock undergoing ductile deformation can at the same time develop joints, for flowage of the rock will eradicate any jointing the rock may possess (Turner, 1963). From this, it may be inferred, that joints develop at higher levels in the crust than that at which the rocks undergo plastic deformation.

THEORETICAL BASIS OF INVESTIGATIONS

The theoretical works of Price (1959; 1966) and Hobbs (1967) serve as the foundation upon which this study is based. Price was the first to explain the mechanical origins of regional jointing. His analysis showed that all master joints, and many minor joints, in both competent and incompetent material, result from the release of stored strain energy accumulated during burial and compaction. As these rocks undergo uplift, lateral expansion and extensional stresses are generated which produce jointing. The joint frequency is determined by the amount of strain energy stored in the rock prior to the initiation of uplift. By considering the strain energy stored in an elastic body as being equal to the work performed in producing a given amount of strain, he was able to estimate relative joint frequencies for particular lithologies.

The problem of the frequency was further investigated by Hobbs, who examined the mechanical reaction of brittle sedimentary rock to these changing conditions of stress. By considering the Griffith failure criterion (Appendix A) and the elastic properties of the material, he was able to demonstrate that the frequency of jointing in a bed of rock

is dependent upon several factors; specifically, the physical properties of the rock bed and the surrounding rock beds, the thickness of the rock bed, and the degree of tectonic deformation.

We shall take a more detailed look at how the above results were arrived at, with particular attention to any assumptions made and the evidence offered in their support. It will be shown that on the basis of these investigations, a consistent theoretical framework supporting this study can be established.

The State of Stress in the Crust

Before considering the problem of stress fields which give rise to jointing, we will first examine the state of stress present in the crust. In the analysis that follows, compressive stresses will be considered positive, tensile stresses will be considered negative, and $\sigma_1 > \sigma_2 > \sigma_3$.

It was proposed by Anderson (1951) that a hydrostatic state of stress was maintained in the crust, provided that it was not subject to additional tectonic stresses. He called this the standard state of stress. Using a rectangular system of coordinates with the vertical direction as the z axis, the state of stress at a depth z can be written as

$$\sigma_x = \sigma_y = \sigma_z = \bar{\rho} g h \qquad (1)$$

where $\bar{\rho}$ is the average density of the crustal material above this point and g is the acceleration due to gravity. This expression describes crustal material as being in a state of fluid equilibrium. If we assume that $\bar{\rho} = 2650$ kg/m^3, g = 9.8 m/sec^2, and z = 1.0 km, σ_z at this point is approximately equal to 26 MPa, where the units of the

MPa (megapascal) are 10^6 kg/m sec^2.

The phenomena of jointing requires that competent rocks behave as brittle materials, that is, that they act elastically up to the point of failure. Laboratory experiments (Handin and Hager, 1957) have shown that competent rocks may fail as brittle materials at loads as high as 965 MPa when acted upon by a confining pressure of 193 MPa, conditions found in the upper crust. Since we are concerned with jointing in relatively undeformed, horizontal sediments that have not been subjected to stress conditions which would exceed the elastic limits of the materials, the sediments may be rheologically modelled as a Hookean substance.

Consequently, the material of the uppermost 10 kilometers of the crust was considered by Price (1959, 1966) to approximate an elastic body. Using the same coordinate system and expressing Young's modulus for crustal material as E and Poisson's ratio as ν, an expression for the strain in the horizontal direction may be found. Rearrangement of equations B5 and B6 from the section on linear elastic theory (Appendix B) yields the following:

$$e_x = \frac{1}{E}\left[\sigma_x - \nu\left(\sigma_y + \sigma_z\right)\right] \qquad (2)$$

$$e_y = \frac{1}{E}\left[\sigma_y - \nu\left(\sigma_x + \sigma_z\right)\right] \qquad (3)$$

These equations can be used to establish the stress conditions in the earth's crust. Consider a small unit cube of rock in the crust subjected to a vertical gravitational stress $\bar{\rho} g z$. This cube tends to expand laterally due to its elastic nature, but is restricted by the pressure of the surrounding rock, which is also behaving elastically. If the rock is not free to expand laterally ($e_x = e_y = 0$), a

transverse stress is created, which can be calculated from equations (2) or (3):

$$\sigma_x = \sigma_y = \frac{\nu}{1-\nu}\sigma_z = \frac{\nu}{1-\nu}\bar{\rho}gz \qquad (4)$$

Equation (4) is called Price's standard state and it more accurately describes conditions in the crust at shallow depths (<10 km) than does the Anderson state, which represents deep crustal conditions at elevated temperatures and pressures. It has been demonstrated experimentally by Simmons and Brace (1965) and Price (1966), that due to elastic behavior, the value of ν increases as the pressure due to overburden increases. Since ν will be less than 1/2, σ_x and σ_y will be less than under Anderson's standard state. The stress condition of equation (4) is generally supported by hydrofracture data published in Haimson (1976).

By assuming that the fracturing of crustal material would be of a brittle nature within the limits of elastic deformation, Price (1959, 1966) examined whether or not it was possible to produce regional joints solely by the application of compressive stress σ_x in a horizontal direction to his standard state of stress. Taking the vertical stress due to the weight of the overburden as σ_z, he demonstrated that σ_x is limited to the range

$$\frac{m-2}{m-1}\sigma_z < \sigma_x < \frac{m-2}{m-1}m\sigma_z \qquad (5)$$

where m (Poisson's number) is equal to $1/\nu$.

He then examined the fracture criterion from the coefficient of internal friction and Poisson's number obtained through rock tests. It was found that under the conditions of stress that occur in the uppermost crust, neither the tensile strength nor the compressional strength of the rocks were exceeded. Since it is not possible to form either

extensional or shear fractures, the conclusion is reached that regional joints cannot be the products of severe horizontal compression during a vigorous period of mountain building. Instead, fractures develop in a subsequent period of decreasing horizontal compressive stress associated with the orogenic movement of rocks to progressively shallower levels in the crust. Thus, the problem of regional jointing is controlled by the relationship between the vertical stress, which gradually decreases as uplift progresses, and the newly emergent horizontal stress, which will become tensile. By tracing changes in the stress field associated with the processes of uplift, the conditions required to produce jointing may be accounted for.

Stress Due to Lateral Extension

One factor which causes variation in the stress field is due to lateral strain which develops in rocks during uplift. Let us consider an unfolded, horizontal unit of competent sedimentary rock originally deposited at or very close to sea level, as is the case in our coal-bearing sequences. These sediments generally have considerable lateral extent and can be represented in section as an arc of radius R from the center of the earth. If uplift takes place without tilting of the beds, the radius becomes (R + dR) where dR is the amount of uplift. As is shown in figure 1, there has been an increase in the lateral extent of the rock unit due to tectonic uplift. Originally at AB it had a length r, while after uplift to CD it has a length (r + dr).

From the figure it is clear that $r = R \cdot \theta$ and $dr = dR \cdot \theta$, so the resultant lateral strain in the bed is given by $dr/r = dR/R$. Assuming that dR is equal to 1.50 km, a value representative of three of our field areas, and that R is equal to 6371 km, we see $dr/r = dR/R = 1.50/6371 =$

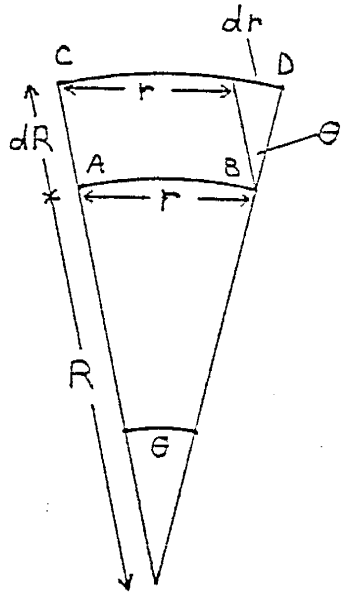

Figure 1. Development of lateral strain accompanying uplift. (after Price, 1959.)

2.35×10^{-4}. This lateral extension shown in figure 1 will be equal in all directions in the horizontal plane. If brought about by purely elastic processes, this horizontal expansion will develop a tensile stress σ_e, so that

$$\sigma_e = E \frac{dr}{r} \tag{6}$$

where E is Young's modulus of the rocks involved.

Thermally Induced Stresses

A second manner by which the stress field is altered is through the temperature change rocks experience as they are uplifted to higher levels in the crust. When a homogeneous rock is slowly heated or cooled, it will homogeneously expand or contract. The relationship between the strain produced, e, and the change in temperature, ΔQ, may be expressed as

$$e = \alpha_\ell \, \Delta Q \tag{7}$$

where α_ℓ is the linear coefficient of thermal expansion. If the rock is not free to expand or contract, stresses will be generated. Such a mechanism of stress generation is called thermal loading, and can be described using the elastic stress-strain relationship (equations 2 or 3) with thermal effects included:

$$e_t = \frac{1}{E}\left[\sigma_t - \nu\left(\sigma_t + \sigma_z\right)\right] + \alpha_\ell \Delta Q \tag{8}$$

Here e_t is thermal strain in the horizontal plane, σ_t is thermal stress $\left(\sigma_t = \sigma_x = \sigma_y\right)$, and σ_z is stress due to gravitational load.

The confinement of rock that is essential for thermal loading is provided by two mechanisms: spatial variation of ΔQ and inhomogeneous material properties. If the rock is confined (thermal strain $e_t = 0$)

and undergoes cooling through a temperature interval ΔQ, the induced thermal stress (neglecting any overburden stress σ_z) is then:

$$\sigma_x = \frac{\alpha_\ell E \Delta Q}{1 - \nu} \tag{9}$$

We can further specify the history of cooling during uplift and erosion by substituting for the temperature change, ΔQ, the gradient dQ/dz and variation in elevation Δz:

$$\sigma_x = \frac{\alpha_\ell E \Delta z}{1 - \nu} \frac{dQ}{dz} \tag{10}$$

This expression provides an estimate of the maximum thermal stress (Turcotte and Schubert, 1982; Suppe, 1985).

Stresses Due to the Gravitational Unloading

As horizontally bedded rocks are uplifted, they are subject to a pronounced variation of the existing stress field. During burial the sediments undergo compaction and thereby attain their ultimate physical properties, such as strength and elasticity. If these sediments are uplifted without the addition of significant horizontal, tectonic compressive stresses, then one can assume that the initial stress condition is close to the hydrostatic state. Figure 2 shows the variations in stress due to burial, compaction, uplift, and erosion. The stress level is plotted along the abscissa and is composed of two parts: a component due to thermal stresses and a gravitational component.

Thermal stresses are stresses locked into a body even in the absence of forces acting on the outside of the body. Because most rocks are heterogeneous intergrowths of minerals of differing elastic

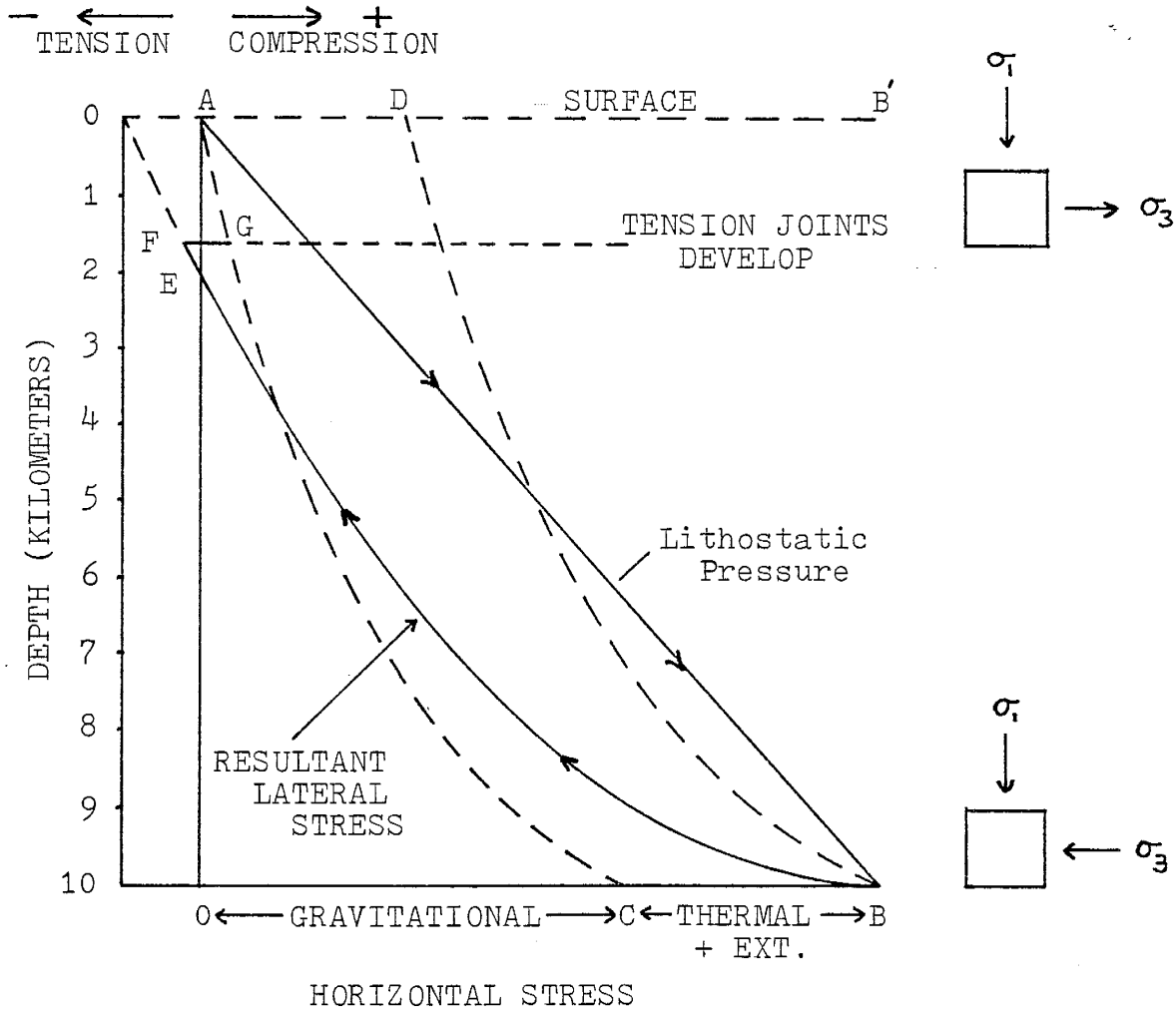

Figure 2. Stress variations due to uplift - Initial conditions approximately hydrostatic. (after Price, 1966)

constants and thermal expansion coefficients, these stresses are produced by pressure release and cooling during uplift and erosion, and can play an important role in the formation of joints. The effects produced by lateral stretching due to uplift will also be included in residual stresses.

The release of gravitational load due to the erosion of superincumbent material causes the compressed rock to expand. Since expansion is restricted in the horizontal direction by the surrounding rocks, which are also expanding, much of the horizontal compressive stress will remain after erosion.

Through Poisson's ratio, ν, the change in horizonal stress $\Delta\sigma_G$ is related to the change in gravitational load, $\bar{\rho} g \Delta z$:

$$\Delta\sigma_G = \frac{\nu}{1-\nu} \bar{\rho} g \Delta z \qquad (11)$$

Substituting a value of $\nu = 0.25$, we see that the decrease in horizontal stress is one-third the decrease in gravitational load.

Along the ordinate in Fig. 2 is plotted the depth of burial in kilometers. The maximum depth at which strictly brittle behavior is experienced (assuming no abnormal temperature gradients) is about ten kilometers and the greatest pressure, the initial condition, approximately 250 MPa (Price 1966; Paterson, 1978).

If we start with unconsolidated sediments at the surface of the earth at point A, and subject them to increasing loads from overburden we obtain the straight line AB. This represents the vertical gravitational loading, which is directly proportional to depth. The lateral stresses OC and CB represent the horizontal components produced by gravitational loading (eqn. (4)) and the thermal stresses (eqns. (6) and (10)), respectively. To the right of point B is shown a unit volume of

material and the nature of the stresses acting upon it. An inspection shows that they are all compressive, so at this point in the sedimentary loading history, tensional jointing is not possible.

As uplift takes place, the gravitational component of the lateral stress, OC, decreases in the manner shown by CGA (because of the pressure dependence of ν), so that B'D (=OC) represents the total decrease in lateral stress due to this factor. The thermal component, which is comprised of the factors due to thermal loading and lateral stretching accompanying uplift, will increase in magnitude as the rocks approach the surface. This is due to cooling effects produced in rocks which have been moved from conditions in which they were in equilibrium with the existing thermal gradient at depth to more shallow conditions at which they are no longer in thermal equilibrium, and the stretching of rocks formed at depth as uplift proceeds. The resultant variation in the lateral stresses which will take place in competent rocks, therefore, is represented by the curve BEF. When the rocks reach point E the lateral stresses equal zero, and if uplift continues, the rocks will enter the tensile field. The tensional stress will increase until it reaches the tensile strength of the material at point F, and a vertical tension joint will form. This is illustrated by the stress orientation shown on the unit volume at level FG.

The moment jointing occurs the tensile stresses are relieved; the least principal stress changes from a tensile stress to a compressive stress of value $\frac{\nu}{1-\nu}\sigma_z$ represented by point G. Here, the orientation of the stresses on the unit volume will again be compressive. The other horizontal principal stress, formerly σ_2, the intermediate principal stress, now becomes the least principal stress.

With further uplift a second set of tension joints will develop, the second set forming perpendicular to the first. In the case of the initial lateral stresses being very nearly equal, the formation of these joints sets will be practically simultaneous. The orientation of the residual stresses will reflect the original state of stress in existence during tectonic compression, even after an extended period of relaxation (Griggs and Handin, 1960).

The combined effect of the release of gravitational load, thermal contraction and lateral extension may be expressed as a horizontal stress in the following form by combining equations 4, 6, 10, and 11:

$$\sigma_x = \sigma_y = \frac{\upsilon}{1-\upsilon} \bar{\rho} g z + \Delta\sigma_G + \Delta\sigma_T + \Delta\sigma_e \qquad (12)$$

$$\sigma_x = \frac{\upsilon}{1-\upsilon} \bar{\rho} g z + \frac{\upsilon}{1-\upsilon} \bar{\rho} g \Delta z + \frac{\alpha_e E \Delta z}{1-\upsilon} \frac{dQ}{dz} + E \frac{dr}{r} \qquad (13)$$

In this formulation, the first quantity represents the initial conditions, and the last three quantities refer to effects produced by uplift.

Stress Distributions and the Mechanics of Jointing

Figure 3a shows a uniform tensile stress which has built up in an imbedded layer of rock due to uplift. With further extensional strain the state of stress will increase to a point where it equals the materials' tensile strength and a fracture will form. The resulting stress distribution due to joint formation in the embedded layer is illustrated in figure 3b. Joint formation at P-P' has produced a change in the uniform stress field that existed prior to jointing. We see that the tensile stress σ_T is zero at the fracture surface and increases in magnitude as you move into the unjointed regions of the bed.

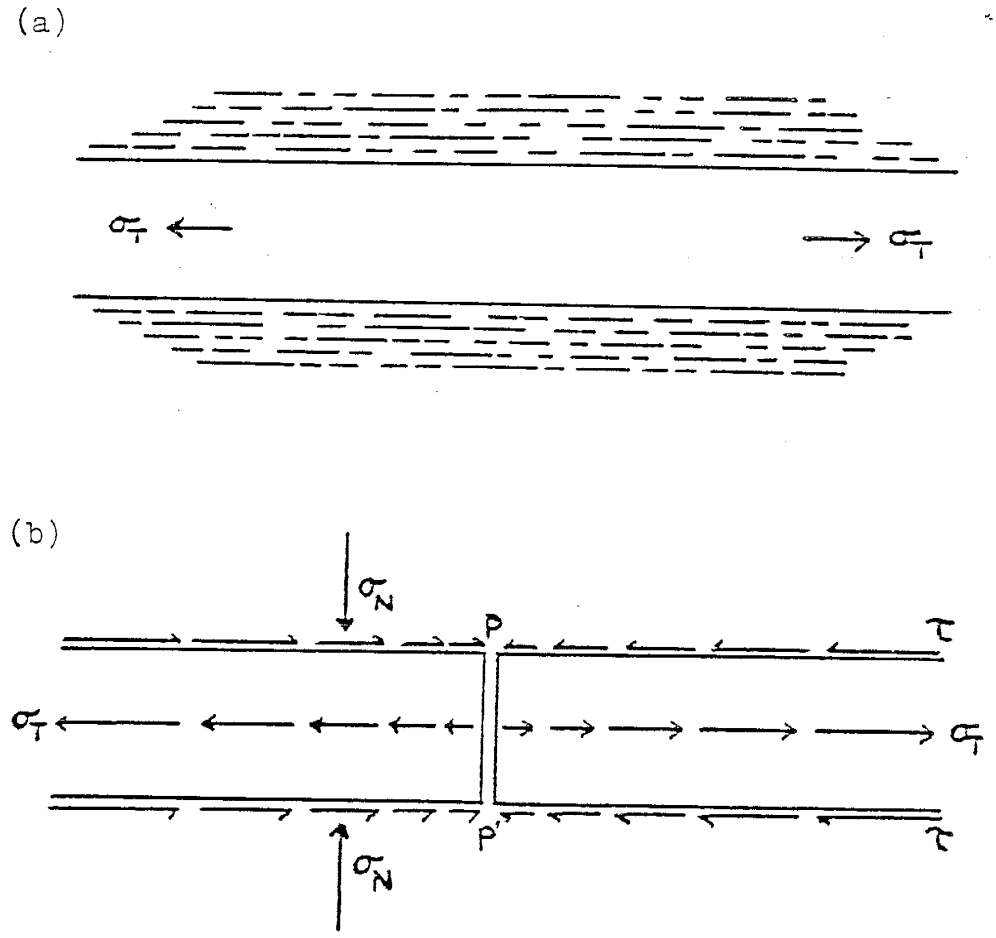

Figure 3. (a) Uniform tensile stress σ_T acting in embedded layer. (b) Resulting tensile stress distribution due to formation of joint at P-P'. (after Price, 1966.)

Also shown are shear stresses, τ, which are produced along the upper and lower surfaces of the bed in response to jointing. These stresses have a maximum value of $\sigma_N \mu_S$, where σ_N is the normal compressive stress due to the weight of overburden and μ_S is the coefficient of static friction.

We will now consider the effects of joint formation on the neighboring beds (fig. 4). When jointing occurs (P-P') in the embedded layer, strain energy is released into the overlying and underlying beds. The amount of energy exchanged will depend upon the elastic properties (E, G, T) and the thickness, d, of the jointed bed.

Because the elastic properties of the rock beds are different, the elastic displacements in the jointed bed and the neighboring beds will be different. Subsequent to joint formation, shearing stresses are produced on planes parallel to the tensile strain e. This shear stress is superposed on the uniform tensile stress which exists in the bed and increases the stress in the adjacent beds in the region of the boundaries of the joint.

Assuming no slippage occurs, the perturbation of the original state of stress in the neighboring beds caused by the formation of the joint will decrease linearly in the vertical direction. A rough approximation for this disturbing effect is given by

$$\tau = \tau_h (h - y)/h \qquad (14)$$

where y is the vertical distance from the interface, h is the distance the perturbation extends, and τ_h is the additional shearing stress.

If the original state of stress in the unjointed neighboring bed is close to its tensile strength T_n, the additional input of energy may

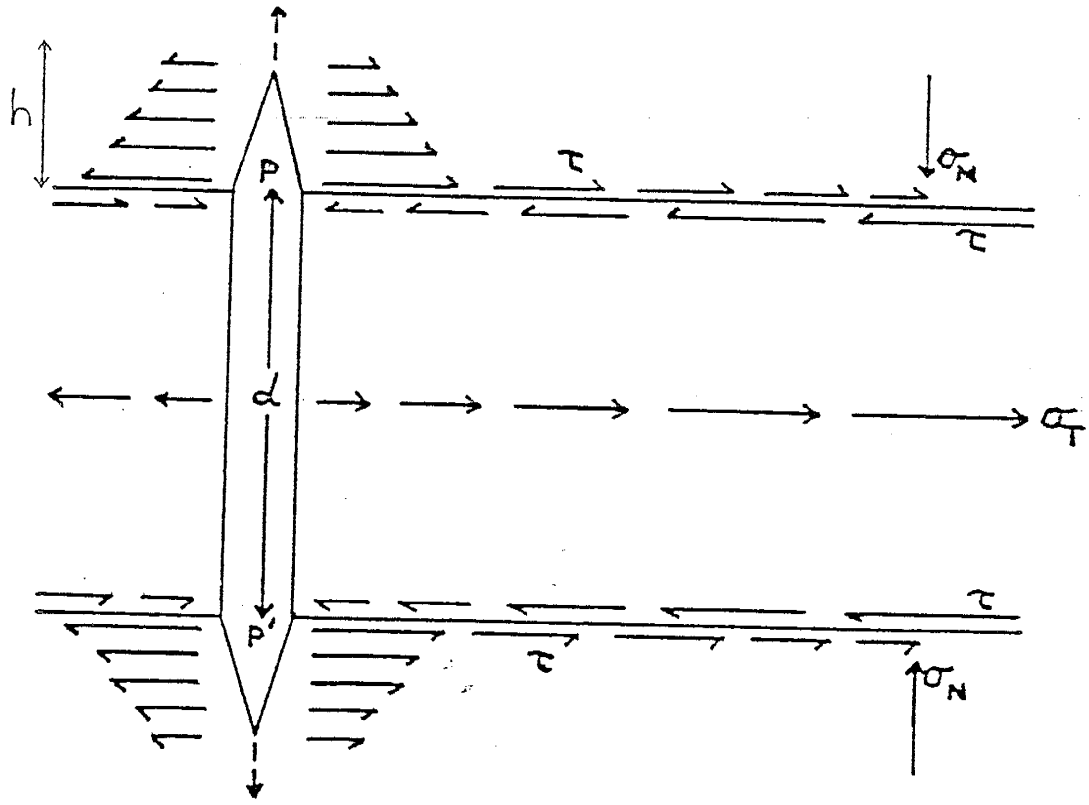

Figure 4. Effects of joint formation in the embedded layer on the neighboring beds.

precipitate rupture in the neighboring beds. This process will continue until the energy available for crack extension (Segall, 1984) has been dissipated (see Appendix A).

Hobbs (1967) has described the horizontal distribution of stress in the jointed bed as

$$\sigma_T = E e \left(1 + \sinh Dx - \cosh Dx\right) \qquad (15)$$

where E is Young's modulus, e is the strain, D is a constant equal to $2/d * (G_n/E)^{1/2}$, and x is the distance from the joint. The d in the constant represents bed thickness, and G_n is the shear modulus of the neighboring bed. For x = 0 we see that $\sigma_T = 0$ at the fracture surface, as it should be, and so our boundary condition is satisfied.

By entering values for d, E and G_n, a curve illustrating the buildup of σ_T/T as a function of x/d may be constructed, as shown in figure 5. The values used were experimentally determined for coal samples taken from the Manilla Mine, one of the field areas studied. A computer program for performing these calculations is provided in Appendix C.

It is instructive to note that at x = d the stress level is approximately equal to 96.7% of the original value of σ_T prior to jointing and at x = 2d the stress level is virtually 100% σ_T. Thus, in accordance with St. Venant's principle, for areas sufficiently removed from the position at which jointing has taken place, the effect on the preexisting state of stress will be negligable (Mase, 1970). The remainder of the bed is on the threshold of tensile failure, so that with an additional incremental strain e, another joint will form (Q-Q', Fig. 6a) at a distance L characteristic of the material the bed is

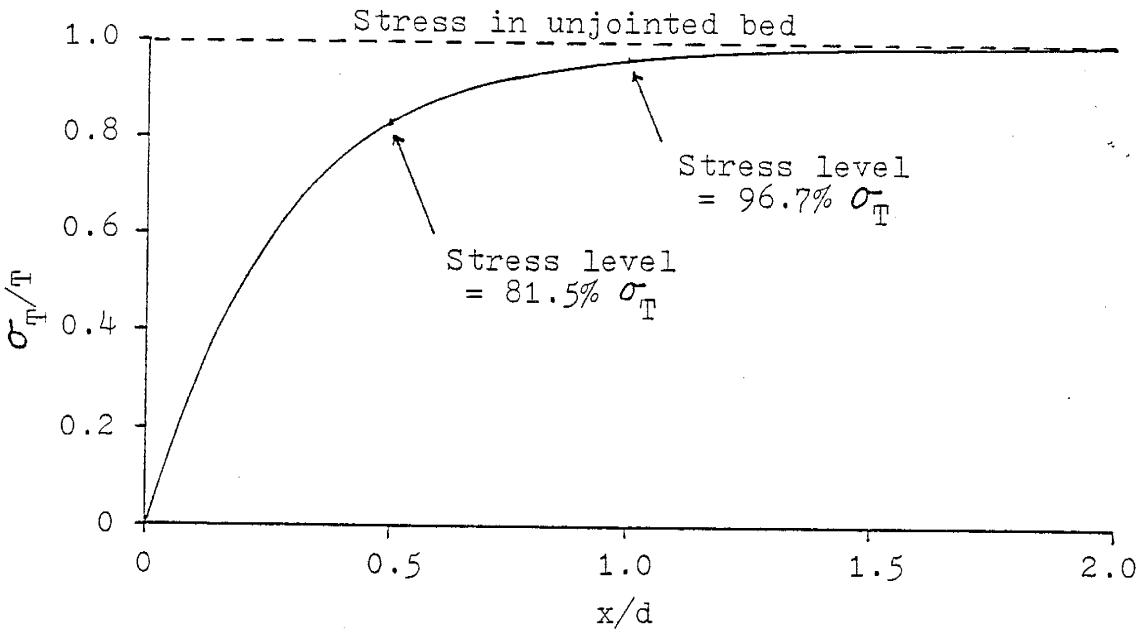

Figure 5. Buildup of tensile stress/tensile strength as a function of distance from joint/bed thickness. Values determined for Carthage Coal.

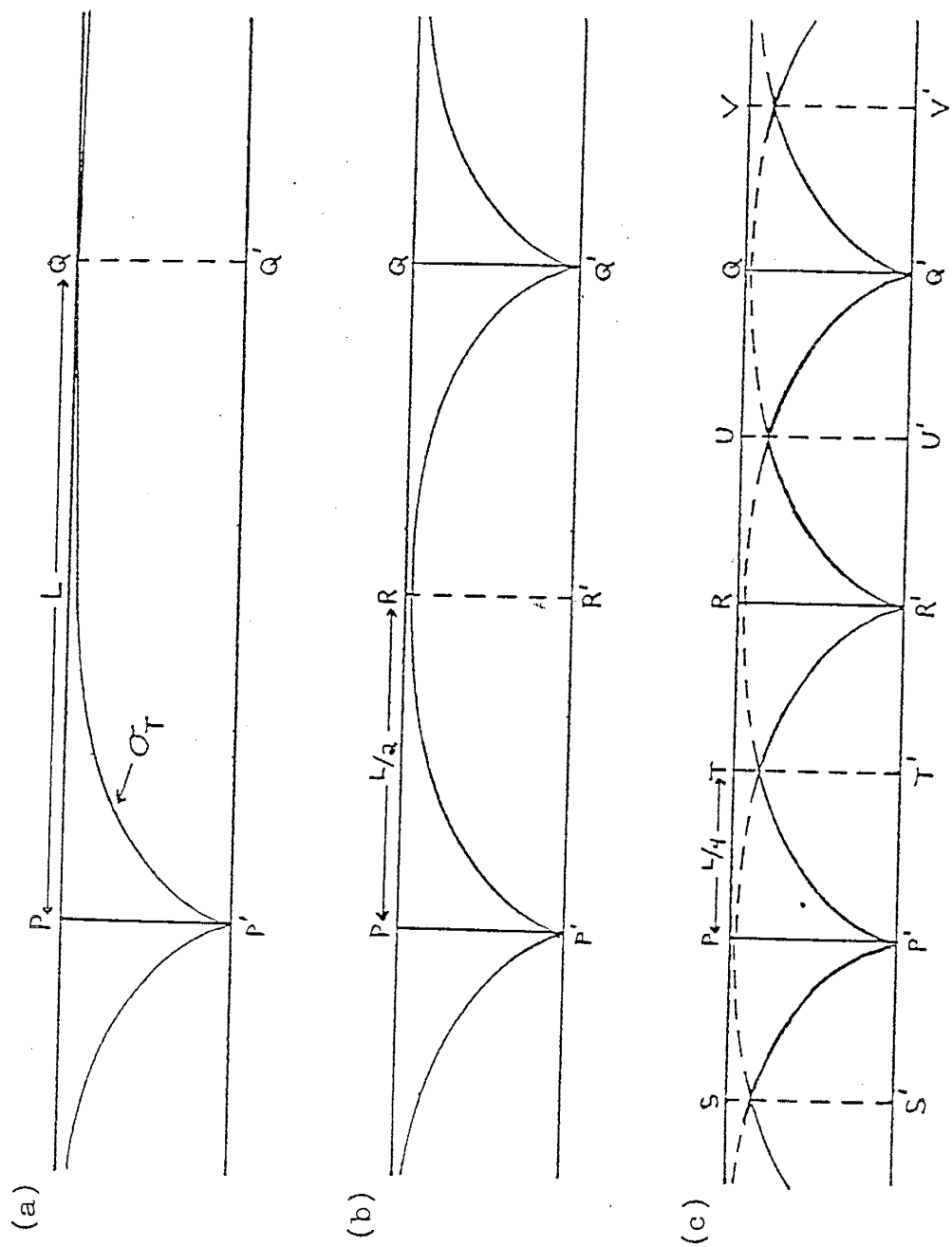

Figure 6. Tensile stress distributions due to formation of subsequent joint sets.

composed of. With the formation of this second joint there is a change in the stress distribution. The position at which the stress level is greatest now lies midway between the two fractures at distance L/2 (Fig. 6b). This position (R-R') will be the next location at which failure will take place as the strain increases. The process will be repeated as extensional strain continues (Fig. 6c), producing subsequent jointing at distances L/4, corressponding to positions S-S', T-T', V-V' and U-U'.

Interjoint Spacing

We can describe joints in terms of the spacing between sucessive members of a particular set. This joint spacing is equal to 1/j, where j is joint density, and has the dimensions of a distance. Hobbs' investigations into the factors controlling tensile joint formation may be written as:

$$s = d\left(\frac{E}{G_n}\right)^{1/2} \cosh^{-1}\left(\frac{e_2}{e_2 - e_1}\right) \qquad (16)$$

This expression describes the interjoint spacing s in terms of the bed thickness d, the elastic constants E and G_n, and the degree of tectonic deformation. The e_2 in the inverse hyperbolic cosine function is the final state of strain reached during the jointing process, and e_1 is the strain necessary to produce the first joint. As e_2 increases, $\cosh^{-1}$ (e_2/e_2-e_1) decreases, so s decreases with increasing tectonic deformation.

A sequence of sediments possessing identical elastic properties is displayed in figure 7. In this idealized case, the factors representing the contributions due to the physical properties and degree of deformation of the material are constants. Under these conditions it is

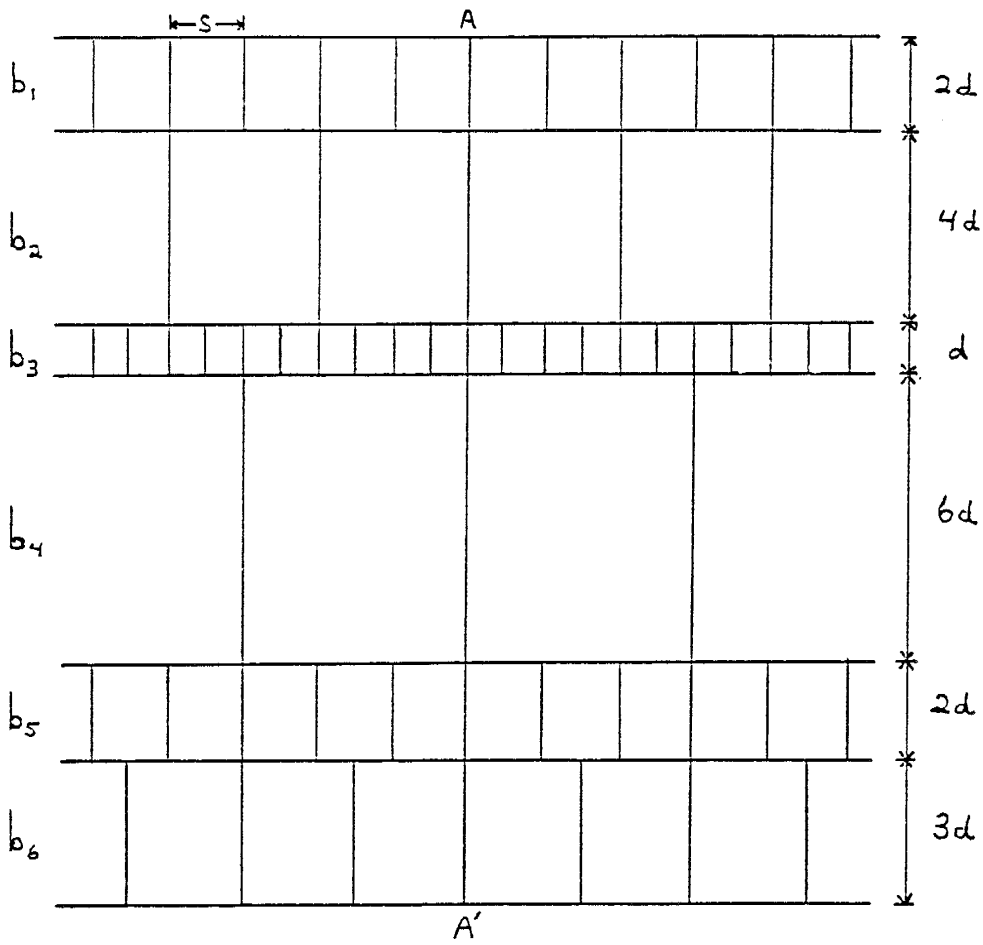

Figure 7. Joint spacing in a sequence of sediments possessing identical elastic properties but differing thicknesses.

seen that the interjoint spacing s is inversely proportional to the bed thickness d. An examinination of beds b_2 and b_3 illustrates this situation: the thickness of b_3 is one-fourth that of b_2, consequently, the joint density of b_3 is four times that of b_2. Also shown in the figure is a master joint A-A' that has developed due to initial failure of bed b_3, the thinnest, most easily fractured bed, and the subsequent propagation of extensional energy into the surrounding mediums.

New groups of joints can only form at specific values of increasing tensile strain e, so joint formation is not a continuous process. Figure 8 is a log-log plot illustrating the relationship between $s/d \cdot (G_n/E)^{1/2}$ and e/e_1. The horizontal sections correspond to conditions when strain is accumulating and the vertical sections correspond to the process of joint formation. If the strain increases linearly, groups of joints will form at a rapidly decreasing rate (Hobbs, 1967).

It was proposed earlier that many, perhaps most, joints in competent rock are post-burial structures and that the stresses which bring about the development of joints are residual and are not due to tectonic forces. Since the residual stresses are only dissipated in the immediate vicinity of the joint plane, in order to relieve stresses throughout a wide area, the formation of a very large number of joints is necessary. We see here a reason for the large number of joints observed in the field, namely, that the process of joint formation is relatively inefficient at dissipating strain energy.

Pore Pressure and Extensional Failure

The theoretical effects of pore pressure on extensional failure have been discussed by Murrell (1964). The concept of effective stress suggests that the criterion for failure would be $\sigma_3' = \sigma_3 - p = T$,

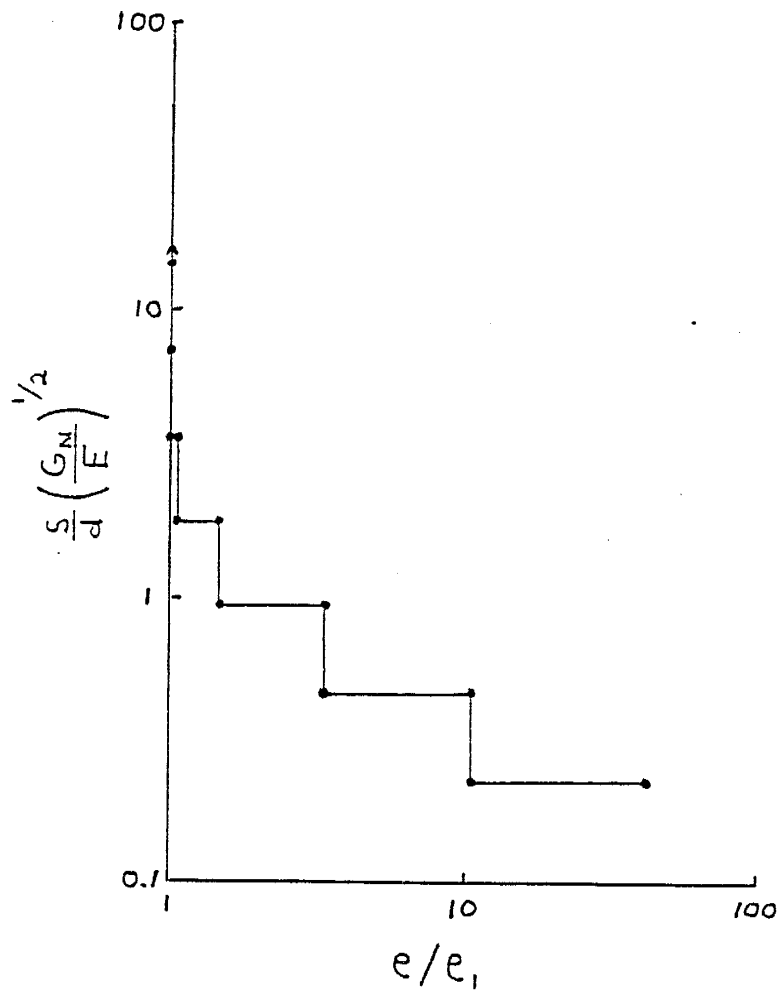

Figure 8. Relationship between the formation of successive generations of joints and the accumulation of tensile strain. (after Hobbs, 1967.)

where σ_3' is the effective stress and p is hydrostatic pressure. This is derived from the Griffith theory for a crack with internal pressure, has been shown to hold experimentally, and is fundamental to the theory of hydraulic fracturing. Flat, open cracks of every orientation are equally affected by a hydrostatic pressure p. They also have the same effect on the Poisson's ratio of a body as they have on its Young's modulus, that is, the lateral strain ratio of a body with open cracks is the same as that of a solid body without cracks (Jaeger and Cook, 1979).

If we extend our previous discussion of the buildup of stress within an imbedded layer to include the effects of pore pressure, we obtain results as shown in figure 9a. While the crack is developing, there will exist a fluid pressure gradient from the low pressure fluid (p_j) in the fracture (due to the volume increase) to higher pressure fluid (p_u) at some distance ℓ in the unfractured rock. Consequently, at distance ℓ the rock is "unaware" of the existence of the joint and the original conditions required for hydraulic fracture are still in existence and a second fracture could develop.

The interjoint spacing s is clearly related to the gradient of fluid pressure dp/dx, as figure 9b illustrates. This gradient, in turn, will be largely determined by (1) the rate of propagation of the fracture (which will be related to the strain rate and therefore reflect the degree of tectonic deformation) and (2) the permeability of the unfractured rock (which is related to the lithology) (Ladeira and Price, 1981).

An increase in pore pressure will reduce the effective mean stress

$$\sigma_m' = \frac{(\sigma_1' + \sigma_2' + \sigma_3')}{3} = \frac{(\sigma_1 + \sigma_2 + \sigma_3 - 3p)}{3} \qquad (17)$$

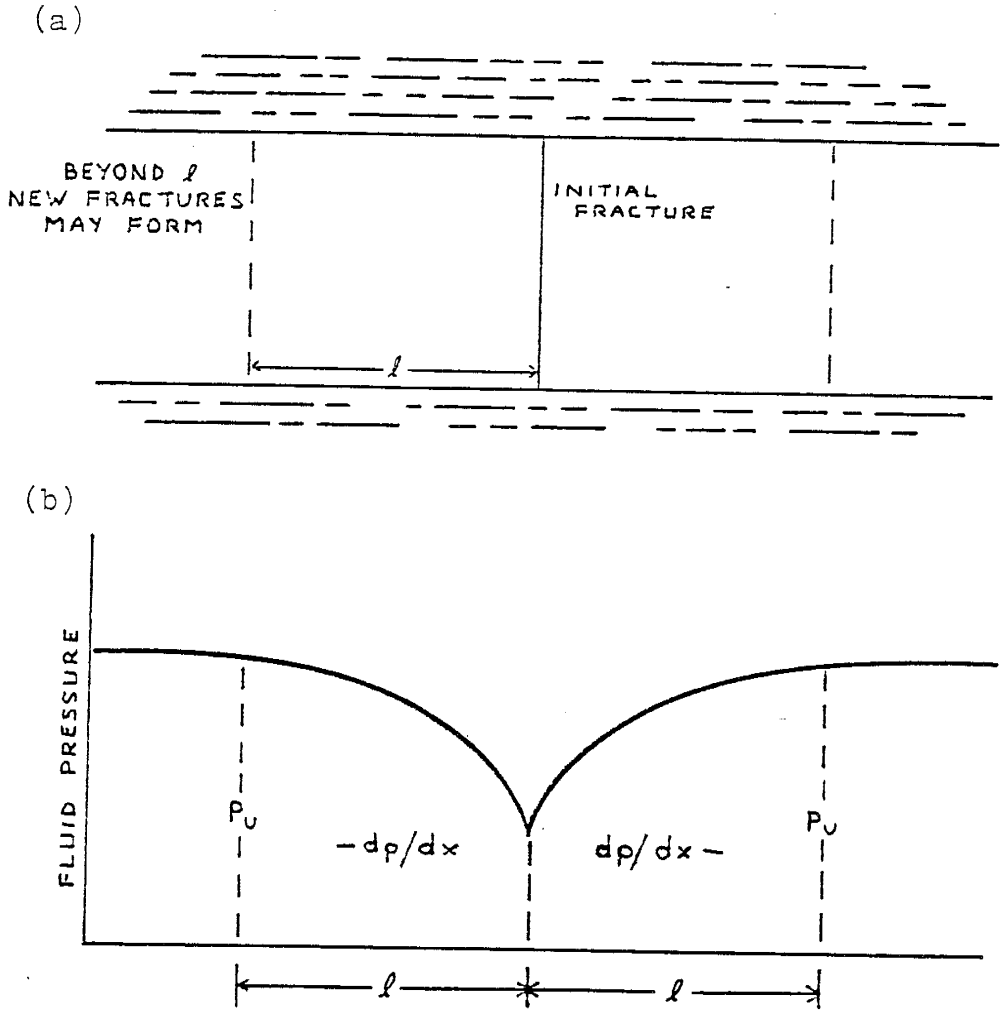

Figure 9. (a) Formation of initial fracture in embedded layer disrupts existing fluid pressure thereby inhibiting fracture growth except at some distance ℓ. (b) Gradient of fluid pressure resulting from initial fracture. (after Ladeira and Price, 1981.)

where σ_1', σ_2', and σ_3' are the effective principal stresses. An illustration of this phenomenon, which is the basis of hydraulic fracturing, is given in figure 10 by use of the Mohr diagram. Here, the Mohr circle is in effect translated to the left by an amount equal to the existing fluid pressure, P_f: both the fracture envelope and the size of the circle (deviatoric stress, $\frac{(\sigma_1 - \sigma_3)}{2}$) are unaffected. Since both strength and ductility decrease as the mean stress decreases, the pressure due to pore fluids makes rocks weaker and more brittle. Therefore, brittle fracture will take place at greater depths than would otherwise be expected.

Suppe (1985) gives the following expression for the maximum depth of true tensile joints

$$z = \frac{3T}{\rho g (1 - \lambda_f)} \qquad (18)$$

where λ_f, the fluid pressure ratio, is equal to the ratio of fluid pressure to vertical stress, $P_f / \bar{\rho} g z$. Figure 11 is a graph of equation 18 showing maximum depth of tensile fracturing as a function of tensile strength and fluid pressure ratio.

Experimental Verification of Hobbs Theory

The theoretical studies of Hobbs (1967) show that joint frequency is dependent upon several factors: (1) the physical properties of both the rock bed and its surroundings, (2) the thickness of the bed, and (3) the degree of tectonic deformation.

In order to investigate the validity of this prediction, a simple experiment was designed that would test each of these factors. Thin layers of plaster (0.25 - 0.55 cm) representing sedimentary beds were affixed to sheets of aluminum (1.6 mm thickness) by means of a light

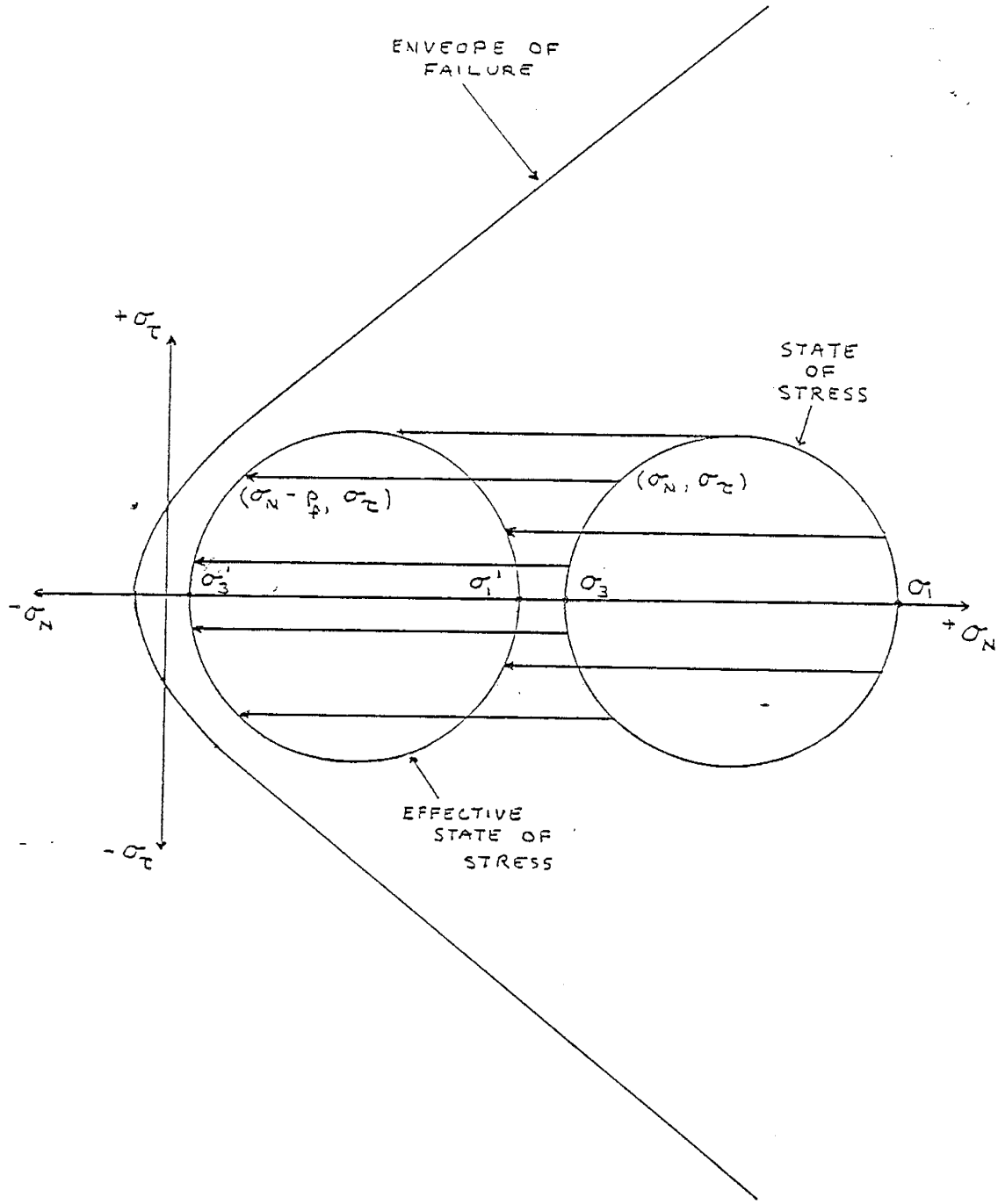

Figure 10 . Mohr diagram illustrating the relationship between state of stress and the effective state of stress due to pore pressure. (after Suppe, 1985.)

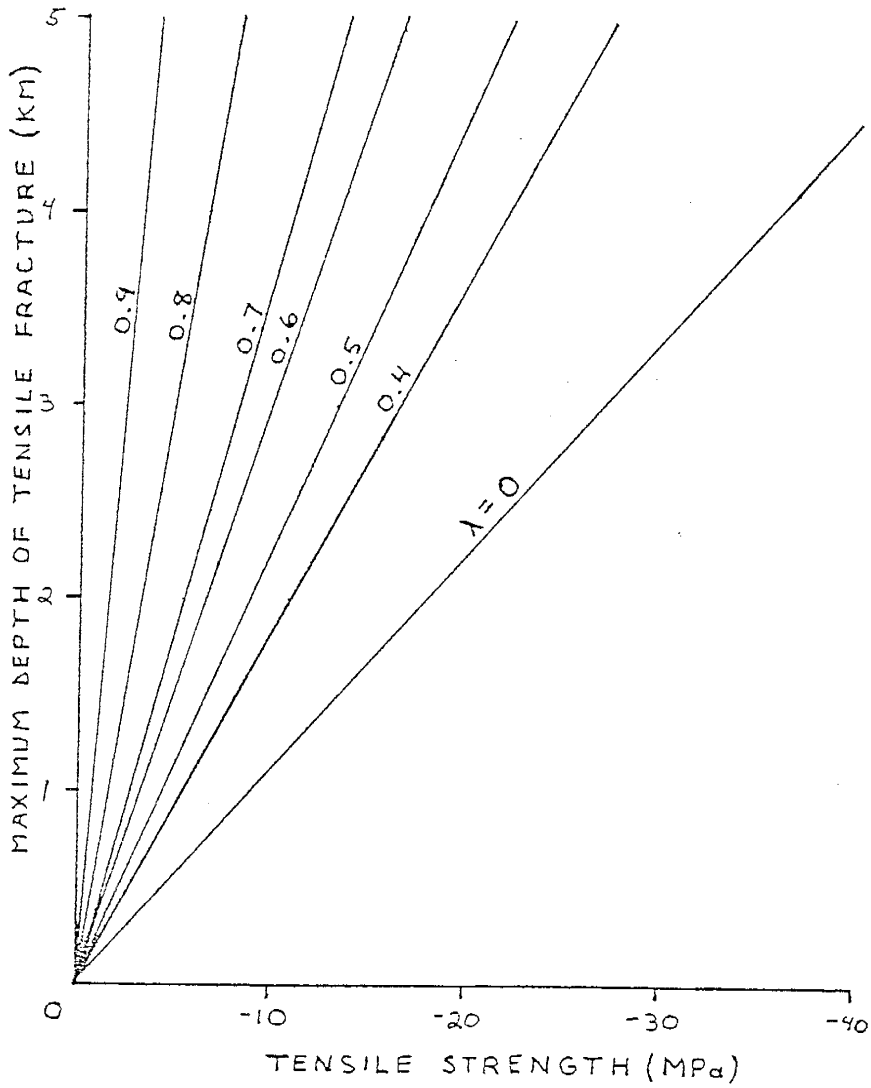

Figure11. Maximum depth of tensile fracturing as a function of tensile strength and fluid pressure ratio.

adhesive spray. The adhesive acted as a cohesive force that might simulate pressures from lithologic overburden. These aluminum sheets were then placed in a device in which they and the attached plaster "beds" could be subject to controlled amounts of extensional strain. The device (fig. 12a) consisted of a frame which held the ends of the sheets immobile, while a screw mechanism, which caused the sheet to deform, was advanced. The advancement of the screw produces vertical displacement and bending of the sheet, which in turn, sets up a tensional stress field in the attached plaster bed. As the amount of deformation is increased, the tensile strength of the bed is eventually reached, and a tensional fracture will form. With repeated strain increments, the tensile strength of the material will be exceeded in the unjointed regions of the material. The general theory and energy considerations are discussed more fully in the section dealing with joint formation.

Sucessive generations of tension joints were observed to form at characteristic distances (see figures 12a, 12b, 12c). The models were composed of various mixtures of plaster and material such as sand and fine sawdust and their elastic constants were determined by use of ultrasonic pulse techniques and are listed in Table 1. By varying the compositions of the layers, the first prediction of theory was tested, and by noting the thickness of the beds and the amount of deformation at which joint formation took place, the last two predictions were evaluated.

Figures 13a and 13b present the results of this experimental approach, where the different symbols used identify the composition of the specimens. In figure 13a, which is a plot of joint spacing vs. bed thickness, we see a strong correlation between these two factors; as the

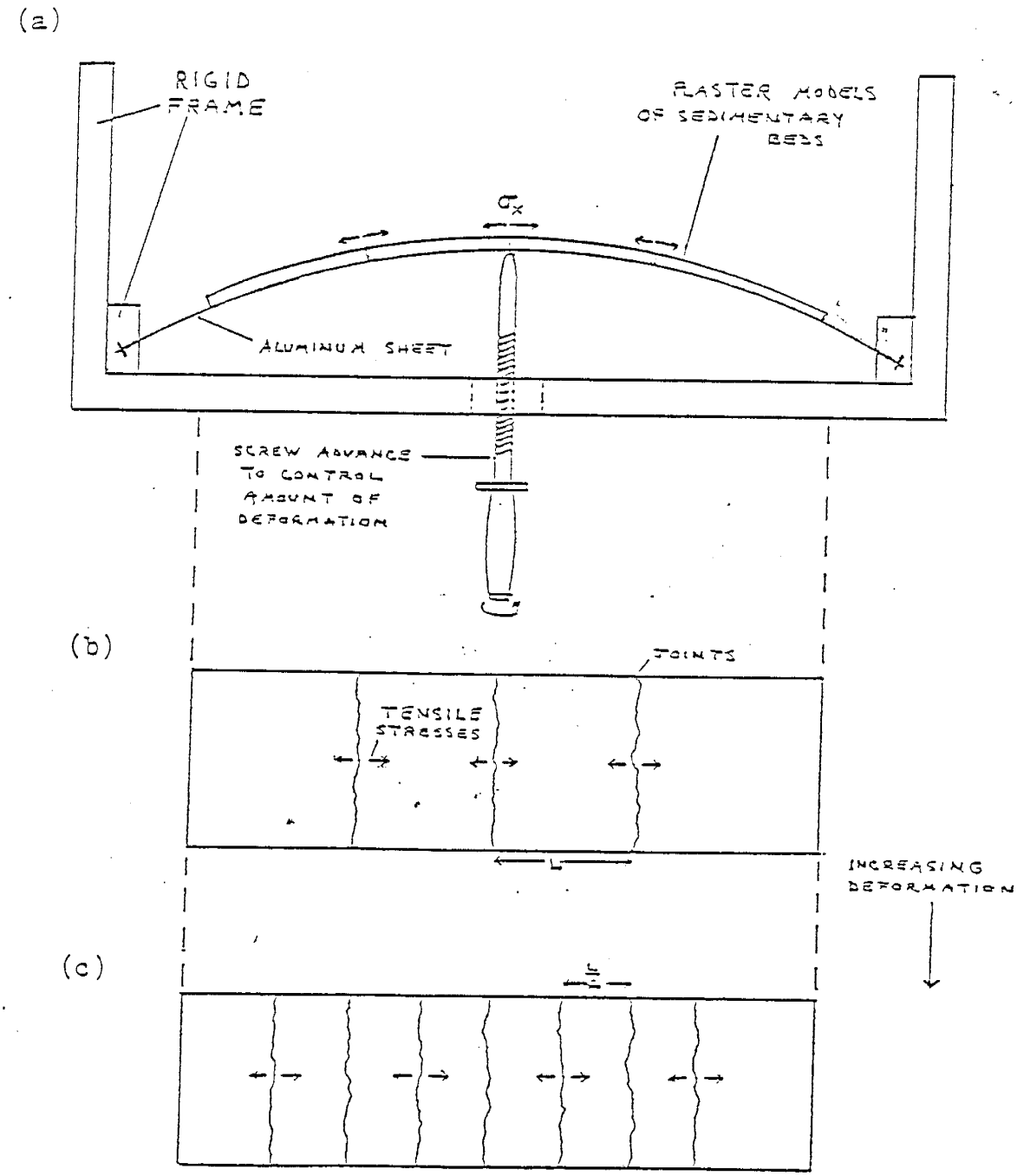

Figure 12. (a) Schematic diagram of device used to impose extensional stress on plaster models.
(b) First generation joints observed to form at characteristic distance L.
(c) Second generation joints observed to form at characteristic distance L/2.

Table 1. Values of elastic constants of various mixtures used to make sedimentary models.

	100% Plaster	80% Plaster 20% Sand	60% Plaster 40% Sand	80% Plaster 20% Sawdust	60% Plaster 40% Sawdust
V_p Compressional velocity * (km/sec)	2.40±0.11	1.29±0.05		1.71±0.09	1.31±0.08
V_s Shear Velocity (km/sec) *	1.84±0.08	0.93±0.05		1.17±0.07	0.81±0.06
ρ Density (g/cm^3)	1.27	1.48	No samples available for testing ++	0.96	0.80
E Young's Mod. (GPa)	6.77	2.45		2.79	1.25
G Shear Mod. (GPa)	4.30	1.28		1.31	0.52

* Values determined by ulrasonic pulse.

** Values calculated using V_p and V_s.

++ Samples broke during removal from aluminum sheets.

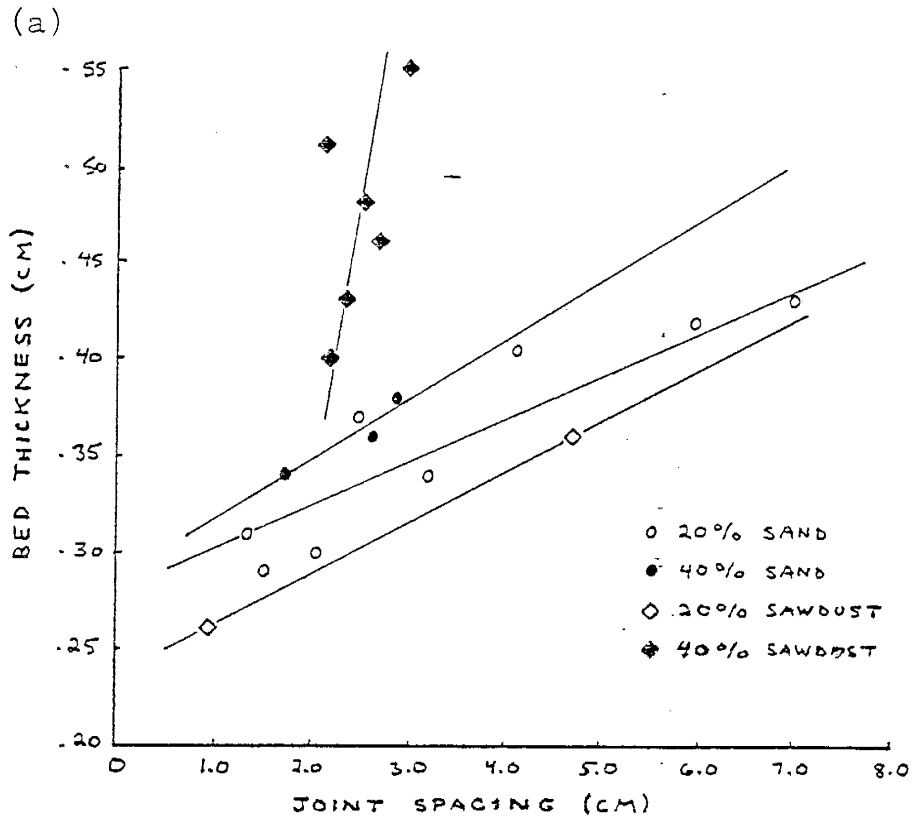

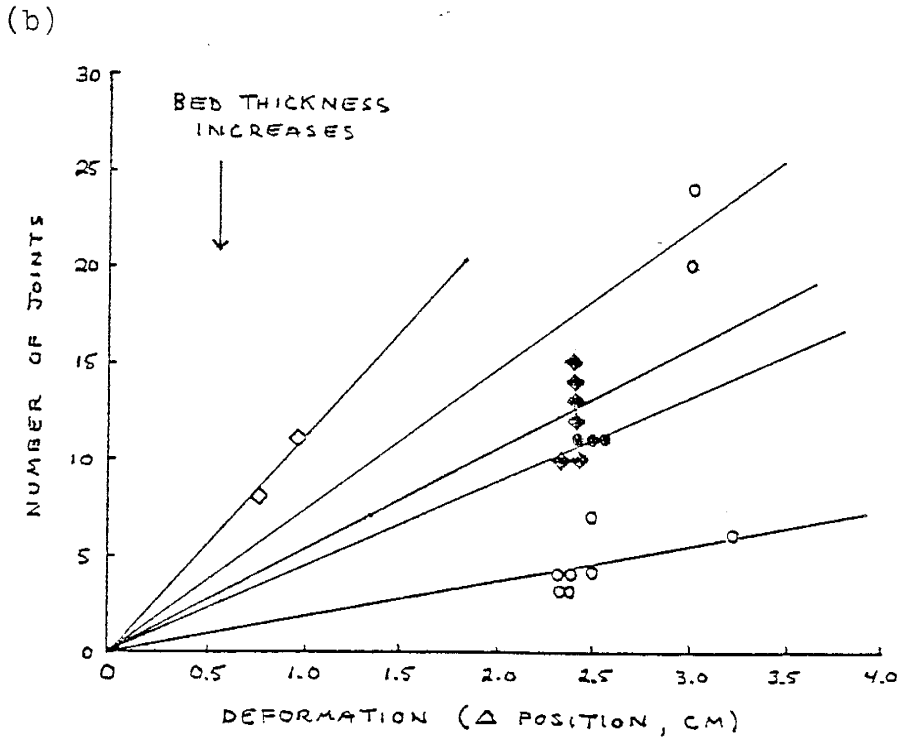

Figure 13. Results of plaster model experiment.
(a) Joint spacing versus bed thickness.
(b) Deformation versus number of joints.

thickness of the bed increases, the spacing between joints increases. The relation between the degree of tectonic deformation and number of joints produced is shown in figure 13b. We require that before the application of deformational strain the beds are unjointed, so that all lines relating deformation and the number of joints produced pass through the point (0,0). The apparent "stacking" of some of the results (for example, 40% sawdust) reflects changes in bed thickness. It is seen that as deformation increases, so does the number of joints (see also figs. 12b, 12c).

Results of this simple approach generally support the theoretical work of Hobbs (1967) which relates joint frequency with the physical properties, deformation, and thickness of the beds. It is felt that these predictions have been experimentally confirmed and that they are indeed valid and can serve as a basis for further research.

Mechanical Nature of Rocks

The theories we have investigated so far require that rocks of the uppermost crust behave as homogenous elastic bodies. A brief look at the structural nature of sedimentary rocks is needed to provide support for this line of inquiry.

Dependent upon the scale and detail on which it is studied, the mechanical structure of a rock presents several different appearances. In sedimentary rocks, which are generally laminated, the rock within a lamina may be relatively isotropic, whereas, at a scale that includes the separation between laminae, the same rock may be anisotropic.

The majority of sedimentary rocks are composed of layered aggregates of particles joined together by varying amounts of cementing materials. Chemical composition may be relatively homogeneous or very

heterogeneous, as in pure arenites and polymictic conglomerates, respectively. The properties of a single mineral are a function of its chemical composition, lattice structure (which will determine glide systems), and lattice defects such as vacancies and dislocations. They also depend on the orientation of the applied stress field and on the mode of load application. These particles generally represent the smallest scale on which the mechanical properties are investigated. The boundaries between particles represent weaknesses in the rocks structure which can otherwise be regarded as continuous.

On a somewhat larger scale, the presence of joints, cracks, bedding and minor faulting poses an important question concerning the continuity of a rock mass. In outcrops ranging in size from meters to hundreds of meters the structure of some rocks is continuous, but more often it is interrupted by cracks, joints, and bedding planes separating different sedimentary layers. The mechanical properties of rocks are dependent upon every one of its structural features, with individual features having varying degrees of importance in different circumstances. While such disturbances may be small in relation to the dimensions of a structure in the rock, they will affect the overall mechanical properties of the rock mass, and allow us to treat the bed as a physical continuum (Jaeger and Cook, 1979).

The specimens used in the experimental studies normally have dimensions of several centimeters and contain a sufficiently large number of structural particles for us to regard them as being grossly homogeneous. Thus, although the properties of individual particles may differ widely from one particle to the next and although the individual crystals of the specimen are often anisotropic, they and the grain

boundaries separating them will interact in a sufficiently random way to give the specimen average homogeneous properties. These average properties will not necessarily be isotropic, due to processes of rock formation and alteration which often align the structural particles. Their interaction will be random with respect to size, composition and distribution, but not with respect to structural alignment. Such rock specimens possess gross anisotropic properties, but nevertheless, may be regarded as homogeneous (Paterson, 1978).

FIELD STUDIES

Having established the theoretical foundations of our hypothesis relating joint formation and strain energy, the next step was to acquire joint data from outcrops in the field. Three field areas (the Manilla, Trinity, and Gateway mines) consist of coal-bearing sequences of sedimentary rocks, with a fourth site being exclusively sandstones. As mentioned previously, coal/sandstone interfaces were chosen because it was felt that the contrast in joint density with respect to lithology would be most pronounced due to their different elastic properties. The additional sandstone study was conducted to provide a comparison in the case of adjacent sediments whose properties were similar.

Procedures and Methodology

At each locality the data on jointing was collected in the following manner. First, the rocks are examined to determine the major joint systems present, noting their attitude and orientation. Information on strike, dip, bed thickness and lithologic characteristics are also recorded. Second, a traverse is selected over which the joint densities will be determined. Joint density, j, will be defined as the

number of joints of a particular set encountered along a unit distance measured perpendicular to the set. The sampling line is chosen so as to provide the best display of one or more joint sets. Sampling traverses were made on both upper (plan view) and cross-sectional surfaces whenever possible. Most outcrops provided only cross-sectional exposures, with the exception of the sandstone study. Third, the surfaces of the joints are examined to see whether there are morphological clues to the nature of the stress system which produced them. Specifically, do the surfaces exhibit slickensides or undulatory behavior as might be expected in shear fractures, or are they planar or hackly such as tension joints? Note is also taken on any fracture fillings present as to composition, structural style, and cross-cutting relationships, which may provide relative ages of joint sets. Finally, the surface trend of the outcrop is recorded, for it is usually necessary to normalize the jointing data to a common direction in order to determine the relative joint density.

The following procedure was used to correct for sampling line bias. Consider a single set of parallel, planar, vertical joints. We will assume that the frequency of jointing of this set, intersected by a sampling line that is perpendicular to the set, is j per unit length. Figure 14 shows a diagramatic representation of the joint set, constructed in the plane that contains the normal to the set and the sampling line. The acute angle between the sampling line and the set normal is δ. A line of length l, parallel to the set normal can, for sufficiently large values of l, be expected to intersect a total number N of joints given by:

$$N = jl \tag{19}$$

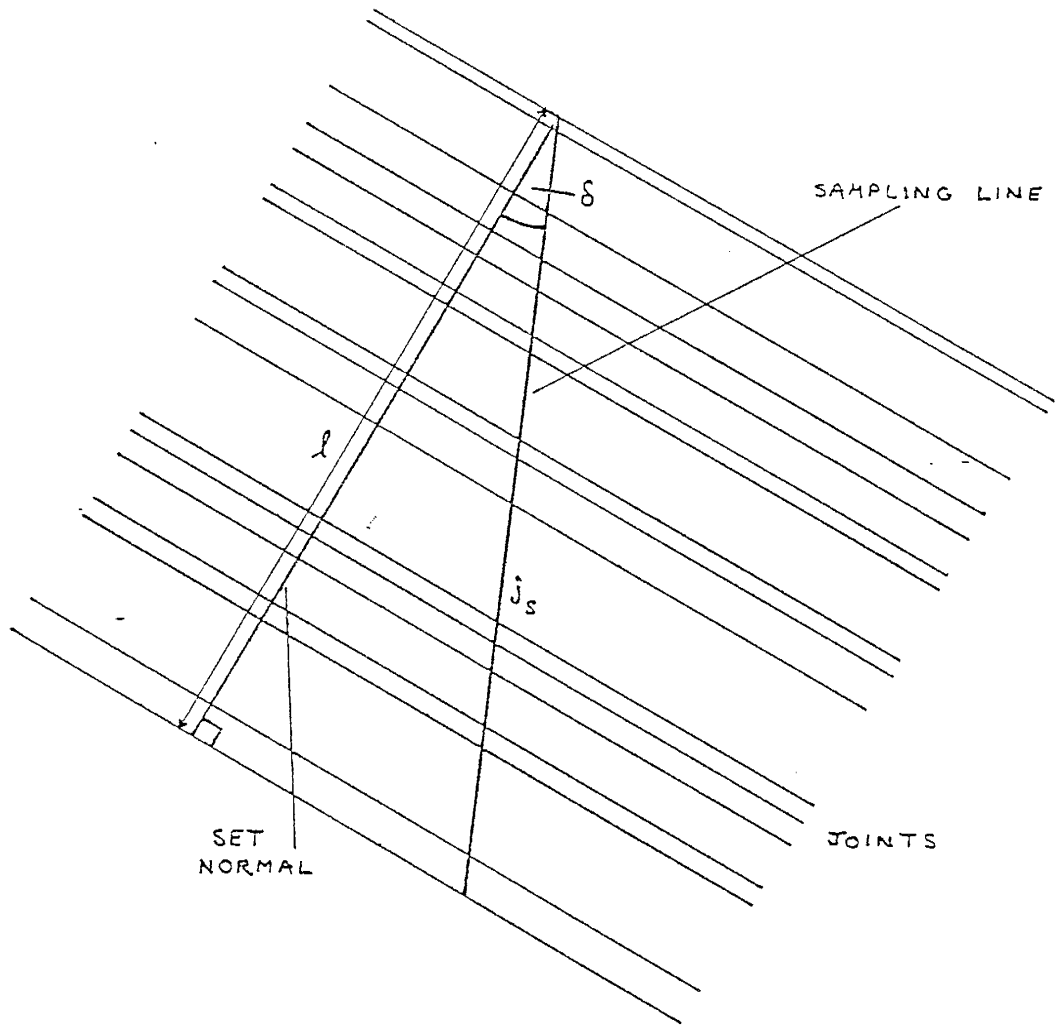

Figure 14. Joint set intersected by a sampling line of general orientation.

A general sampling line, at an angle δ to the set normal, would have to be of length $\ell/\cos\delta$ in order to intersect the same number of joints N. Hence, the frequency observed along this sampling line is given by

$$j_s = N \cos\delta / \ell \qquad (20)$$

and substituting j = N/l from equation 19 we get

$$j_s = j \cos\delta \qquad (21)$$

This demonstrates that the number of joints of a given set, intersected by a sampling line that makes an acute angle δ with the set normal, decreases with increasing values of δ and approaches zero when δ approaches 90°. By noting the joint density and the angle to the set normal, the bias imposed by linear sampling may be avoided.

Samples of rock are collected from each bed to provide specimens for the laboratory tests required to ascertain the elastic properties of the material. Information on specimen orientation is recorded, particularly those aspects concerned with the fracture-face and bedding, for we will later prepare samples of specific orientation with respect to these features. Special note is also made of the nature of the bedding contacts and whether joints propagate into the neighboring beds, or are confined to a single bed. This will give some indication as to how energy has been transferred between beds. Joints will not propagate from one bed to another unless there is sufficient interbed cohesion to effect the transfer of energy.

Carthage Coal Field - Manilla Mine

The Carthage coal field is located just south of U.S. 380 about 11-16 kilometers east of San Antonio in Socorro County, N.M. (see Fig. 15).

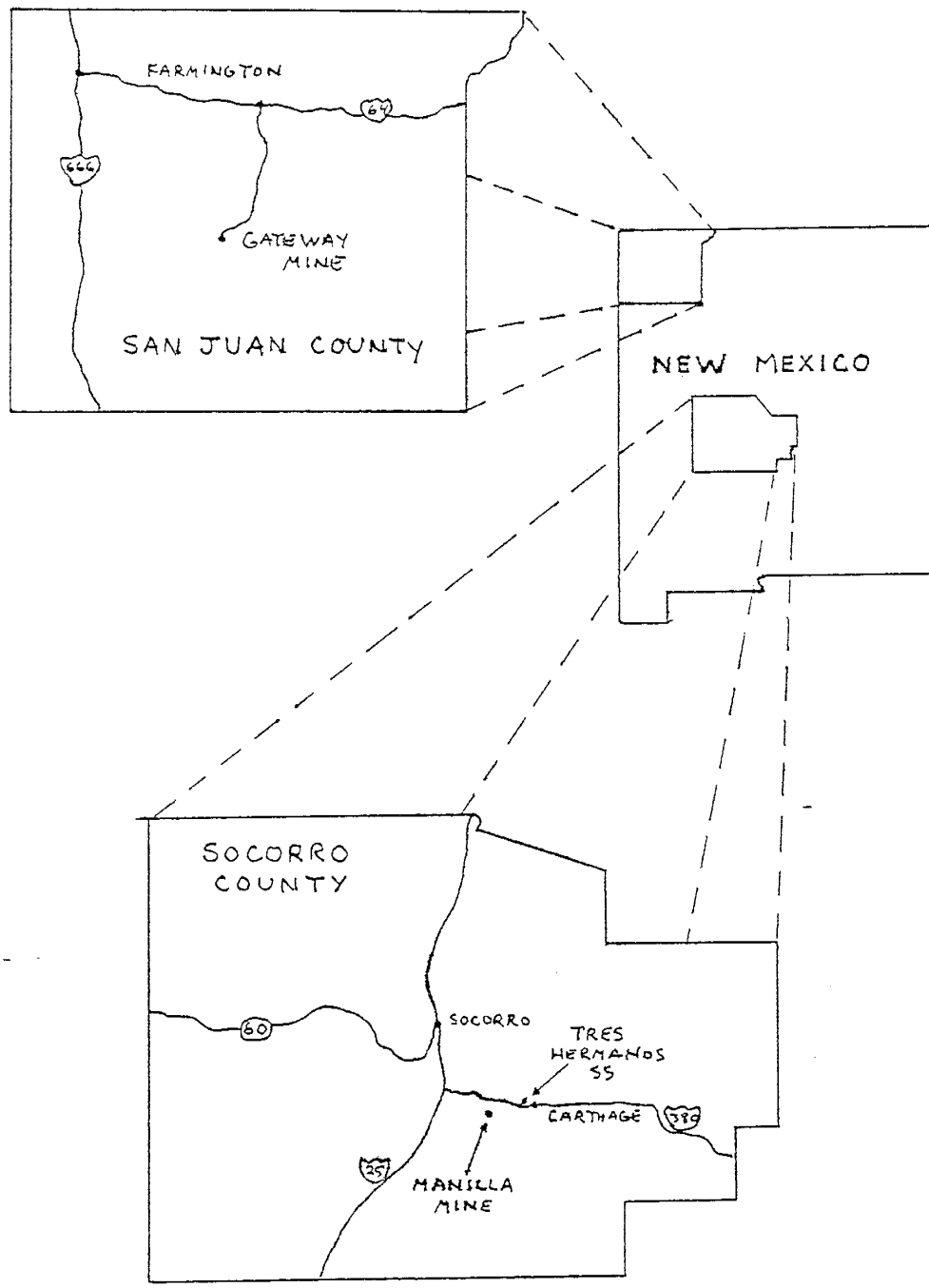

Figure 15 . Index map showing location of the three field study areas in New Mexico: the Gateway Mine, the Manilla Mine, and the Tres Hermanos SS.

The Carthage area is a structurally complex uplifted fault block between two structural depressions, the Rio Grande trough to the west, and the Jornada del Muerto to the east (Budding, 1963). Here, coal of the Upper Cretaceous Crevasse Canyon Formation crops out in several thin and discontinuous beds with strike lengths generally less than a kilometer (Osburn, 1983). The Crevasse Canyon Formation is comprised of a sequence in which fine-grained sediments predominate, with associated coals and fluvial sandstones. This formation records shoreward sedimentation along a regressing seaway and the deposits show a strong fluvial influence.

The coal, ranked as high-volatile A bituminous, is of excellent quality, and has all been mined underground by the room and pillar method. The mines are in a state of decay due to decades of neglect, with collapsed tunnels and rotting timbers, so consequently there are very few exposures one can study. One exception is the Manilla Mine where two beds are exposed at the mine entrance. The beds, which strike N45W and dip 21 SW, are underlain by shales and mudstone and overlain by mudstone capped with sandstone. Upper bed thickness is about 0.5 meters, and that of the lower bed about 1.8 meters, both beds being slightly variable in thickness. Approximately 0.8 meters of poorly consolidated sandy mudstone, which lacks any obvious jointing, separates the two beds. The coal is exposed for about 15.0 meters before caved-in areas of the mine make it inaccessable.

Because the mines in the Carthage area have not been worked for some time, deterioration of the exposed face has occurred due to the elements. This restricted the taking of data to only the most prominent set of cleats, the term referring to a system of joints in a coal seam. In general, the cleating in the coal is in only fair condition;

Table 2. Summary of joint data from field areas.

Location/Lithology	Bed Thickness (d, meters)	Joint Density (j, #/meter)	Joint Spacing (s, meters)
Manilla Mine Socorro Co., NM			
Carthage Coal	0.88	34.48	0.029
Mesa Verde Sandstone	1.22	4.35	0.230
Trinity Mine Scott Co., VA			
Cove Creek Coal	0.10	62.51	0.016
Middesboro Sandstone	2.19	1.85	0.540
Gateway Mine San Juan Co., NM			
Fruitland Coal #2	0.102	10.53	0.095
Fruitland Coal #5	0.152	7.81	0.128
Tres Hermanos Sandstone Socorro Co., NM			
Upper Sandstone	1.18	Set #1 6.67	0.150
		Set #2 2.86	0.350
		Set #3 5.00	0.200
Lower Sandstone	1.02	Set #1 6.67	0.150
		Set #2 2.56	0.390
		Set #3 4.54	0.220

individual cleats do not always continue all the way through the coal, but often become indistinct and difficult to follow. The cleat surfaces vary in shape from planar to undulating.

Data on joint orientation, frequency, and characteristics were also taken on outcrops of Mesa Verde Sandstone located about 70 meters from the mine entrance, the closest well-exposed area to sample. Readings taken on the upper surface (plan view) of the bed for three joint sets show fairly uniform densities. The joints display a tendency to be curvilinear and to cluster in zones where the joint density can increase several fold. Joint direction is quite variable, as is the length of fracture trace. Almost all joints are closed, with but a few scattered specimens showing calcite and gypsum infillings. Table 2 summarizes the data collected on both coal and sandstone at the Manilla Mine.

Cove Creek Seam - Trinity Mine

The Trinity Mine is located in Scott County, Virginia in the southwestern extremity of the state (see Fig 16). Here, continental coal-bearing rocks of Early Pennsylvanian age (Lee Formation) crop out on the southeastern limb of the Powell Valley anticline. Strata of this northeast plunging structure dip between 6° and 20° to the southeast. Structurally, there are seven major overthrust faults in the surrounding area which cut the sedimentary sequence, resulting in subparallel belts which display similar geology for many miles along strike. The lithofacies, stratigraphic thicknesses and structural style change from one fault belt to the next, however (Miller, 1974).

The Lee Formation is comprised of two thick tongues of medium-to-coarse grained sandstone that is partly conglomeratic, separated by about 180 meters of a coal-bearing sequence of interbedded shale, siltstone,

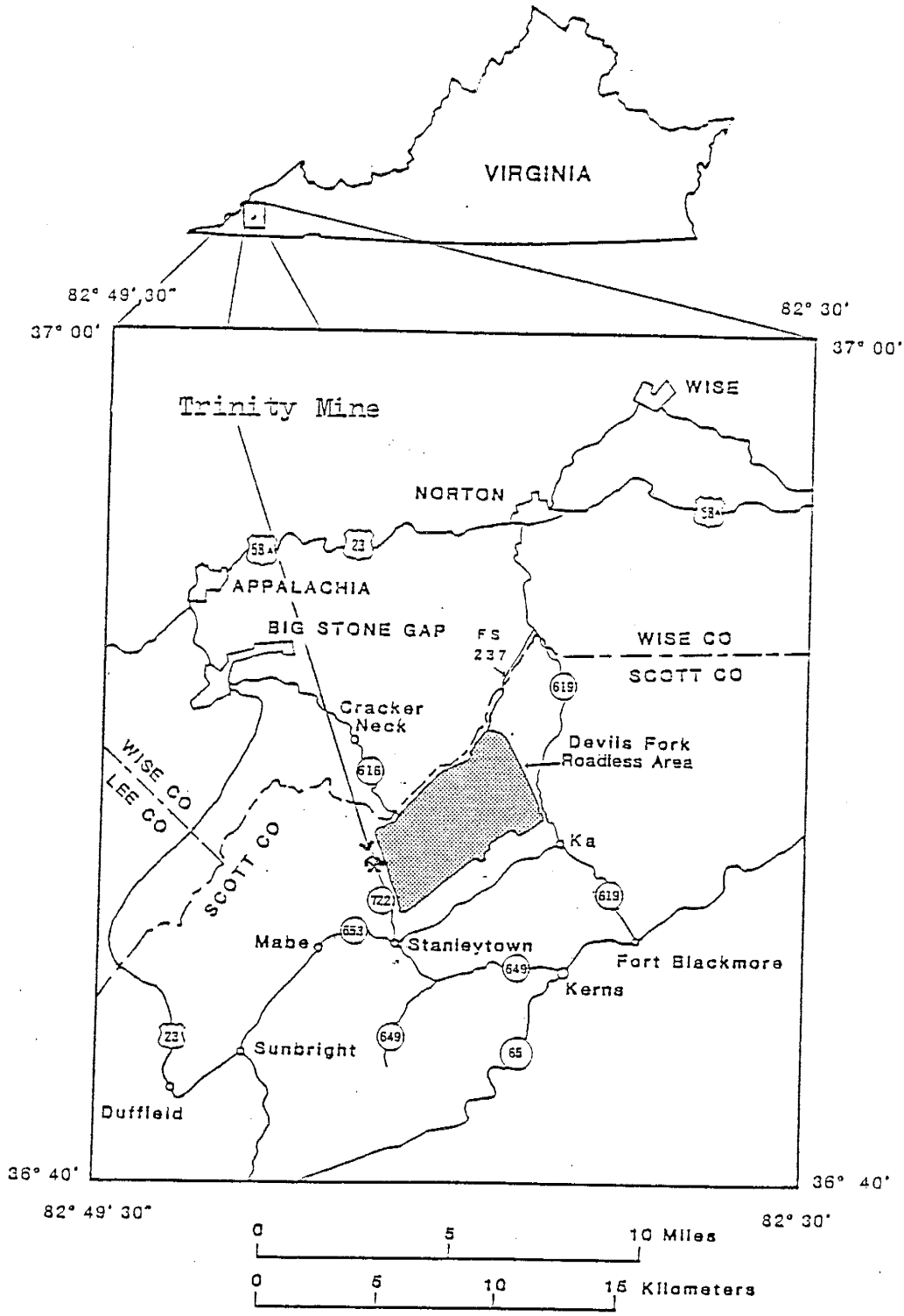

Figure 16. Index map showing location of the Trinity Mine, Scott Co., VA. (after Englund et al., 1983.)

fine-grained sandstone and underclay, totalling more than 330 meters in all (Englund et al., 1983). The principal coal bed of this sequence, the Cove Creek, is ranked as high-volatile A bituminous, and has a thickness of 1.0 to 1.5 meters. It is this bed that is being worked at the Trinity Mine via drift entries and the room and pillar method. The coal is overlain by a bed of massive, fine-grained, well-cemented, cross-bedded sandstone. Whereas cleat in the coal is perpendicular to bedding, well-developed, and easily readable, fractures in the overlying sandstone display a tendency to follow the curvature of the cross-bedding surfaces and are not always distinct. The data collected at the site are presented in Table 2, page 43.

Gateway Mine - Bisti Fruitland Field

Field studies were conducted at the Gateway Mine (operated by Sunbelt Mining) located about 50 kilometers south of Farmington, New Mexico (see Fig. 15), where coals of the Fruitland Formation (Upper Cretaceous) are being worked. The fluviatile, lagoonal, and nearshore marine origin of this formation resulted in great variation in lithology in short distances, both laterally and vertically, and a wide range of clastic rock types. Here the Fruitland is a sequence of highly lenticular nonmarine claystones, silty and sandy shales, and soft cross-bedded sandstones, with seams of coal. It is overlain by the Kirtland Shale, of similar lithology but lacking coal, and is underlain by the Picture Cliffs Sandstone, marine sediments of Late Cretaceous age.

From a physiographical standpoint, the Bisti Fruitland field lies on a broad, gently northward dipping plain which is dissected by tributaries of the Chaco River. Within the Bisti field the economically valuable coals are found in the lower 50 meters of the Fruitland

Formation (Shoemaker et al., 1971). The coal is of subbituminous rank A, with a mild decrease in quality (owing to increase in ash content) as one proceeds from north to south. The ash content (9.0 - 12.0%) is present as thin layers (0.5 - 5.0 cm) or intimately mingled with the coal itself (Fig. 17). Observations of the relation of cleats infilled with volcanic ash to cleats lacking fillings suggest that the first set to form had an extensional stress axis oriented at N33W, a direction possibly associated with movement of the Uncompahgre Uplift to the north. Two coal seams, referred to as seam #2 and seam #5 for the lower and upper beds, respectively, are currently being strip-mined. These beds, approximately 2 meters thick in total, are separated by about 20.0 meters of poorly consolidated, light gray, muddy sandstone. Another similar muddy sandstone overlies the upper coal seam #5 and is about 6.0 meters thick (Fig. 18). The jointing data obtained from these two coal seam/overlying muddy sandstone sequences are contained in Table 2.

Tres Hermanos Sandstone - Carthage Area

The Tres Hermanos Formation, like the Crevasse Canyon, is composed of sediments which record sedimentation shoreward of a regressing seaway. Beds of sandstone showing well-developed jointing are found in the Carthage area, about 1.0 kilometer further east of the Manilla mine study site (see Fig. 15). Roadcuts on U.S. 380 give good cross-sectional views and exposures about 100 meters north of the road provide both section and plan views.

The sandstone sequence selected for this study consisted of two medium-to-fine grained, well-sorted, well-cemented beds, hereafter referred to as the upper and lower beds. The attitude of these

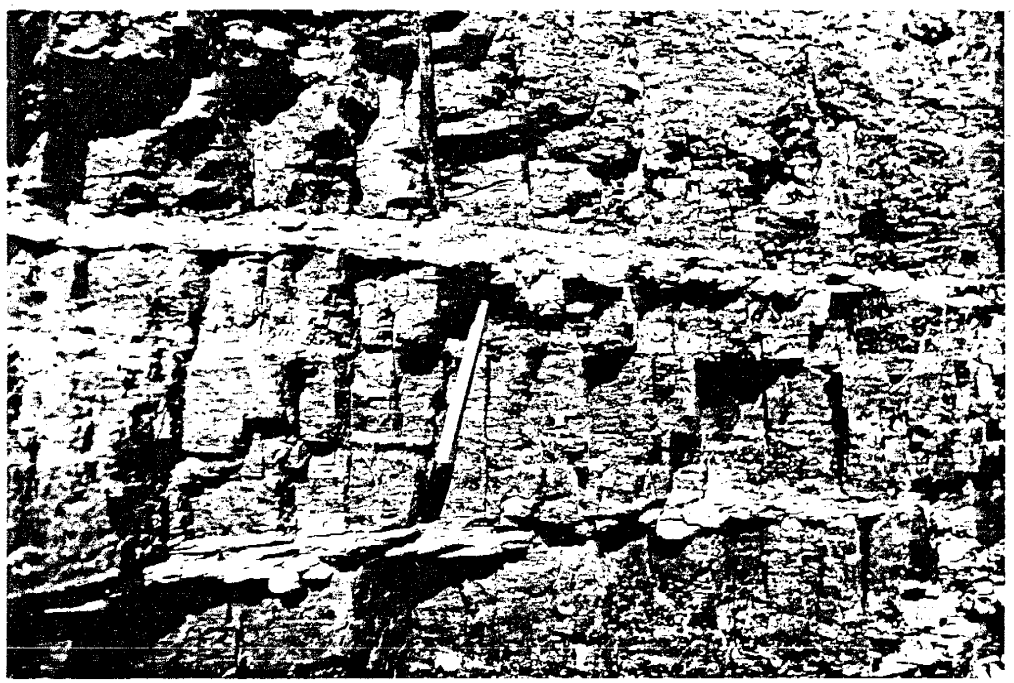

Figure 17. Volcanic ash is present as continuous layers and intimately mingled with the coal of seam #5, Gateway Mine.

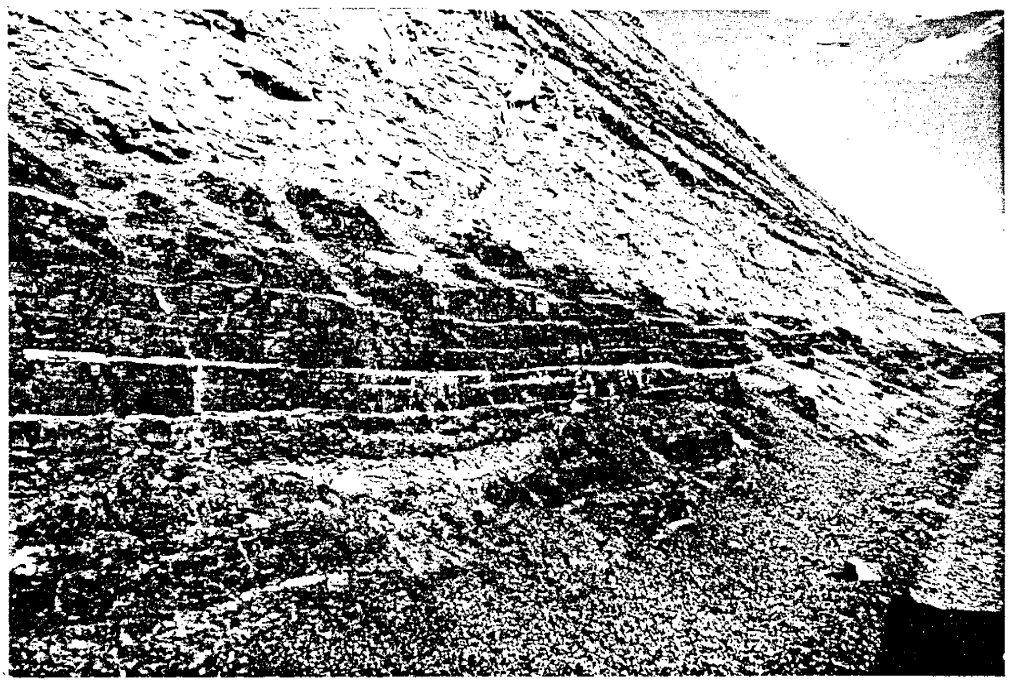

Figure 18. View of seam #5, Gateway Mine, showing overlying muddy sandstone and the continuous nature of ash layers within the coal. Notice the lack of discernible jointing within the sandstone.

sediments was measured as having a strike of N7W and a dip of 13° E. Plan views of the upper bed (Fig. 19) display a well-developed, regularly spaced, pattern of fractures which show little variation in direction. No signs of relative dating of the joint sets are obvious, for in general, the joints lack infillings. Average bed thicknesses are 1.18 m and 1.02 m for the upper and lower beds respectively, and both beds exhibit some cross-bedding. Many of the joints penetrate the entire section of sediments with only minor departures in direction. Jointing information from both beds was recorded in 10 meter sections on three joint sets having average directions of N77W, N35W and N45E (see Table 2).

EXPERIMENTAL DETERMINATION OF ELASTIC PROPERTIES

Having established the required theoretical foundations and the actual joint densities of the sediments in our study areas, we now need to determine the values of the elastic constants of the rocks so that theoretical joint densities may be calculated. This was accomplished by subjecting the various rock types to a number of tests employed in experimental rock mechanics. In the sections that follow, a brief explanation of the theory of each technique will be given, along with a synopsis of sample preparation and experimental procedures.

Tensile Strength - the Brazilian Test

As the name suggests, the Brazilian test originated in South America (Hondros, 1959). In this test, a solid circular disk is compressed to failure across a diameter. The formation of extension fractures along a diameter which is subject to compression and tension

Figure 19. Plan view of joint system in upper Tres Hermanos Sandstone.

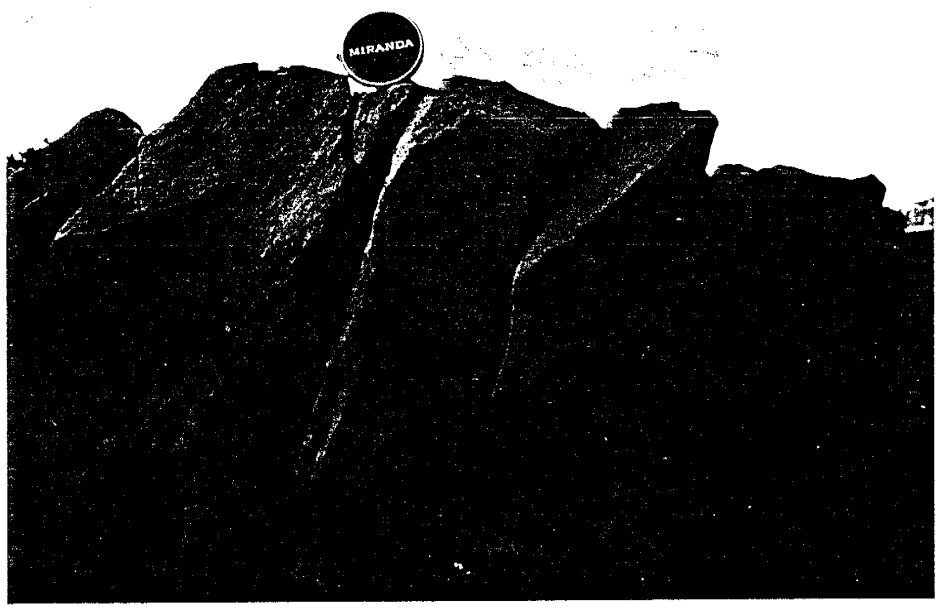

Figure 20. Cross-sectional view of joint system in upper Tres Hermanos Sandstone.

is of prime interest because these stresses probably more closely approximate those obtained when extensional fractures occur in the field than does uniaxial tension (Jaeger, 1967). The justification for this test is based on the experimental fact that most rocks in biaxial stress fields will fail in tension at their uniaxial tensile strength when one of the principal stresses is tensile and the other principal stress is compressive with a magnitude not exceeding three times that of the principal tensile stress (Brown, 1981).

The stress distribution in a thin disk loaded by uniform pressure applied radially over a short strip of the circumference at each end of the diameter was analysed by Hondros, assuming that the material is homogeneous, isotropic and linearly elastic (Figs. 21a, 21b). It was shown that there exists across this loaded diameter a principal tensile stress of constant magnitude which tends to pull the disk in half along this line. The magnitude of this stress T is given by

$$T = \frac{2F}{\pi D t} \qquad (22)$$

where F is the applied load, and t and D are the thickness and diameter of the disk, respectively (Hondros, 1959).

Sample Preparation and Experimental Procedure - Tensile Strength

Specimens may be either thin disks cut from cylindrical cores or rectangular prisms fashioned from irregularly shaped specimens. For the purposes of this study, best results were obtained for sandstone and coal by using cylindrical disks and rectangular prisms, respectively. The test specimens obtained by coring or slabbing the desired materal are then cut on a trim saw. Care is taken to insure that the surfaces are free from obvious tool marks and that any irregularities across the specimen do not exceed 0.25 mm. The end faces should be as flat as

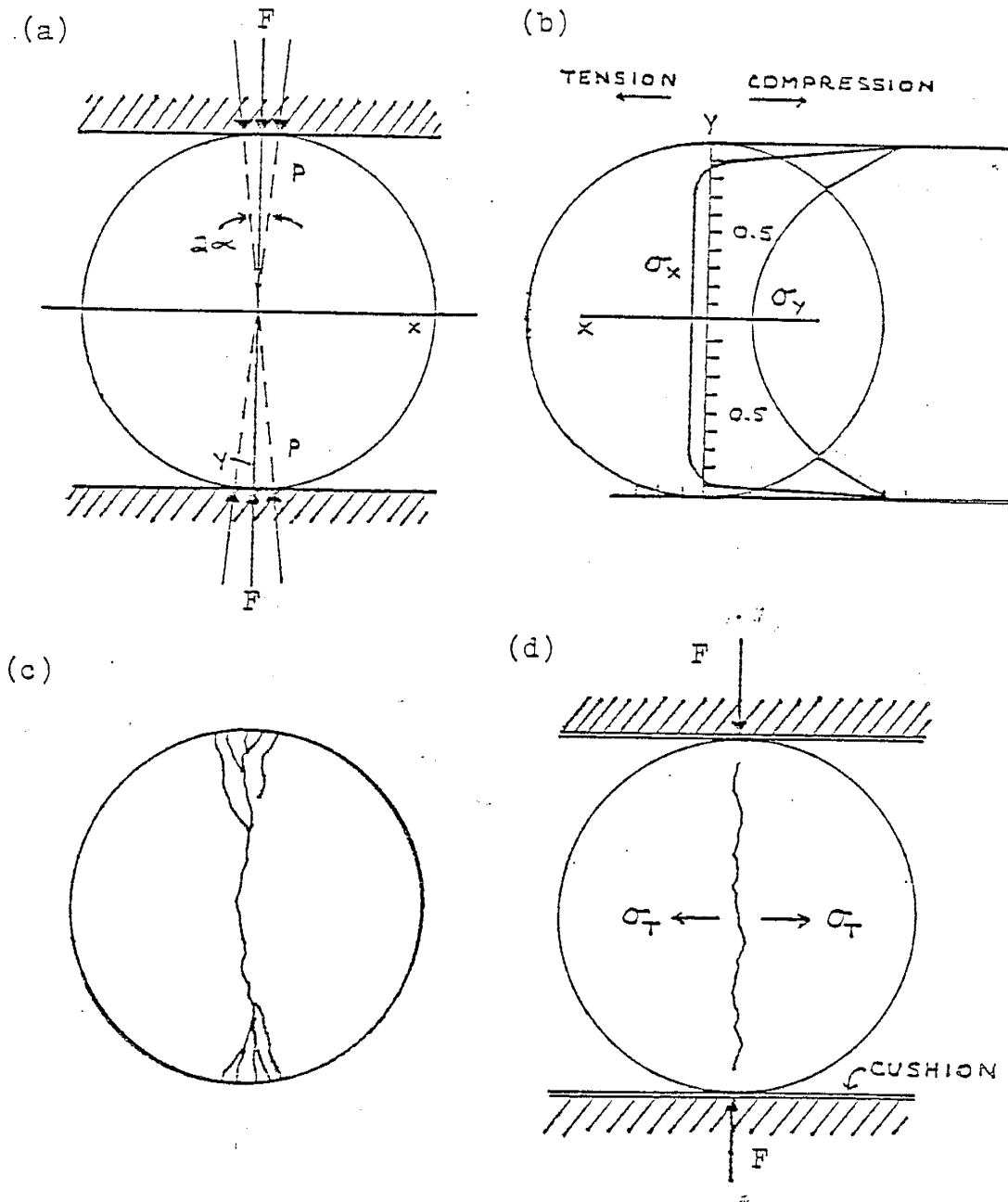

Figure 21. (a) Disk compressed by a diametral load due to uniform pressure over arc 2α.
(b) Stresses along loaded diameter of disk.
(c) Typical fractures resulting from (a).
(d) Modifying effect of inserting cushions between disk and platens.

possible (0.25mm), and in the case of rectangular prisms, ms, square and parallel to within 1°. The ratio of specimen thickness to diameter was from 0.5 to 1.0 with all specimens having a diameter of 2.50 ± 0.02 centimeters.

Orientation of the axis of loading with respect to any specimen anisotropy, such as bedding planes, foliation, and inclusions, is also noted. Load on the specimen was applied at a constant rate (200 N/s) which resulted in failure in 15-30 seconds for the weakest rocks. The testing machine is fitted with a chart recorder so that the load for primary fracture can be precisely determined (in some cases load will continue to increase after failure as the split specimen is still bearing load).

For the Brazilian test to be valid, disk failure should take place with the developement of a vertical crack initiated from the center of the specimen, which proceeds upward and downward along the loading axis YY'. In practice, however, these conditions are seldom realized, for appreciable tangential stresses are developed in the region of contact which can modify the local stress distribution. Their effect is to create a horizontal compressive stress which results in the formation of small shear wedges (Fig. 21c). This condition was avoided by inserting thin sheets of cardboard between the loading platens and the disk (Mellor and Hawkes, 1971)(Fig. 21d). The thickness of the cardboard platen cushions should be about 0.01 D where D is the specimen's diameter. Employing this modification has the effect of dissipating the shearing stresses that are usually generated along the loading surfaces. In this case, cracking does not begin at the platen contact but often starts instead from the center and terminates at about one-tenth of the

diameter from the boundary, thus proving conclusively that the test is indeed determining a true tensile strength.

In the event that the specimen failed due to shearing, as evidenced by cracks radiating out from a crushed zone below the loading points and the absence of any cracks in the center of the disk, the test was considered invalid.

Ultrasonic Pulse Velocity Determinations

In this method a mechanical pulse in imparted to the specimen by placing it in physical contact between two piezoelectric transducers; one acts as a driver, and the other acts as a receiver. It is necessary to use different piezoelectric transducers for the generation of compressional and shear waves. Small piezoelectric ceramic cylinders (0.64 cm diameter, 0.64 cm length) of barium titanate acting in the thickness mode will transmit and receive compressional waves. In order for shear waves to be transmitted and received, it is required that these cylinders be cut so that the applied voltage generates shear waves.

A pulse generator supplies a short-duration electrical pulse to the driver which converts it into a mechanical or impact wave and transmits this energy to the specimen. After traveling through the specimen, the pulse is picked up by the receiving transducer, reconverted into an electrical signal and displayed on an oscilloscope (see Fig. 22). From the oscilloscope setting the transit time can be determined and this in turn allows us to calculate the velocity of the wave. The elastic constants are obtained from the density and the velocities, using the following expressions derived from the theory of elasticity for homogeneous, isotropic solids (Lama, 1978).

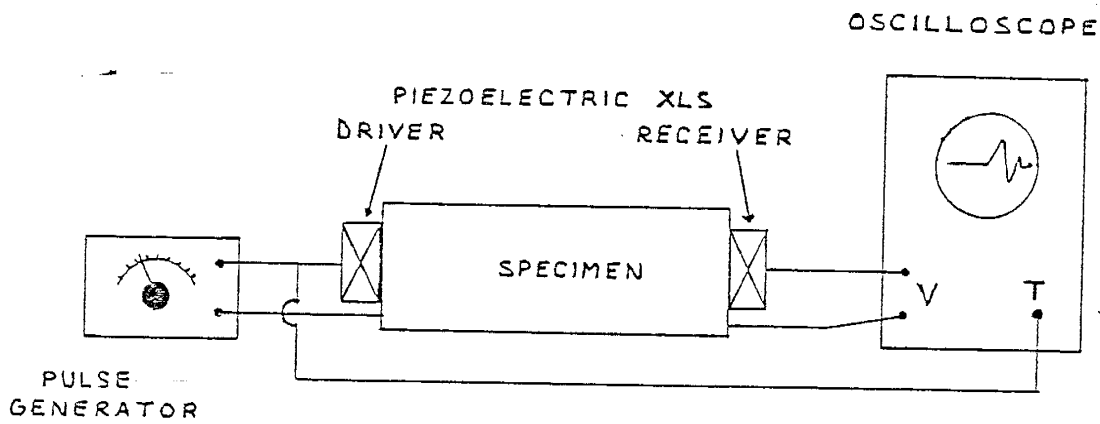

Figure 22. Schematic diagram of apparatus used in determinations of elastic properties by the ultrasonic pulse method. (after Lama and Vutukuri, 1978.)

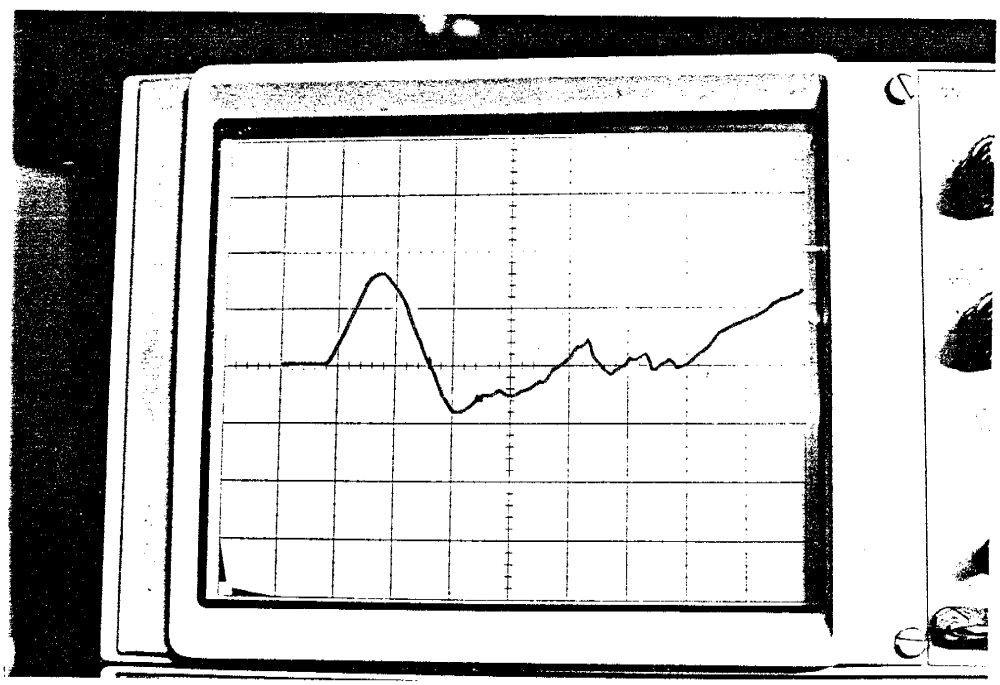

Figure 23. Compressional waveform recorded for sample #1 Manilla Mine coal (scale - 20 microseconds per centimeter; delay time = 15 microseconds).

$$E = \frac{\rho V_s^2 (3 V_p^2 - 4 V_s^2)}{V_p^2 - V_s^2} \quad (23)$$

$$G = \rho V_s^2 \quad (24)$$

$$\nu = \frac{V_p^2 - 2 V_s^2}{2 (V_p^2 - V_s^2)} \quad (25)$$

where E = modulus of elasticity, Pa
G = modulus of rigidity, Pa
ν = Poisson's ratio
ρ = density, kg/m_3
V_p = longitudinal infinite medium velocity, m/s
V_s = shear velocity, m/s

In order to use equations 23, 24, and 25, the rock specimen must be isotropic or possess only a small degree of anistropy. An estimate of the degree of anisotropy of the rock is obtained by measuring the compressional wave velocity in three orthogonal directions.

Sample Preparation and Experimental Procedure - Ultrasonic Pulse

A steel cylinder (length 52.50 mm) was used as a standard and yielded compressional and shear wave velocities of 5.83 and 3.50 km/sec, respectively. These values were repeatable and compare well with values reported in the Handbook of Chemistry and Physics, 63rd edition. Tests were performed at atmospheric pressure and record first major pulse in waveform so as avoid effects due to long-wavelength standing waves.

Specimens may be either cylindrical or prismatic, but must possess two parallel, flat surfaces between which the velocity is to be measured. Measurements are made across the shortest dimension of the specimen so that V_s results will not be compromised by shear waves being converted to compressional waves. Care should be exercised during the drilling, handling, sawing and lapping of the test specimens to minimize mechanical damage. The size of the specimens can vary somewhat (1.0 -

5.0 cm), the primary consideration being to select a sample size for which a strong, easily readable waveform (Fig. 23) is displayed on the oscilloscope. To provide good coupling between the specimen and transducers, the surface area of contact should be sufficiently plane. In the case of granular materials such as sandstone, it is desireable to employ a layer of electrical tape to improve the efficiency of energy transfer. Significant attenuation of the pulse may occur due to randomly oriented discontinuities. Factors of internal structure such as porosity, inclusions and grain size can limit the application of the technique.

Uniaxial Compression

The uniaxial compression test was used to obtain static values of Young's modulus of the materials collected at the study sites for the purpose of comparison with dynamically determined values. In this test, right circular cylinders are compressed parallel to their longitudinal axis in a compression tester. Loading and deformation are monitored by a load cell and LVDT (linear variable differential transformer; see Appendix D), respectively, and both are displayed on a chart recorder (Fig. 24).

In uniaxial compression the specimen is uniformly loaded in one direction and free to move in the other two; $\sigma_1 \neq 0$, $\sigma_2 = \sigma_3 = 0$. There is a contraction in the direction of σ_1, and an expansion $e_2 = e_3$ in the orthogonal directions. Figure 25 illustrates a plot of axial stress versus axial strain showing typical behavior for rock materials from zero stress up to the ultimate strength. This complete curve gives the best description of the deformational behavior of rocks having non-linear stress-strain behavior at low and high stress levels. Young's

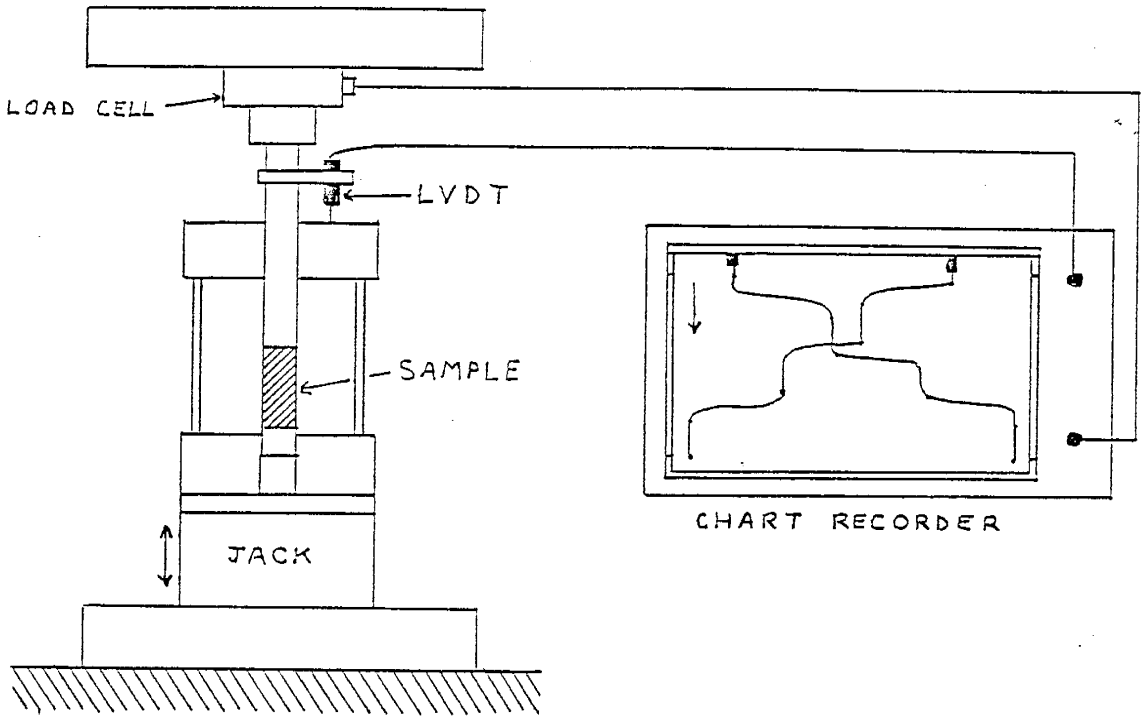

Figure 24. Schematic diagram of compression tester and devices used to record load and deformation of specimen in uniaxial compression.

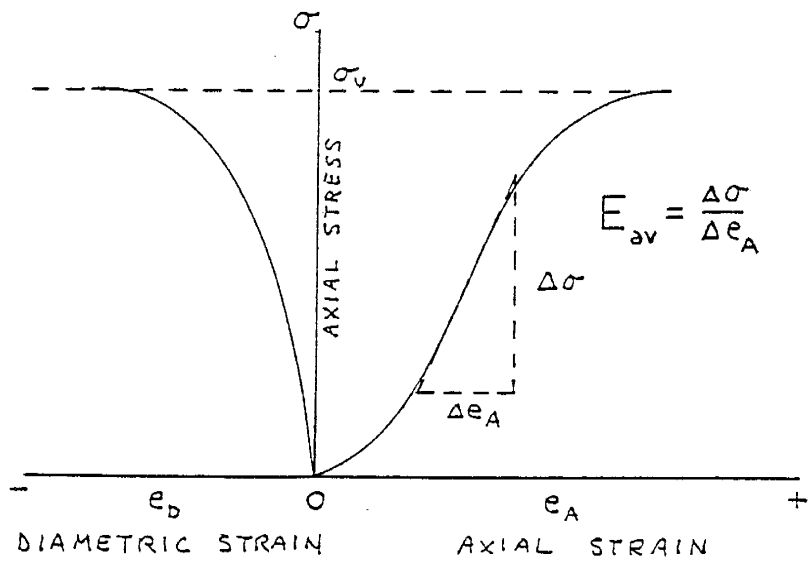

Figure 25. Graphical presentation of axial and diametric stress/strain curves showing method for calculating the average Young's modulus.

modulus, E, is determined from the average slope of the straight line portion of the axial stress versus axial strain curve.

Sample Preparation and Experimental Procedure - Uniaxial Compression

Test specimens were right circular cylinders having a height to diameter ratio of 2.5-3.0, and a diameter of 2.50 $\pm$ 0.02 cm. The ends of the specimens were lapped flat to 0.05 mm and did not depart from perpendicularity to the axis of the specimen by more than 0.01 radian. The sides of the specimens were smooth and free of abrupt irregularites and straight to within 1.0 mm over the full length of the specimen. Diameters of the test specimens were measured to the nearest 0.1 mm by averaging two diameters measured at right angles to each other at about the upper-height, mid-height, and lower height of the specimen. This average diameter is used for calculating the cross-sectional area. Specimen height is determined to the nearest 1.0 mm.

The load to the specimens was applied at a constant stress rate such that failure occurred within 5-10 minutes of loading. Loading stress rates were within the limits of 0.5 - 1.0 MPa/s as determined from strip chart recordings. Uniaxial compressive strength, C_o, of the specimen can be calculated by dividing the maximum load, F_{max}, carried by the specimen during the test, by the original cross-sectional area ($C_o = F_{max}/\text{area}$). Not all test specimens were compressed to failure; some were stressed to only moderate levels so that they could later be used in tensile strength experiments.

The LVDT was calibrated by using a traveling microscope and chart recorder. Displacement of the LVDT produced movement on the chart recorder which was noted and checked via the microscope. In this manner, consistent, reproducible results were obtained. Then, knowing

the response of the chart recorder, the load cell was calibrated by a separate pressure measuring device on the hydraulic pump. Response of both the LVDT and the load cell are in good agreement with published data on Young's modulus when standard steel cylinders were tested.

ADDITIONAL METHODS

The following additional methods and experimental techniques were used to obtain information that was useful in solving problems concerned with determination of the required elastic constants and mechanisms of failure.

Petrographic Analysis of Thin-Sections

Results of tests performed on samples of Mesa Verde sandstone to determine the tensile strength of the material displayed a considerable degree of experimental scatter. To obtain a better idea of the reasons for the observed scatter, thin-sections of a number of samples (10) were made from cores used in the tensile strength determinations and a point-count analysis was performed.

The analysis showed that the samples could be separated into two groups: those cemented with calcite and those cemented with chert. The group cemented with calcite consistently displayed smaller values of tensile strength (average T = -0.74 MPa) compared to those cemented with chert (average T = -2.57 MPa). All samples showed similar grain size (average grain diameter = 1.4×10^{-1} mm), and similar compositional ratios of quartz, chert, amount of cementing material, and opaques and minor constituents (plagioclase and muscovite). For these reasons it is believed that the observed scatter of the tensile strength values can be

considered as due to differences in the physical properties of the cementing material.

Shear Strength Determinations

A method for determining the shear strength of rock was also designed and constructed. A cube, rectangular prism or cylindrically shaped specimen is placed between two beveled dies set up in a compression testing machine and sheared along a predetermined plane. A set of rollers is placed between the bottom die and platen so as to allow a horizontal displacement. In the 45-degree dies (Figs. 26, 27), the loading device transfers the vertical load to the rock specimen, automatically splitting it into components normal to and parallel to the shearing plane. For using cylindrical specimens obtained by coring, special grooved inserts are employed (Fig. 27).

The method is particularly simple, and test results show little scatter. Knowledge of the shear strength S is used as a check on the values obtained for the tensile strength T, and aids in the construction of the Mohr envelope.

Fracture Surface Profiles

The surface morphology of joints is the primary observational criterion for distinguishing shear joints as Coulomb fractures or transitional - tensile fractures, so a method was developed by which the surface roughness of joints may be evaluated. Accurate profiles illustrating the morphology of joint surfaces are produced by attaching an LVDT (linear variable differential transformer) to a traveling microscrope adapted for this purpose (Figure 28). As the electrically driven microscope carriage traverses the joint surface, the LVDT records

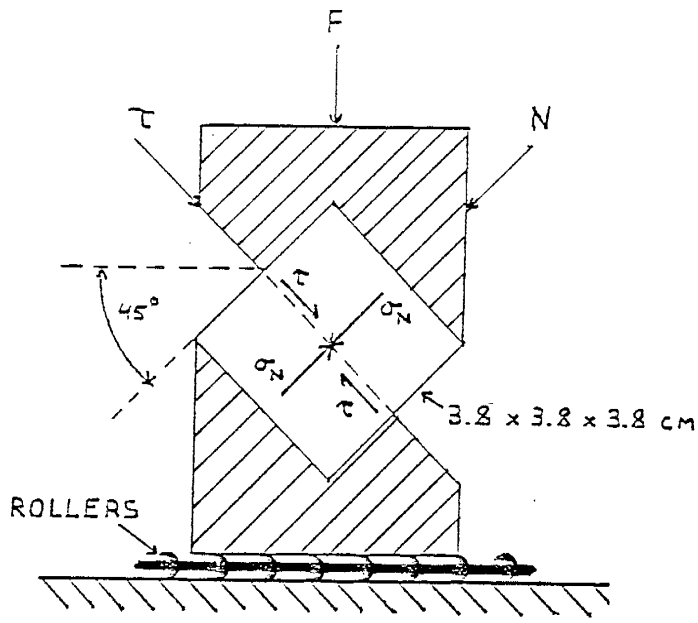

Figure 26 . Diagram showing resolution of forces resulting from the application of load to specimen being sheared in beveled dies. (after Jumikis, 1979.)

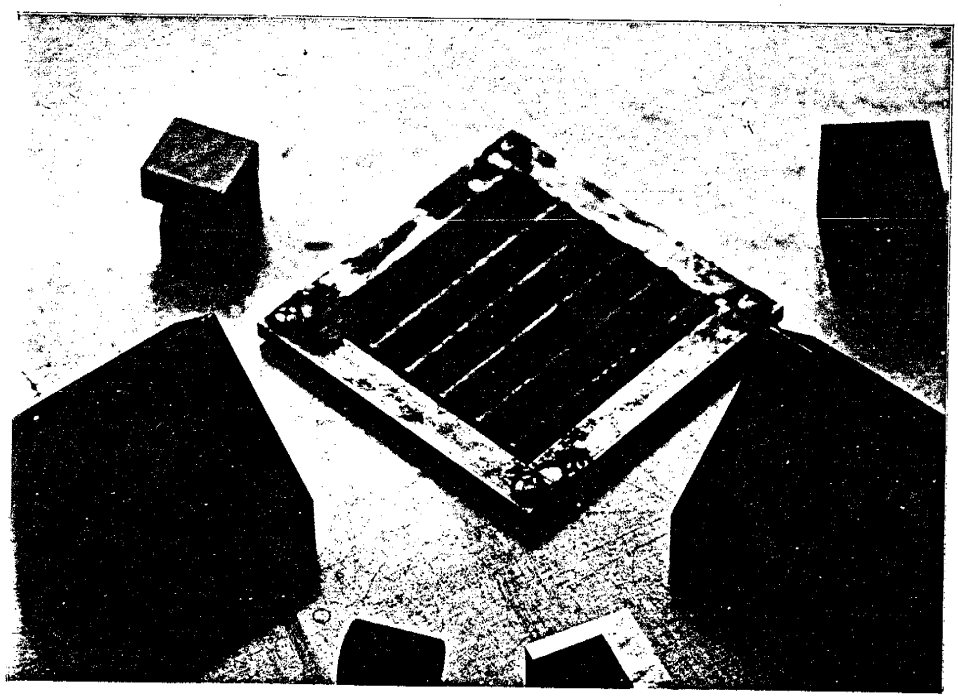

Figure 27 . Photograph of beveled dies, grooved inserts, roller assembly, and typical samples (both sheared and unsheared) used in shear strength determinations.

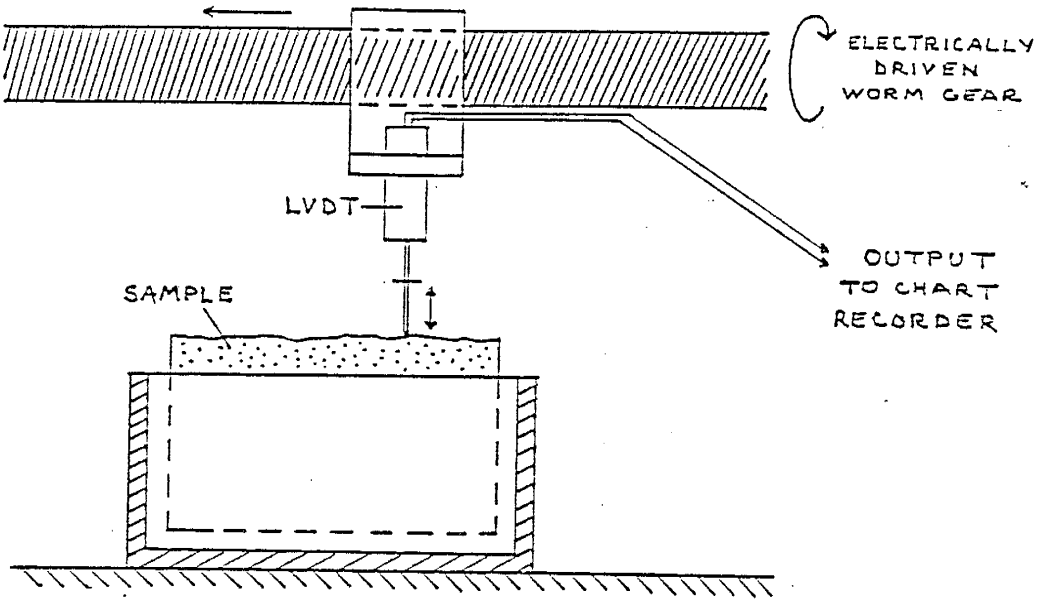

Figure 28. Schematic diagram of device used to produce profiles illustrating the morphology of joint surfaces.

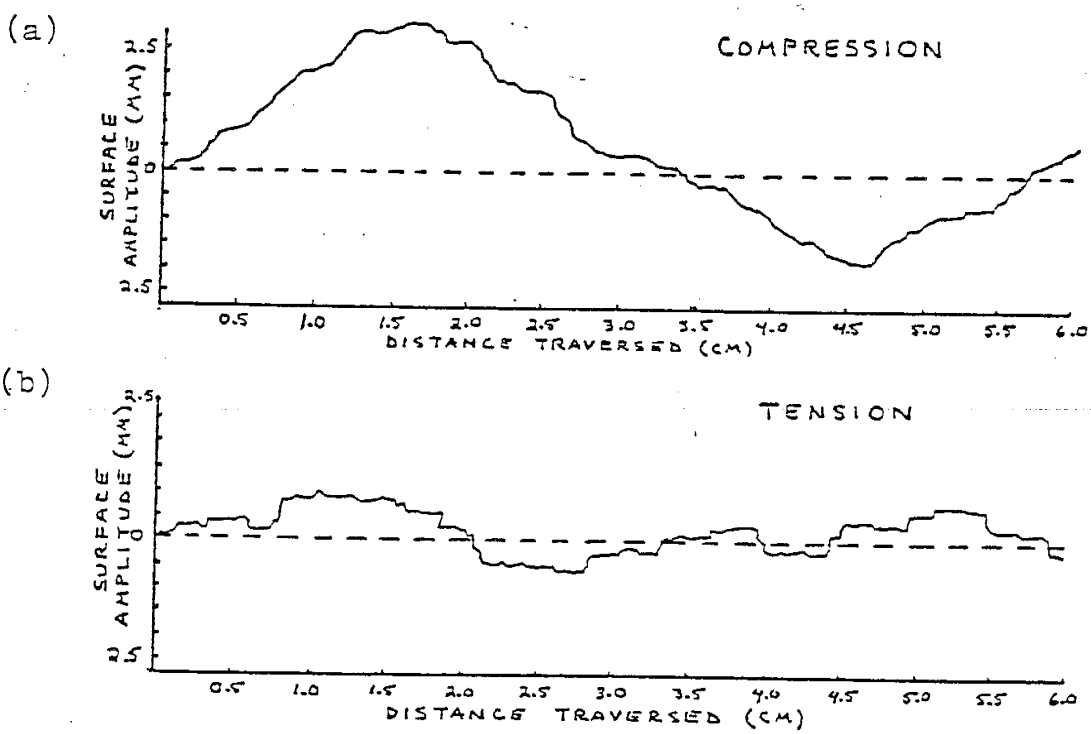

Figure 29. Profiles obtained from experimentally produced joint surfaces in Mesa Verde sandstone.
(a) Compressional profile.
(b) Tensional profile.

changes in the surface configuration which are displayed on a chart recorder. Magnifications of approximately 200 : 1 are obtained and surface asperities as small as 100 microns can routinely be observed.

These "profilograms" show that within any one rock type there are recognizable quantitative and qualitative differences in the character of joint surfaces formed in tension versus joints produced by shearing (Weissback, 1978). Figure 29 shows typical profiles recorded for compressional joints and tensile joints produced experimentally in Mesa Verde Sandstone. The compressional profile is characterized by broad, relatively smooth deflections of large surface amplitude and wavelength. The action of the two rock surfaces moving past one another creates the smoothness and the initial mechanisms of fracture are responsible for the amplitude and wavelength effects. In comparison, fracture surfaces produced in tension exhibit abrupt changes in amplitude and direction distinctive of brittle materials that have been pulled apart; none of the asperities have been smoothed over and the total surface amplitude remains relatively small. Profiles such as these were used to decide whether some specimens in tensile strength tests indeed failed in tension.

We can now present a table summarizing the elastic properties obtained by the use of both the experimental and additional methods for the various lithologies at each particular study site. Table 3 gives the values obtained, the methods employed, and limits of accuracy. Data for the specific tests and lithologies are collected in Appendix E.

COMPARISON OF OBSERVED AND THEORETICAL JOINT SPACINGS

Using the information contained in Table 2 on observed joint spacing and bed thickness, together with the values of the elastic

Table 3. Summary of elastic properties.

Lithology	E Young's Mod. (GPa)	G Shear Mod. (GPa)	T Tensile Strength (MPa)	Density (g/cm^3)
Carthage Coal	3.43	1.73	-1.44 ± 0.26	1.22 ± 0.02
Mesa Verde SS	20.75 (21.96 ± 4.91)*	9.75	-3.16 ± 1.71	2.39 ± 0.02
Cove Creek Coal	12.37	6.19	-2.07 ± 0.56	1.28 ± 0.02
Middesboro SS	37.36 (37.30 ± 5.54)*	16.99	-7.68 ± 2.92	2.40 ± 0.02
Fruitland Coal #2	3.33	1.49	-1.65 ± 0.49	1.19 ± 0.02
Muddy SS #2	5.54	3.12	---------- +	1.96 ± 0.02
Fruitland Coal #5	2.76	1.31	-1.06 ± 0.77	1.24 ± 0.02
Tres Hermanos SS				
Upper bed	33.95 (34.58 ± 7.59)*	16.76	-7.50 ± 2.50	2.20 ± 0.02
Lower bed	43.84 (40.12 ± 6.67)*	20.20	-10.74 ± 2.76	2.29 ± 0.02

* Values of E and G were calculated from V_p and V_s; those values of E which appear in parentheses were obtained by uniaxial compression.

+ Specimens displayed ductile behavior under diametral compression.

Table 3. Summary of elastic properties. (continued)

Lithology	V_p Compressional Velocity (km/sec)	V_s Shear Velocity (km/sec)	S Shear Strength (MPa)
Carthage Coal	1.68 ± 0.07	1.19 ± 0.04	---------- **
Mesa Verde SS	2.96 ± 0.15	2.02 ± 0.10	5.64 ± 1.54
Cove Creek Coal	3.11 ± 0.11	2.20 ± 0.07	5.86 ± 1.81
Middesboro SS	3.99 ± 0.36	2.66 ± 0.18	15.04 ± 1.74
Fruitland Coal #2	1.70 ± 0.09	1.12 ± 0.02	---------- **
Muddy SS #2	1.70 ± 0.12	1.26 ± 0.11	---------- **
Fruitland Coal #5	1.50 ± 0.08	1.03 ± 0.05	---------- **
Tres Hermanos SS			
Upper bed	3.93 ± 0.24	2.76 ± 0.16	12.96 ± 3.25
Lower bed	4.41 ± 0.08	2.97 ± 0.05	20.56 ± 4.99

** Specimens displayed splintery or ductile behavior rendering unreliable results.

constants found in Table 3, we can now proceed to calculate joint spacings expected on the basis of theory and compare them to the actual values observed in the field. In the case of joint data actually recorded in the field, this will simply be S_{obs}, which is given in Table 2. The situation involving the theoretical joint spacing requires some calculation, however.

Earlier, in equation 16 (page 22), an expression was given which described the interjoint spacing s in terms of the bed thickness, the elastic constants E and G_n, and the degree of tectonic deformation as:

$$s = d\left(\frac{E}{G_n}\right)^{1/2} \cosh^{-1}\left(\frac{e_2}{e_2 - e_1}\right) \qquad (16)$$

We will now use this expression to obtain the theoretical results we require. Values for d, E, and G may be taken from the tables, and e_1 and e_2 are found in the following manner.

The strain required to produce the first joint, e_1, can be determined from the relationship $e = \sigma/E$. At failure this may be written as $e_1 = T/E$. Taking the known values of T and E from Table 3, e_1 may be readily calculated. Hobbs (1967) provides an expression for the ratio e_1/e_2 as

$$\frac{e_1}{e_2} = 1 - \frac{1}{\cosh\left[\frac{s}{d}\left(\frac{G_n}{E}\right)^{1/2}\right]} \qquad (26)$$

and solving for e_2, the final state of strain, we obtain:

$$e_2 = e_1 \Big/ \left(1 - \frac{1}{\cosh\left[\frac{s}{d}\left(\frac{G_n}{E}\right)^{1/2}\right]}\right) \qquad (27)$$

The assumption is made that both beds of a particular study sequence undergo equal amounts of strain, which we will call e_2 of the

system. In order to standardize our treatment of the data, this e_2 will be calculated in terms of the stronger of the two lithologies as determined from their values of tensile strength. For example, e_2 for the Manilla Mine study would be calculated by using e_1, s, d, and E of the sandstone, the stronger bed, and G of the coal in equation (27).

In order to obtain a theoretical joint spacing for the Manilla Mine, we would now use the computed value of e_2 for the system in equation (16), along with values of e_1, d, and E for the coal and G of the sandstone. This yields an s_{theor} value for the coal, the weaker of the two lithologies, which can now be compared to s_{obs}, the observed joint spacing in the coal. Thus our final s_{obs}/s_{theor} ratio will be expressed in terms of the weaker, more jointed lithology.

Table 4 lists the calculated values of e_1, e_2, the deformation factor $\cosh^{-1}(e_2/e_2-e_1)$, s_{obs}, s_{theor} and the s_{obs}/s_{theor} ratio. This s_{obs}/s_{theor} ratio is the object of all our investigations, so the results will need to be considered in detail.

Discussion of s_{obs}/s_{theor} Results

Figure 30 is a logarithimic plot of the theoretically predicted joint spacing vs. observed joint spacing for the data presented in Table 4. Included in the figure is a reference line signifying perfect correlation between theory and observations. Those points that plot above this line represent studies in which more joints were observed than are predicted from theory. Conversely, points plotting below the line correspond to observations of joint densities falling short of predictions. We will first take a look at the reasons behind the large error bars on the s_{theor} values, and then consider the linear trend of the data.

Error is introduced due to inaccuracies in the determination of the

Table 4. Summary of strain values and joint spacing ratios.

Location/Lithology	e_1	e_2	$\cosh^{-1}(e_2/e_2-e_1)$
Manilla Mine			
Carthage Coal	4.20×10^{-4} (W)	1.03×10^{-1}	9.05×10^{-2}
Mesa Verde Sandstone	1.52×10^{-4} (S)		
Trinity Mine			
Cove Creek Coal	1.67×10^{-4} (W)	4.09×10^{-2}	9.05×10^{-2}
Middesboro Sandstone	2.06×10^{-4} (S)		
Gateway Mine			
Fruitland Coal #2	4.95×10^{-4} (S)	1.63×10^{-3}	7.66×10^{-1}
Fruitland Coal #5	3.84×10^{-4} (W)		
Tres Hermanos Sandstone			
Upper bed Set #1	2.21×10^{-4} (W)	5.96×10^{-2}	8.62×10^{-2}
Lower bed Set #1	2.45×10^{-4} (S)		
Upper bed Set #2	2.21×10^{-4} (W)	9.01×10^{-3}	2.24×10^{-1}
Lower bed Set #2	2.45×10^{-4} (S)		
Upper bed Set #3	2.21×10^{-4} (W)	2.79×10^{-2}	1.26×10^{-1}
Lower bed Set #3	2.45×10^{-4} (S)		

Table 4. Summary of strain values and joint spacing ratios. (continued)

Location	s_{obs}	s_{theor}	s_{obs} / s_{theor}
Manilla Mine	2.90×10^{-2}	4.70×10^{-2}	0.62
Trinity Mine	1.60×10^{-2}	7.72×10^{-3}	2.07
Gateway Mine	1.28×10^{-1}	1.09×10^{-1}	1.17
Tres Hermanos SS			
Set #1	1.50×10^{-1}	1.32×10^{-1}	1.14
Set #2	3.50×10^{-1}	3.43×10^{-1}	1.02
Set #3	2.00×10^{-1}	1.93×10^{-1}	1.04

Values of e_1 represent the strain necessary to produce the first joint.
The (S) and (W) specify the stronger and weaker of the two lithologies, respectively, as determined from their tensile strengths.
Those values of e_1 followed by (S) were used to calculate e_2.
Those values of e_1 followed by (W) were used to calculate s_{theor}.
Values of e_2 represent the final state of strain of the system, assuming both beds undergo equal amounts of strain.
Values of s_{obs}/s_{theor} are expressed in terms of the weaker, more jointed lithology.

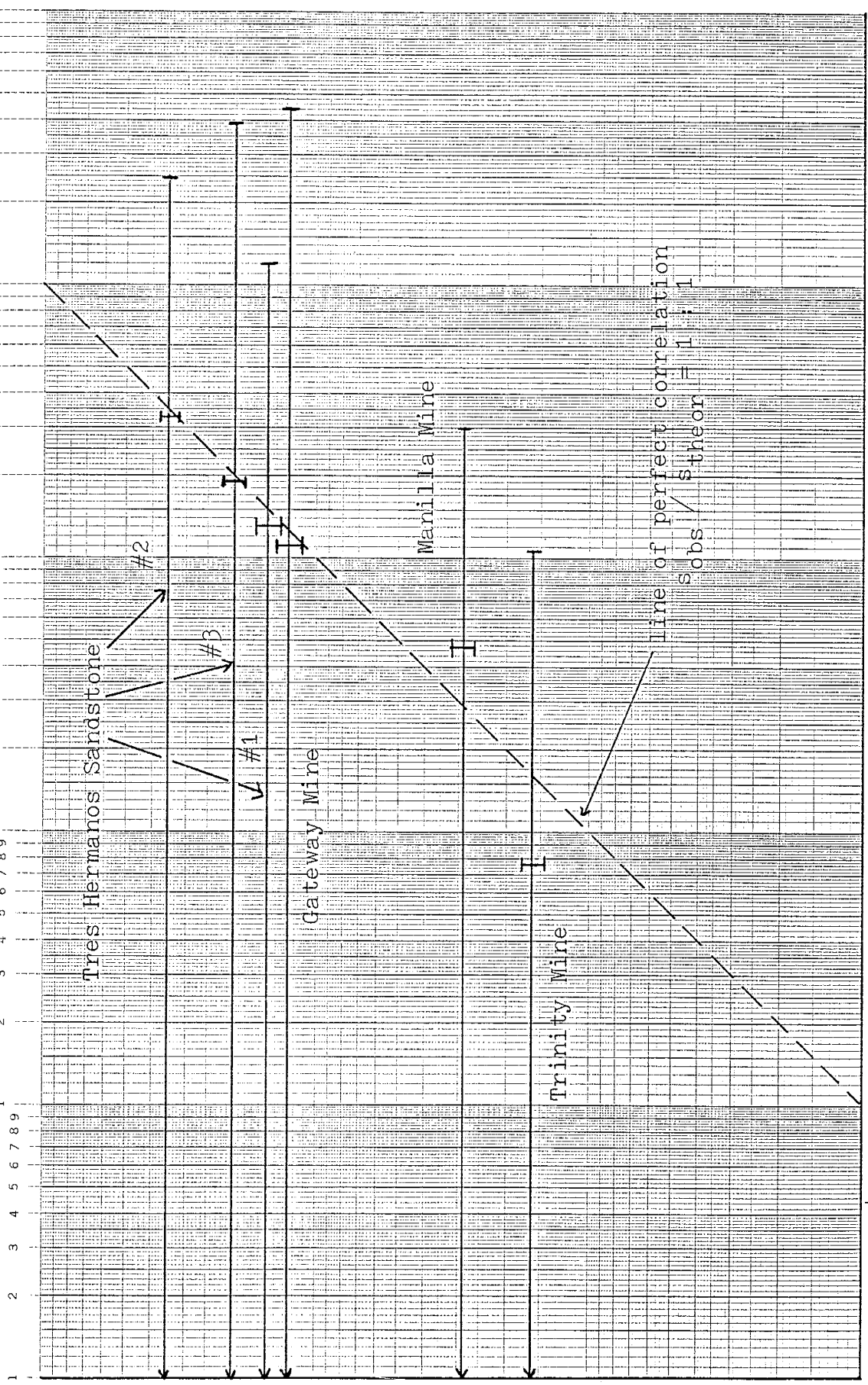

Figure 30. Graphic log/log plot of s_{theor} vs. s_{obs}.

elastic constants T, E and G. The results of tensile strength determinations for the various lithologies given in Table 3 exhibit a fairly large degree of uncertainty. This is due to the nature of tensile failure, which is affected by a number of variables, such as fluid content and porosity, quantity and nature of cementation, grain size, and uniformity of the applied stress field (Jaeger, 1967; Vutukuri et al, 1974). Nevertheless, the values reported fall within the range given for both coals and sandstones listed in the Handbook of Mechanical Properties of Rocks (Lama and Vutukuri, 1978) and are believed to be representative of the rock types tested. The values of tensile strength are used to calculate the strain at which a particular rock type will fail from the relation $e_1 = T/E$. This e_1, which appears in the deformation factor of equation (16), is at least an order of magnitude less than e_2, and so is of only minor consequence in the value of this term. Hence, the rather large degree of scatter to the experimental results, which is common to virtualy all tensile strength determinations, will have only a modest effect on the results of this study.

The values obtained for V_p and V_s (Table 3) show relatively small amounts of uncertainty in most cases (< 5%), with the exception of some of the sandstones (6-9%). This range of results for sandstone is probably due to variations in cementation of these rocks. The effect of the uncertainty in the determination of V_p and V_s on the calculated values of E and G tends to be minimized by the way E and G appear in the material properties term in equation (16), specifially, as the square root of the ratio of these quantities. Young's modulus, E, is also used in the computation of e_1, but here too it is involved as a ratio, and will not drastically alter the result. Values determined for E and G

using V_p and V_s are found to be very similar to values tabulated in Lama (1978). The generally good agreement between the statically and dynamically determined values of E (Table 3) also support their reliability.

In the case of e_2 and s_{theor}, however, propagation of uncertainty in the determination of V_s has proven to be an unwieldy problem. This is due to the nature of the expressions which contain G or functions of G. The value of the shear modulus is calculated from the relation $G = \rho V_s^2$ (equation 24). This G, in turn, appears in equation 27 and is involved in the calculation of e_2. The quantity e_2 appears in both the numerator and denominator of the deformation term $\cosh^{-1} (e_2/(e_2-e_1))$ of equation 16, the expression by which the theoretical joint spacing is computed. The respective magnitudes of e_2 and e_1 are commonly 10^{-1} to 10^{-3} and 10^{-4}, so the argument of the $\cosh^{-1}$ function is usually quite close to 1.0 (values for this study range from 1.0037 to 1.3082). Figure 31 illustrates the behavior of $\cosh^{-1} (X)$, where $X = e_2/(e_2-e_1)$, for a range of values of X. It is seen that for values of X very close to 1.0 there is an extremely rapid increase in Y, so that even small amounts of uncertainty in the calculation of X will yield a large range of possible Y's. This accounts for the wide range of uncertainty in s_{theor} indicated by the error bars in Figure 30. Error bars on s_{obs} show a $\pm$ 10% accuracy on joint data recorded in the field.

The behavior of the deformation term $\cosh^{-1} (e_2/(e_2-e_1))$ near 1.0 and the relative magnitudes of e_2 and e_1 place strict limitations on the amount of uncertainty in V_p and V_s and the quantities derived from them. Attempts to reduce these large uncertainties to a more geologically realistic magnitude have not met with success. Recalculation of the error bars using the standard deviation of E and G does not improve matters much, and in some cases makes it worse. It appears that

(a)

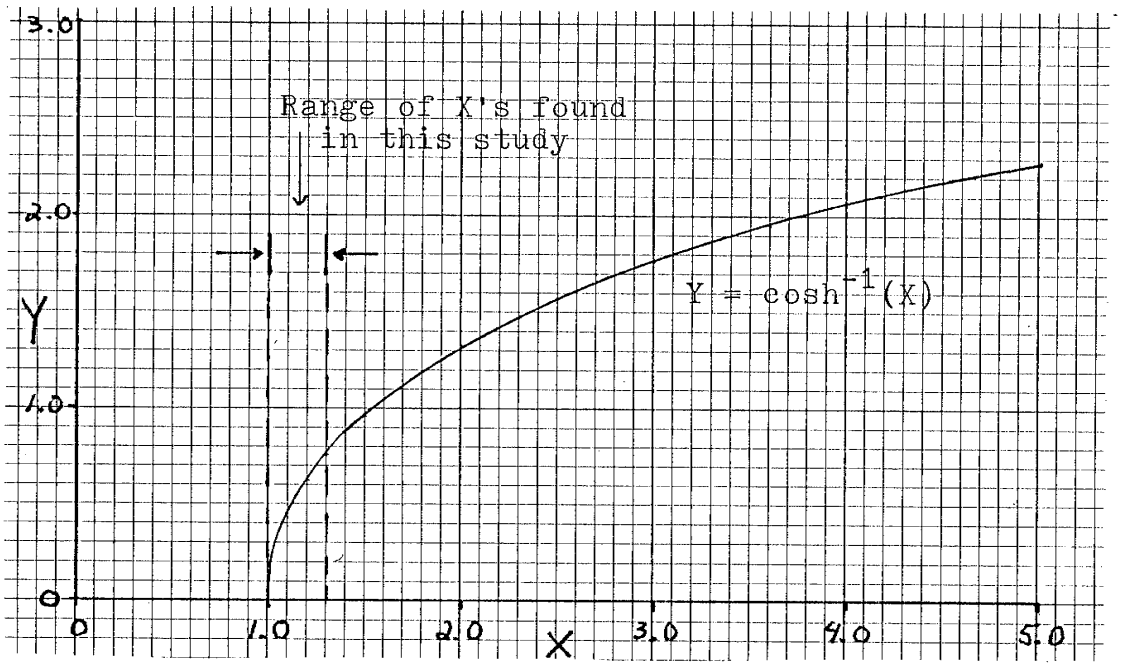

(b)

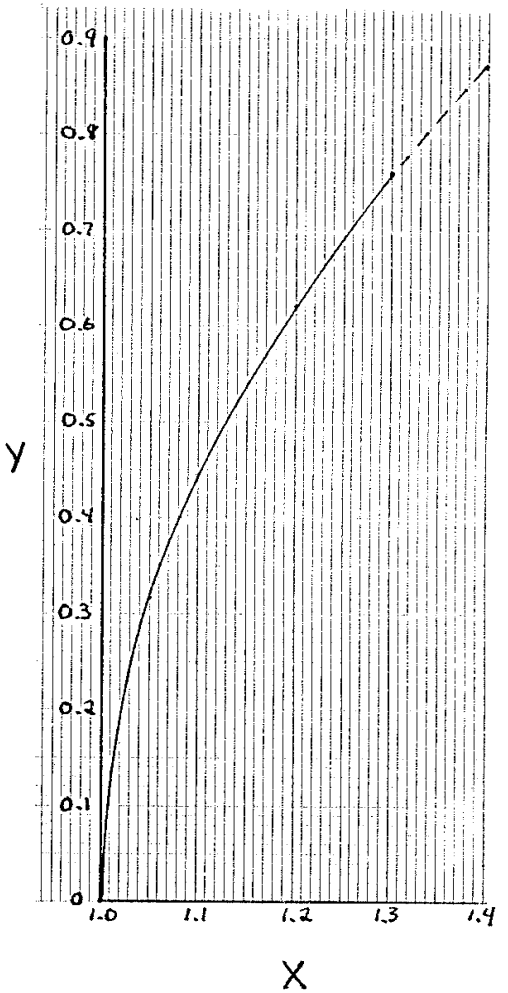

Figure 31. Graph of $Y = \cosh^{-1}(X)$.
(a) X = 0.0 to 5.0.
(b) X = 1.0 to 1.4.

investigations into the relationship between strain energy, jointing, and the mechanical properties of rocks are incapable of being solved without large uncertainty using the formulation of Hobbs (1967). Improvements in observational and experimental techniques would essentially require perfect precision (zero error) in order to yield an accurate s_{obs}/s_{theor} ratio.

Despite the large error bars, the data still show a pronounced linear trend. If we attribute the major portion of the calculated error to the behavior of the $\cosh^{-1}$ function near 1.0, we can investigate the linear trend displayed by the data via other methods and see what the results indicate.

Only one study produced a s_{obs}/s_{theor} ratio in which there were more joints predicted than actually observed; the Manilla Mine study. This is probably due to the poor state of preservation of the joints within the coal, which did not allow an accurate accounting of joint density. Consequently, the theoretically expected value is substantially larger than that which was recorded, resulting in a s_{obs}/s_{theor} ratio of 0.62.

An inspection of the remaining values reported for the s_{obs}/s_{theor} ratio shows that in all cases more joints were observed in the field than predictions from our theoretical calculations would indicate, with values ranging from 1.02 to 2.07. Conditions of joint preservation were generally good for the remainder of the studies, so the reasons for this apparent discrepancy are believed to be due to inadequacies in our simplified model. In particular, effects due to pore-pressure have not been included in the computations. Virtually all sediments at depth are subject to the effects of pore pressure to some degree, and due to the

relatively shallow depths of burial (<2.0 km) to which the sediments investigated in this study have been subjected, it is assumed that minimum fluid pressure ratios of between 0.1 - 0.4 may have influenced the jointing process. These values seem reasonable since no evidence of over-pressuring phenomena were observed at any of the study sites. As stated earlier, the pressure due to pore fluids makes rocks weaker and more brittle, so we would expect a corresponding increase in joint densities recorded at the surface. For this reason the disparity between the s_{obs} and s_{theor} joint spacings are thought to be due in large part to embrittlement caused by hydraulic fracturing.

The results reported in Table 4 yield an average value of 1.18 for the s_{obs}/s_{theor} ratio. Considering the number of experimental tests that had to be performed and the variables associated with field work and theory, these results appear quite good. It should be remembered, however, that several assumptions were employed in order to facilitate our task, particularly, the absence of additional tectonic stress and the assumption of equal strain in both beds, and manageably low uncertainty; these values may in fact be fortuitous. It is also possible that the ratios obtained are indeed reasonable approximations to the actual ratios, but this cannot be proven on the basis of error calculations. So, despite a sound theoretical basis as to the origins of jointing and the mechanics of joint formation, carefully conducted field observations, and experimental results which show relatively small amounts of uncertainty, it is not possible to claim that the s_{obs}/s_{theor} ratios obtained are accurate estimates. It is likely that the limits of accuracy are on the order of $\pm$ several hundred percent. Considerable refinement of this estimate would be possible if information regarding state of stress and pore pressure were known.

Comparative Stress Contributions to the Jointing Process

A number of theoretical, observational, and experimental parameters have been incorporated into the s_{obs}/s_{theor} results reported in column four of Table 4. From the theoretical perspective, the calculations reflect contributions to the existing stress from processes associated with uplift. To illustrate the relative magnitude of these contributions to the energy available for jointing, a rough calculation of each of these components was conducted and appears in Table 5. These values were computed using the last three terms of equation 13 which describe the effects of gravitational unloading, thermal contraction, and lateral extension, respectively, and the elastic constants reported in Table 3. Also supplied are specific values of quantities not shown in the tables along with the source of information where applicable.

The tensile strengths of the various lithologies are shown to be exceeded by the tensile stresses generated during uplift in all cases. It is also seen that in all of the coal/sandstone studies, the gravitational and thermal contributions account for the bulk of the energy available for jointing, with the contributions from lateral extension being comparatively minor. Only in cases where the rocks have a large Young's modulus or have undergone ample uplift does this factor become significant.

Applications and Suggestions for Future Studies

It is unfortunate that the form of Hobbs solution to the mechanical process of jointing restricts us from obtaining an s_{theor} value without unduly large uncertainty, for a method of estimating subsurface fracture densities would be a most desirable thing. Such a capacity has possible applications in several areas of hydrology and petroleum geology. Joint

Table 5. Stress contributions to the jointing process from various sources during tectonic uplift.

Location/ Lithology	Gravitational Unloading (σ_G, MPa)	Thermal Contraction (σ_t, MPa)	Lateral Stretching (σ_e, MPa)	Specific Values Used/ References/Comments
Manilla Mine				
Carthage Coal	12.40	-13.72	-0.81	$\bar{\rho}$ = 2350 kg/m^3 ν_c = 0.35, ν_{ss} = 0.25 (Lama, 1978) Δz = 1.0 km (Wilpolt and Wanek, 1951) α_ℓ = 1.0x10^{-5}/°C, assumed (Turcotte and Schubert, 1982) dQ/dz = 30°C/km (Reiter et al., 1986) dR = 1.52 km, R = 6371 km T_c = -1.44 MPa, T_{ss} = -3.16 MPa
Mesa Verde SS	7.60	-8.30	-4.95	
Trinity Mine				
Cove Creek Coal	25.33	-7.61	-1.48	$\bar{\rho}$ = 2400 kg/m^3 ν_c = 0.35, ν_{ss} = 0.25 (Lama, 1978) Δz = 2.0 km (Miller, 1974) α_ℓ = 1.0x10^{-5}/°C, assumed (Turcotte and Schubert, 1982) dQ/dz = 20°C/km (Miller, 1974) dR = 0.76 km, R = 6371 km T_c = -2.07 MPa, T_{ss} = -7.68 MPa
Middesboro SS	15.52	-19.92	-4.46	

Table 5. Stress contributions to the jointing process from various sources during tectonic uplift. (continued)

Location/ Lithology	Gravitational Unloading (σ_G, MPa)	Thermal Contraction (σ_T, MPa)	Lateral Stretching (σ_e, MPa)	Specific Values Used/ References/ Comments
Gateway Mine				
Fruitland Coal (#2)	11.87	-1.54	-0.87	$\bar{\rho}$ = 2250 kg/m^3 ν_c = 0.35 (Lama, 1978) Δz = 1.0 km (Clarkson, 1984)
Fruitland Coal (#5)	11.87	-1.27	-0.72	α_ℓ = 1.0x10^{-5}/°C, assumed (Turcotte and Schubert, 1982) dQ/dz = 30°C/km (Reiter and Mansure, 1983) dR = 1.67 km, R = 6371 km T_{c2} = -1.65 MPa, T_{c5} = -1.06 MPa
Tres Hermanos				
Upper SS	8.36	-14.94	-8.10	$\bar{\rho}$ = 2350 kg/m^3 ν_c = 0.25 (Lama, 1978) Δz = 1.1 km (Wilpolt and Wanek, 1951) α_ℓ = 1.0x10^{-5}/°C, assumed (Turcotte and Schubert, 1982) dQ/dz = 30° C/km (Reiter et al., 1986) dR = 1.52 km, R = 6371 km T_{uss} = -7.50 MPa, T_{lss} = -10.75 MPa
Lower SS	8.36	-19.29	-10.50	

sets and the spacing of fractures have a strong influence on the permeability and seepage characteristics of rock masses. In general, the hydraulic conductivity of any given joint set will be inversely proportional to the interjoint spacing if individual joint apertures are comparable (Brown, 1981). It may also be possible to estimate the storage capacity within joints in sandstone reservoirs if it is assumed that the extensional strain has been taken up in the formation of joints. From an engineering standpoint, several sets of closely spaced joints tend to give conditions of low mass cohesion, whereas sets that are widely spaced are more likely to result in larger and more stable masses. These effects are dependent upon the areal extent or persistence of individual fractures within a bed. In the case of orientation, joint spacing becomes increasingly important when other conditions for deformation are present; for example, underlying beds of low shear strength, such as shale.

If the problem can be reformulated without involving functions whose behavior is extreme in the region pertinent to the study, it is possible that sufficient improvement may be obtained to yield accurate s_{obs}/s_{theor} ratios. It is hoped that additional efforts will be applied to this aspect of the problem. The results of this study may thus be of use in future investigations concerning strain energy and jointing.

SUMMARY AND CONCLUSIONS

Our objective has been to determine whether the observed differences in joint density found in relatively undeformed, horizontal sedimentary rocks can be explained on the basis of the mechanical properties of the rocks, and the strain energy stored in them. Several

investigative approaches have been utilized to answer this question, particularly those of theory, field work, and experimentation.

Theory suggests that the mechanical origins of jointing may be ascribed to the release of tensile stresses generated during uplift and denudation. These stresses are primarily due to horizontal extension accompanying uplift, expansion through the release of gravitational load, and contraction produced by cooling. Stress buildup will proceed until it eventually equals the material's tensile strength, and joint formation will occur. Studies demonstrate that joint frequency is dependent upon the thickness of the sedimentary layer, the physical properties of the rock bed and its surroundings, and the degree of deformation to which the beds are subjected. It was also shown that in order to effectively dissipate the extensional stress accumulated during uplift, the formation of a large number of joints is necessary. This is because residual stresses are only relieved in the immediate vicinity of the fracture in accordance with St. Venant's principle.

Field work was conducted at four locations in order to acquire joint densities that would serve as the basis upon which the validity of theoretical predictions could be judged. Sequences of coal and sandstone were selected for study because it was felt that joint density contrasts with respect to lithology would be most apparent due to differences in their elastic properties. Note was taken of the joint densities, directions, structural style, surface characteristics and the nature of infillings on all well-displayed joint sets. Rock samples were collected from each bed to provide specimens for the laboratory tests that would determine the elastic properties of the material that the theoretical approach to the problem requires.

The requisite material properties were obtained by the experimental

procedures of uniaxial compression, ultrasonic pulse velocity determinations, and diametral compression of disks and rectangular prisms (Brazilian test). These techniques provided values of Young's modulus, the shear modulus, and tensile strength. Once acquired, these values were then used to calculate theoretical joint spacings for the lithologies in question. The joint spacings are expressed in terms of bed thickness, the mechanical properties of the rock bed and its surroundings, and the degree of tectonic deformation. By comparing the calculated spacings to those observed in the field, the question of whether the physical properties of the rocks and the release of strain energy can account for the differences in joint density recorded in adjacent sedimentary rocks may be evaluated.

Results of such comparisons show that in most cases there were more joints observed in the field than computations based on theory would predict with s_{obs}/s_{theory} values ranging from 0.62 to 2.07 with an average of 1.18. This apparent discrepancy is believed to be due mainly to the effects of pore pressure not included in our simplified model, which would tend to increase the observed joint densities due to hydraulic fracturing of the rocks. Propagation of error involving the determination of the elastic constants produces such large uncertainties however, that the accuracy of these ratios is highly questionable. The conclusion is reached that investigations into the relationship between strain energy and tensional jointing cannot adequately be solved by use of Hobbs' formulation because of the unrealistic requirements it imposes on experimental precision. Investigations have also shown that the bulk of the energy that goes into the formation of joints is produced by the release of gravitational

load and thermal contraction, with contributions from lateral extension being relatively minor.

APPENDIX A

Criterion of Failure

Because we are primarily concerned with tensile failure of material in a biaxial stress field, we can use the Griffith criterion to describe and predict the conditions of failure (Jaeger and Cook, 1979). The basis of the Griffith theory (1924) in biaxial form is that failure will occur when the most vulnerably oriented crack in a population of randomly oriented cracks begins to extend under the application of stress. In order to simplify calculation of the stress distribution, Griffith also assumed that the cracks were of cylindrical shape with a flattened elliptical cross-section. Using the classical theory of linear elasticity, he then calculated the two-dimensional stress distribution around a crack. Crack extension is assumed to occur when the maximum stress component at any point around the crack attains the critical value required to overcome the interatomic cohesion of the material, also called the Griffith compressive strength (Segall, 1984). This critical value will be first attained close to, but not at, the ends of cracks inclined at some narrow angle to the direction of σ_1, the maximum applied compressive stress. As the stress continues to increase, a subsidiary crack begins to extend from the sides of the original fracture, growing towards the position of maximum stability, i.e. so as to parallel the direction of maximum compression (Fig. A1a)(Ode, 1960). Thus a brittle rock loaded just beyond its Griffith compressive strength may be assumed to consist of numerous flaws with extensions parallel to the direction of loading (Fig. A1b).

An energy argument, originally proposed by Griffith, which

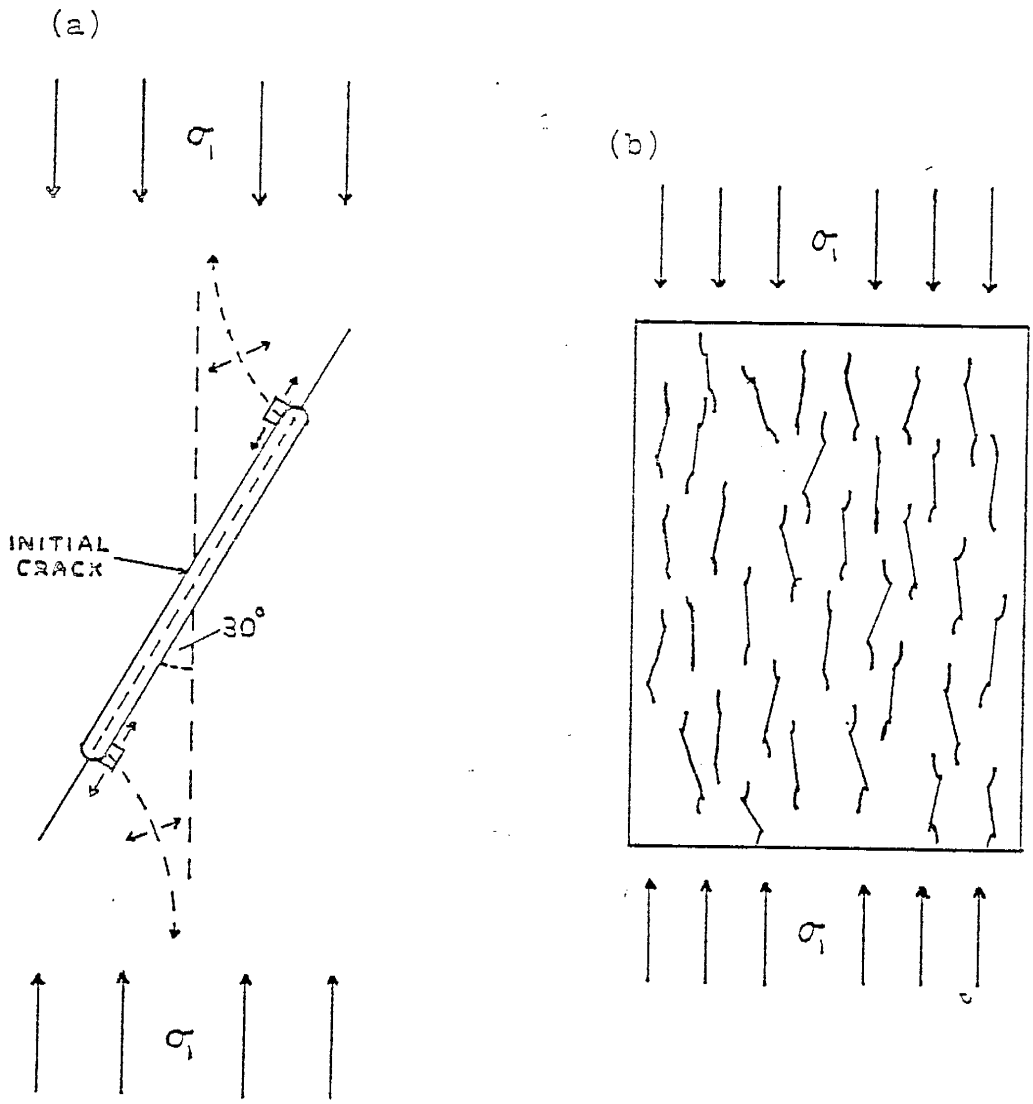

Figure A1. (a) Tensile fracture initiation from a Griffith crack in uniaxial compression.
(b) Crack growth in rock at stresses near the Griffith compressive strength.

is used to describe the conditions under which crack propagation will take place, employs the surface energy as a measure of the local cohesive strength of the material. The criterion of failure, based on the principle that the potential energy of a system will tend to a minimum, states that the crack will propagate if in doing so the sum of the following three terms is ≤ 0:

1. the surface energy of the new crack created,
2. the change in the elastic strain energy of the body, and
3. the change in the potential energy of the loading system.

These terms specify that a system will become unstable and catastrophic brittle fracture will result if the surface energy expended per increment of crack growth is less than the elastic energy released.

The Griffith theory of fracture predicts the size and shape of the fracture envelope (Fig. A2) as:

$$\tau^2 - 4T\sigma_N - 4T^2 = 0 \qquad \text{(A1)}$$

where τ is shear stress, σ_N is normal stress, and T is the tensile strength. It is also sucessful in predicting the approximate orientation of fractures in the tensile and transitional-tensile regions. The cracks most likely to grow in the tensile region according to this theory, are those oriented perpendicular to the principal tensile stress σ_3, as experimental observations confirm (Paterson, 1978; Jaeger and Cook, 1979).

The Mohr circle is tangent to the envelope of failure at only one point, so only one direction of potential fracture exists. Above a critical value of the most compressive stress σ_1, transitional tensile behavior is exhibited. Beyond this value, which is approximately $\sigma_1 = |3T|$, the Mohr circle is now tangent to the fracture envelope at two points,

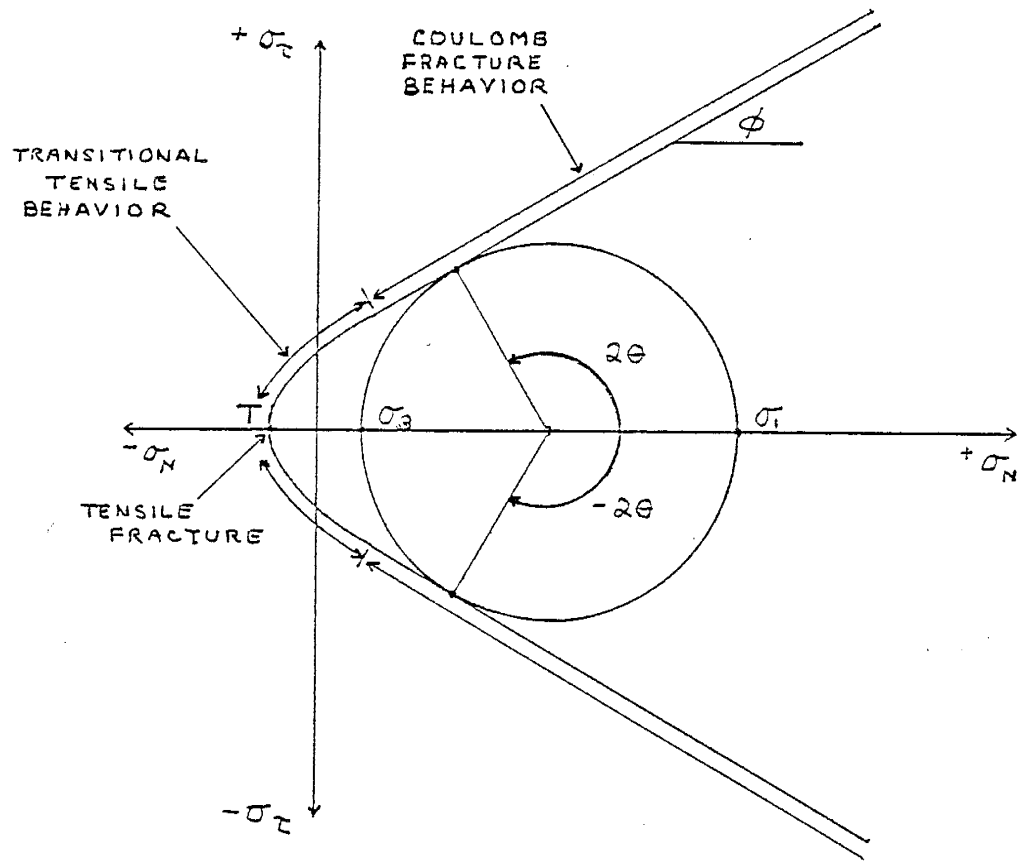

Figure A2. Mohr diagram illustrating the three fields of fracture.

rather than one, at time of failure, and subsequently two directions of potential fracture exist. In the transitional tensile field (Fig. A2) we see a rapid, nonlinear increase in strength ($\sigma_1 - \sigma_3$) with increasing pressure, and a change in the fracture orientation from parallel to about 30° to the direction of maximum compression. It is in the tensile and transitional fields that most joints are formed.

APPENDIX B

Elastic Solids and Linear Elasticity

The general problem of elasticity concerns that of determining the state of stress and displacement in a body of known shape subject to prescribed conditions at its surface. A linear, isotropic, elastic solid is one in which stresses are directly proportional to strains, and there is no preferred orientation of the mechanical properties. In such a medium the principal axes of stress and strain coincide, so that the relationship between stress and strain may be written as

$$\sigma_1 = (\lambda + 2G)e_1 + \lambda e_2 + \lambda e_3 \qquad \text{(B1)}$$

$$\sigma_2 = \lambda e_1 + (\lambda + 2G)e_2 + \lambda e_3 \qquad \text{(B2)}$$

$$\sigma_3 = \lambda e_1 + \lambda e_2 + (\lambda + 2G)e_3 \qquad \text{(B3)}$$

where λ and G, the material properties, are known as the Lamé parameters (G is also called the shear modulus). This form is chosen to express the fact that one constant, $(\lambda+2G)$, connects stress and strain in the same direction, while a different one, λ, relates stress and strain in the two perpendicular directions (Jaeger and Cook, 1979).

Equations (B1) to (B3) may be written in inverse form as

$$e_1 = \frac{1}{E}\sigma_1 - \frac{\nu}{E}\sigma_2 - \frac{\nu}{E}\sigma_3 \qquad \text{(B4)}$$

$$e_2 = -\frac{\nu}{E}\sigma_1 + \frac{1}{E}\sigma_2 - \frac{\nu}{E}\sigma_3 \qquad \text{(B5)}$$

$$e_3 = -\frac{\nu}{E}\sigma_1 - \frac{\nu}{E}\sigma_2 + \frac{1}{E}\sigma_3 \qquad \text{(B6)}$$

Here the material properties E and ν are known as Young's modulus and

Poisson's ratio, respectively.

An elastic material has the property that, upon application of an axial load σ, a strain e, proportional to the applied load, is produced (Fig. B1). Also, upon removal of the load, the material instantly regains its original length. Generally the strains produced in elastic materials are small (less than 2%) and come under the catagory of infinitesimal strain. A linearly elastic or Hookean substance has the stress-strain relationship

$$\sigma = Ke \tag{B7}$$

and may be rheologically modelled by a spring of stiffness K. Apart from a change in sign convention, there is no difference in the effects of compression or tension on the elastic deformation except that in compression (taken as positive), the limit of elastic deformation is considerably larger than in tension (see Fig. B1).

Joint Frequency Estimates Based on Strain Energy

The strain energy stored in an elastic body is equal to the work performed in producing of a given amount of strain. In a unit cube of material that has a linear stress-strain relationship, the strain energy w is given by

$$w = \frac{\sigma e}{2} \tag{B8}$$

where σ is the applied stress and e is the resultant strain. Substituting a value of $e = \sigma/E$ from the stress-strain graph of figure B1 yields:

$$w = \frac{\sigma^2}{2E} \tag{B9}$$

Combining this result with equations B4 to B6 (after suitable

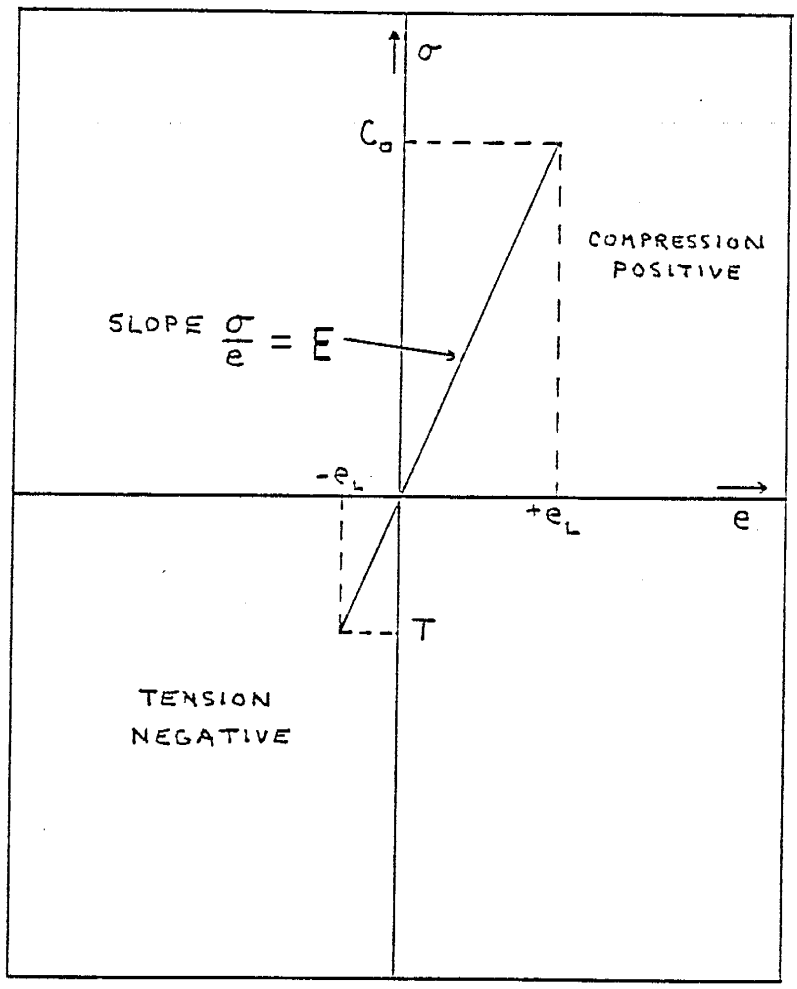

Figure B1. Stress/strain relationship for substance possessing linear-elastic properties.

rearrangement) which relate the conditions of strain in triaxial stress, an expression describing the strain energy stored in this cube is obtained:

$$W = \frac{1}{2E}\left[\sigma_1^2 + \sigma_2^2 + \sigma_3^2 - 2\nu\left(\sigma_1\sigma_2 + \sigma_2\sigma_3 + \sigma_1\sigma_2\right)\right] \quad (B10)$$

In this case of adjacent sedimentary rocks, the stresses will be virtually the same, and consequently, the strain energy contained in the rocks will be dependent on the elastic constants of the materials. When typical values of E and ν for coal and sandstone are entered into equation B10 the relative amounts of strain energy contained within the separate lithologies may be determined (Price, 1966).

APPENDIX C

Program for calculating buildup of tensile stress/tensile strength as a function of the distance from the joint/bed thickness.

```
      PROGRAM STRESS
      REAL E, G, T, TS, D, JF, X, Y, P, SIGXX, Z

C     WHERE E = YOUNG'S MODULUS (GPa'S)
C           G = SHEAR MODULUS (GPa'S)
C           T = TENSILE STRENGTH (MPa'S)
C          TS = TENSILE STRAIN (DIMENSIONLESS)
C           D = BED THICKNESS (METERS)
C          JF = JOINT FREQUENCY (#/METER)
C           X = DISTANCE FROM JOINT (METERS)
C           P = DISTRIBUTION OF LOAD IN BED (NEWTONS/METER)
C       SIGXX = TENSILE STRESS (NEWTONS/METER SQUARED =(PASCALS))
C           Y = RATIO OF TENSILE STRESS TO TENSILE STRENGTH

C     FOLLOWING CALCULATIONS ARE FOR MANILLA MINE COAL BED
C     E AND T ARE FOR COAL
C     G IS FOR NEIGHBORING MESA VERDE SANDSTONE

      E = 3.43E + 9
      G = 2.07E + 10
      T = 1.44E + 6
      TS = T/E
      D = 0.88
      X = 0.0
      JF = (2.0/D) * SQRT (G/E)
      WRITE (5,*) '  '
      WRITE (5, 1000)

      DO 10 Z = 0.0, 3.5, 0.1
         P = E*D*TS*(1.0 + SINH (JF*X))-(COSH (JF*X)))
         SIGXX = P/D
         Y = SIGXX/T
         WRITE (5, 1001) X, SIGXX, Y
         X = X + 0.1
   10 CONTINUE
      STOP

 1000 FORMAT (10X, 'X COORDINATE = ', 10X, 'SIGXX = ', 18X, 'Y = ')
 1001 FORMAT (15X, F4.2, 13X, F10.2, 13X, F7.2)
      END
```

APPENDIX D

LVDT

The linear variable differential transformer (LVDT) is an electromechanical device which produces an electrical output proportional to the displacement of a moveable core. It consists of three equally spaced coils on a cylindrical coil, with the central coil forming the primary and the outer two forming the secondary coils (Fig. D1a). A cylindrical movable magnetic core inside this assemblage generates the magnetic flux inside the coils. The secondary coils are connected in series opposition so that the two voltages in the secondary circuit are opposite in phase and the net output is the difference of these voltages. When the core is in the central position, the net output is zero; this point is called the balance or null point. As the core is moved to either side, the induced voltage increases in the coil in the direction of movement and decreases in the other, yielding a differential output of the proper sign. This output varies linearly with the displacement of the core as shown in figure D1b (Lama, 1978). Sensitivity to displacements as small as 5.0×10^{-6} meter (5.0 microns) are possible on the apparatus used in this study.

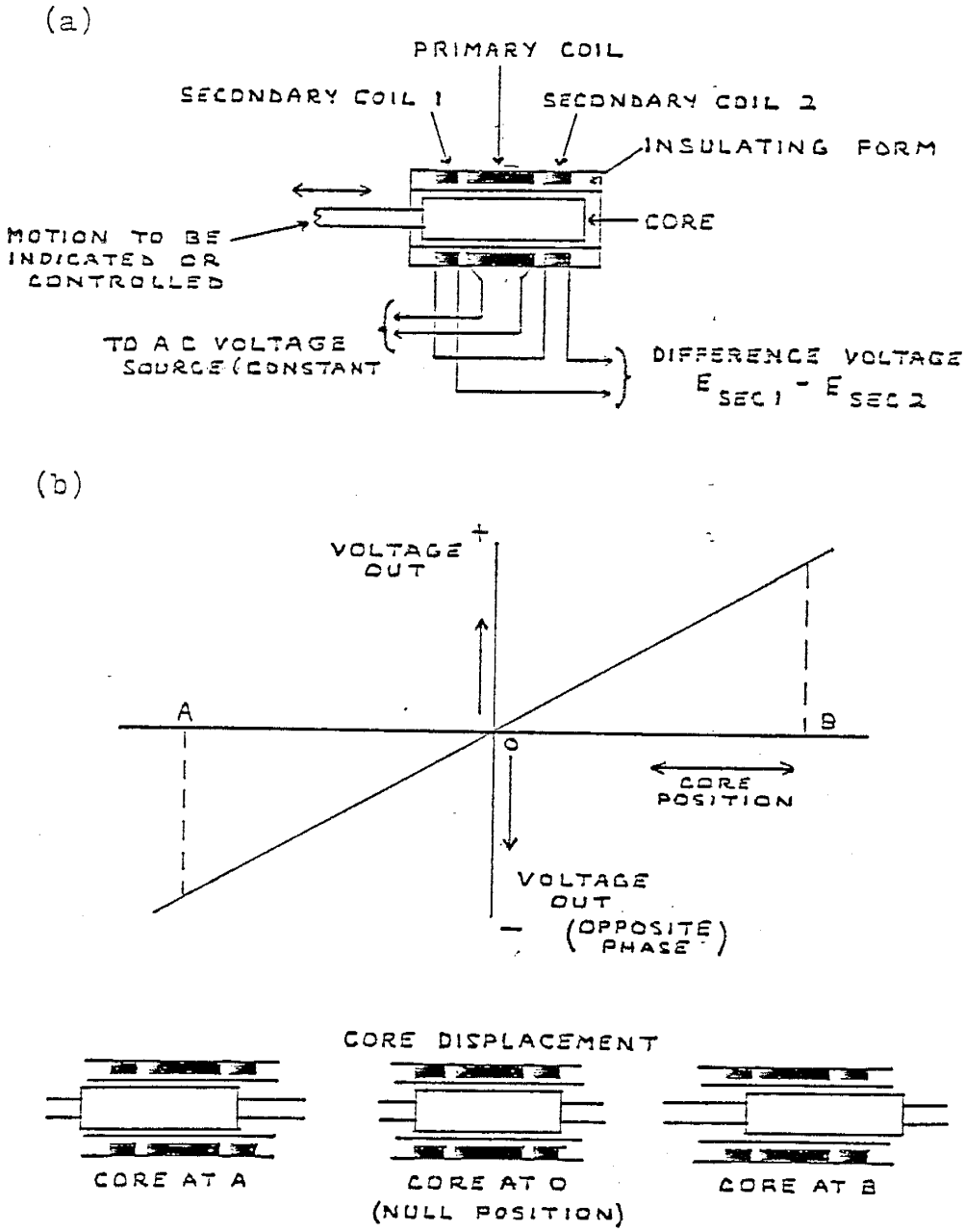

Figure D1. (a) Operation of the linear variable differential transformer (LVDT). (b) Linear graph of LVDT output voltage and phase as a function of core position. (after Lama, 1978.)

Appendix E
Test Data

Manilla Mine

Test Performed: Determination of V_p and V_s (ultrasonic pulse).

Lithology: Carthage Coal

Sample #	Length (mm)	Travel Time (microsec)	V_p (km/sec)	V_s (km/sec)
1	26.70	16.00	1.67	
		25.00		1.07
2	26.05	15.00	1.74	
		22.00		1.18
3	26.55	16.00	1.66	
		23.00		1.15
4	25.95	15.00	1.73	
		24.00		1.08
5	26.10	15.00	1.74	
		23.00		1.13
6	26.50	17.00	1.56	
		24.00		1.10

Average V_p = 1.68 km/sec
Standard deviation = 0.07 km/sec

Average V_s = 1.12 km/sec
Standard deviation = 0.04 km/sec

Comments: All velocities measured perpendicular to bedding.
Specimen length accurate to 0.10 mm.
Travel times accurate to 1.00 microsecond (V_p) and 2.00 microsecond (V_s).
Tests conducted at atmospheric pressure.

Manilla Mine

Test Performed: Determination of V_p and V_s (ultrasonic pulse).

Lithology: Mesa Verde Sandstone

Sample #	Length (mm)	Travel Time (microsec)	V_p (km/sec)	V_s (km/sec)
1	24.72	8.40	2.94	
		12.00		2.06
2	16.45	5.50	2.99	
		8.50		1.98
5	15.90	5.00	3.18	
		7.25		2.19
6	29.50	10.10	2.92	
		15.00		1.97
7	28.90	10.50	2.75	
		15.00		1.93

Average V_p = 2.96 km/sec

Standard deviation = 0.15 km/sec

Average V_s = 2.03 km/sec

Standard deviation = 0.10 km/sec

Comments: All velocities measured perpendicular to bedding.
Specimen length accurate to 0.10 mm.
Travel times accurate to 0.25 microseconds (V_p) and 0.50 microseconds (V_s).
Tests conducted at atmospheric pressure.

Manilla Mine

Test Performed: Tensile strength determination (Brazilian test); method of Davies and Stagg (1970).

Lithology: Carthage Coal

Sample #	D Diameter (inches)	t Thickness (inches)	F Load (lbs.)	T Tensile Strength (MPa)
2	0.543	1.420	237	-1.35
3A	0.533	1.520	350	-1.90
3B	0.533	1.520	238	-1.24
4	0.540	1.600	362	-1.64
5	0.586	1.280	175	-1.02
6	0.550	1.330	263	-1.58
7	0.549	1.260	212	-1.35
8	0.550	1.340	230	-1.37
9	0.545	1.440	250	-1.40
10	0.536	1.590	238	-1.22
11	0.550	1.470	325	-1.76

Average tensile strength = -1.44 MPa

Standard deviation = 0.26 MPa

Comments: All samples compressed perpendicular to bedding.
Tensile strength values calculated according to the relation $T = 2F/Dt\,\pi$.
Specimens in fair-to-good condition; specimens generally disintegrated upon failure.
1 PSI = 6.895×10^3 Pa.

Manilla Mine

Test Performed: Tensile strength determination (Brazilian test); method of Hondros (1959).

Lithology: Mesa Verde Sandstone

Sample #	D Diameter (inches)	t Thickness (inches)	F Load (lbs.)	T Tensile Strength (MPa)
4	0.975	0.415	140	-1.52
5	0.973	1.320	875	-5.98
11	0.974	0.539	155	-1.30
12	0.975	0.550	670	-5.48
13	0.975	1.870	1300	-3.13
14	0.975	1.150	615	-2.41
15	0.974	1.105	335	-4.29
17	0.975	1.016	485	-2.15
18	0.973	0.722	355	-2.21

Average tensile strength = -3.16 MPa

Standard deviation = 1.71 MPa

Comments: All specimens compressed perpendicular to bedding.
Tensile strength values calculated according to the relation $T = 2F/Dt\pi$.
Specimens generally very good; variation in cementation properties produced two groups of results; above values represent most reliable data.
1 PSI = 6.895×10^{3} Pa

Manilla Mine

Test Performed: Determination of Young's modulus by uniaxial compression.

Lithology: Mesa Verde Sandstone

Sample #	Diameter (inches)	Length (in.)	Load (lbs)	Displacement (inches)	Young's Modulus (GPa)
1	0.975	2.52	502	0.00410	
			938	0.00789	
			1775	0.01210	
			2886	0.01652	
			3616	0.01946	
			4319	0.02188	
			4989	0.02456	
			5793	0.02751	
			6329	0.02935	18.92
2	0.975	2.03	669	0.01115	
			1239	0.01394	
			2170	0.01725	
			3549	0.02109	
			4165	0.02262	
			4889	0.02420	
			6094	0.02725	28.49
4	0.975	2.48	904	0.00852	
			1306	0.01023	
			1942	0.01310	
			3201	0.01799	
			4139	0.02104	
			4674	0.02299	
			5659	0.02630	20.40
5	0.975	2.54	335	0.00384	
			502	0.00516	
			1842	0.01330	
			2947	0.01830	
			4179	0.02314	
			5491	0.02893	16.51
6	0.975	2.10	469	0.00452	
			1379	0.00852	
			2310	0.01205	
			3683	0.01615	
			4520	0.01836	
			5659	0.02157	
			6851	0.02472	25.49

Average Young's modulus = 21.96 GPa

Standard deviation = 4.91 GPa

Comments: 1 PSI = 6.895×10^3 Pa.

Manilla Mine

Test Performed: Determination of shear strength with bevelled dies.

Lithology: Mesa Verde Sandstone

Sample #	Dimensions (inches)	Load (lbs)	Shear Strength (MPa)
1	1.18 x 1.00	660	3.96
2	1.13 x 1.00	1250	7.83
3	1.07 x 1.00	820	5.42
4	1.16 x 1.00	1060	6.46
5	1.05 x 1.00	675	4.55

Average shear strength = 5.64 MPa

Standard deviation = 1.54 MPa

Comments: Cylindrical specimens used with grooved inserts. Shear strength calculated from the relation $S = F \cos \theta / A$
$\theta = 45°$, A = area, F = load

Trinity Mine

Test Performed: Determination of V_p and V_s (ultrasonic pulse).

Lithology: Cove Creek Coal

Sample #	Length (mm)	Travel Time (microsec)	V_p (km/sec)	V_s (km/sec)
1	17.15	5.50	3.12	
		8.00		2.14
13	18.22	6.00	3.04	
		8.25		2.21
14	17.00	5.75	2.96	
		8.00		2.12
16	17.70	5.50	3.22	
		7.75		2.21
17	18.20	5.90	3.08	
		7.90		2.30
18	17.92	5.50	3.26	
		8.00		2.24

Average V_p = 3.11 km/sec

Standard deviation = 0.11 km/sec

Average V_s = 2.20 km/sec

Standard deviation = 0.07 km/sec

Comments: All velocities measured perpendicular to bedding.
Specimen length accurate to 0.10 mm.
Travel times accurate to 0.25 microseconds (V_p) and 0.50 microseconds (V_s).
Tests performed at atmospheric pressure.

Trinity Mine

Test Performed: Determination of V_p and V_s (ultrasonic pulse).
Lithology: Middesboro Sandstone

Sample #	Length (mm)	Travel Time (microsec)	V_p (km/sec)	V_s (km/sec)
1	11.70	3.00	3.90	
		4.50		2.60
2	10.23	2.25	4.55	
		3.50		2.92
3	11.99	2.80	4.25	
		4.20		2.85
4	12.00	3.40	3.53	
		4.75		2.53
5	12.01	3.20	3.75	
		4.75		2.53
6	11.85	3.00	3.95	
		4.60		2.53

Average V_p = 3.99 km/sec

Standard deviation = 0.36 km/sec

Average V_s = 2.66 km/sec

Standard deviation = 0.18 km/sec

Comments: All velocities measured perpendicular to bedding.
Specimen length accurate to 0.10 mm.
Travel times accurate to 0.25 microseconds (V_p) and 0.50 microseconds (V_s).
Tests conducted at atmospheric pressure.

Trinity Mine

Test Performed: Tensile strength determination (Brazilian test); method of Davies and Stagg (1970).

Lithology:-Cove Creek Coal

Sample #	D Diameter (inches)	t Thickness (inches)	F Load (lbs.)	T Tensile Strength (MPa)
1	1.162	0.575	365	-2.40
2	1.097	0.540	183	-1.35
3	1.126	0.661	350	-2.06
4	1.178	0.581	302	-1.94
5	1.186	0.650	440	-2.51
6	1.266	0.571	100	-0.61 *
7	1.235	0.619	415	-2.38
8	1.299	0.610	400	-2.22
9	1.158	0.582	283	-1.84
10	1.095	0.570	365	-2.57
11	1.157	0.631	175	-1.05
12	1.256	0.479	327	-2.39
13	1.218	0.582	252	-1.56
14	0.995	0.569	180	-1.40
15	1.273	0.590	350	-2.05
16	1.075	0.591	265	-1.83
17	1.205	0.701	625	-3.25
18	1.060	0.628	263	-1.73
19	0.979	0.500	335	-3.00
20	1.015	0.476	197	-1.79

Average tensile strength = -2.07 MPa

Standard deviation = 0.56 MPa

Comments: All samples compressed perpendicular to bedding.
* - not included in calculations due to premature failure.
Tensile Strength values calculated according to the relation $T = 2F/Dt\pi$.
Specimens generally very good.
1 PSI = 6.895×10^{3} Pa.

Trinity Mine

Test Performed: Tensile strength determination (Brazilian test); method of Davies and Stagg (1970).

Lithology: Middesboro Sandstone

Sample #	D Diameter (inches)	t Thickness (inches)	F Load (lbs.)	T Tensile Strength (MPa)
1	1.53	0.51	1500	-8.44
2	1.37	0.40	1030	-8.25
3	1.33	0.41	1100	-8.85
4	1.24	0.47	540	-4.07
5	1.36	0.73	1590	-7.03
6	1.30	0.40	1600	-13.51
7	1.37	0.47	1625	-11.08
8	1.26	0.59	862	-5.09
9	1.48	0.51	1200	-6.98
10	1.48	0.63	1825	-8.59
11	1.51	0.46	513	-3.24
12	1.43	0.47	1550	-10.12
13	1.43	0.51	800	-4.82
14	1.48	0.51	975	-5.67
15	1.34	0.57	2025	-11.64
16	1.07	0.40	510	-5.49

Average tensile strength = -7.68 MPa

Standard deviation = 2.92 MPa

Comments: All specimens compressed perpendicular to bedding.
Tensile strength values calculated according to the relation $T = 2F/Dt\pi$.
Specimens generally very good; some variation in cementation observed.
1 PSI = 6.895×10^3 Pa.

Trinity Mine

Test Performed: Determination of shear strength with bevelled dies.

Lithology: Middesboro Sandstone

Sample #	Dimensions (inches)	Load (lbs)	Shear Strength (MPa)
6	1.24 x 1.00	2310	13.17
7	1.19 x 1.00	2500	14.86
8	1.13 x 1.00	2780	17.38
9	1.17 x 1.00	2440	14.75

Average shear strength = 15.04 MPa

Standard deviation = 1.74 MPa

Comments: Cylindrical specimens used with grooved inserts. Shear strength calculated from the relation $S = F \cos \theta / A$ $\theta = 45°$, A = area, F = load

Gateway Mine

Test Performed: Determination of V_p and V_s (ultrasonic pulse)

Lithology: Fruitland Coal #2

Sample #	Length (mm)	Travel Time (microsec)	V_p (km/sec)	V_s (km/sec)
1	39.05	23.00	1.70	
		35.00		1.12
2	36.40	20.00	1.82	
		32.00		1.14
3	36.10	22.00	1.64	
		32.00		1.13
4	40.08	25.00	1.60	
		37.00		1.08
5	36.45	21.00	1.74	
		32.00		1.14

Average V_p = 1.70 km/sec

Standard deviation = 0.09 km/sec

Average V_s = 1.12 km/sec

Standard deviation = 0.02 km/sec

Comments: All velocities measured perpendicular to bedding.
Specimen length accurate to 0.10 mm.
Travel times accurate to 2.00 microseconds (V_p) and 3.00 microseconds (V_s).
Tests conducted at atmospheric pressure.

Gateway Mine

Test Performed: Determination of V_p and V_s (ultrasonic pulse).

Lithology: Muddy Sandstone #2

Sample #	Length (mm)	Travel Time (microsec)	V_p (km/sec)	V_s (km/sec)
1	16.90	9.75	1.73	
		13.00		1.30
2	16.90	9.00	1.88	
		12.00		1.41
3	8.10	5.00	1.62	
		7.00		1.16
4	8.40	4.75	1.77	
		6.50		1.29
5	23.00	15.00	1.53	
		21.00		1.09
6	17.00	10.00	1.70	
		13.00		1.31

Average V_p = 1.70 km/sec

Standard deviation = 0.12 km/sec

Average V_s = 1.26 km/sec

Standard deviation = 0.11 km/sec

Comments: All velocities measured perpendicular to bedding.
Specimen length accurate to 0.10 mm.
Travel times accurate to 0.50 microseconds (V_p) and 1.00 microseconds (V_s).
Tests conducted at atmospheric pressure.

Gateway Mine

Test Performed: Determination of V_p and V_s (ultrasonic pulse).

Lithology: Fruitland Coal #5

Sample #	Length (mm)	Travel Time (microsec)	V_p (km/sec)	V_s (km/sec)
1	36.00	25.00	1.44	
		37.00		0.97
2	36.03	22.00	1.64	
		34.00		1.06
3	39.00	25.00	1.56	
		36.00		1.08
4	36.00	25.00	1.44	
		37.00		0.97
5	25.85	18.00	1.44	
		25.00		1.03
6	40.06	27.00	1.48	
		38.00		1.05

Average V_p = 1.50 km/sec

Standard deviation = 0.08 km/sec

Average V_p = 1.03 km/sec

Standard deviation = 0.05 km/sec

Comments: All velocities measured perpendicular to bedding.
Specimen length accurate to 0.10 mm.
Travel time accurate to 2.00 microseconds (V_p) and 3.00 microseconds (V_s).
Tests conducted at atmospheric pressure.

Gateway Mine

Test Performed: Tensile strength determination (Brazilian test); method of Davies and Stagg (1970).

Lithology: Fruitland Coal #2

Sample #	D Diameter (inches)	t Thickness (inches)	F Load (lbs.)	T Tensile Strength (MPa)
2	0.80	1.38	500	-1.99
3	0.84	1.32	410	-1.62
4	1.07	1.35	550	-1.67
5	1.05	1.31	490	-1.56
6	1.07	1.51	600	-1.63
7	1.07	1.15	250	-0.89
8	1.08	1.58	300	-0.77
9	0.85	1.28	525	-2.12
10	0.85	1.28	525	-2.12
11	0.86	1.57	650	-2.11

Average tensile strength = -1.65 MPa

Standard deviation = 0.49 MPa

Comments: All specimens compressed perpendicular to bedding.
Specimens in fair-to-good condition; somewhat irregularly shaped; generally disintegrated upon failure.
Tensile strength values calculated according to relation $T = 2F/Dt\pi$.
1 PSI = 6.895×10^3 Pa.

Gateway Mine

Test Performed: Tensile strength determination (Brazilian test); method of Davies and Stagg (1970).

Lithology: Fruitland Coal #5 -

Sample #	D Diameter (inches)	t Thickness (inches)	F Load (lbs.)	T Tensile Strength (MPa)
1	1.02	0.92	140	-0.65
2	1.03	0.77	362	-2.01
3	1.54	0.88	335	-1.09
4	1.55	0.71	170	-0.68
5	1.55	0.54	85	-0.45
6	1.42	0.80	88	-0.34
7	1.55	0.86	810	-2.67
10	1.62	0.76	525	-1.87
12	1.54	0.69	170	-0.70
15	1.54	0.93	200	-0.61
16	1.53	0.82	175	-0.61

Average tensile strength =-1.06 MPa

Standard deviation = 0.77 MPa

Comments: All samples compressed perpendicular to bedding.
Tensile strength values calculated according to relation $T = 2F/Dt\pi$.
Specimens in fair-to-good condition; generally disintegrated upon failure.
1 PSI = 6.895×10^3 Pa.

Tres Hermanos

Test Performed: Determination of V_p and V_s (ultrasonic pulse).

Lithology: Tres Hermanos Sandstone (Upper bed)

Sample #	Length (mm)	Travel Time (microsec)	V_p (km/sec)	V_s (km/sec)
2	21.85	5.50	3.97	
		8.00		2.73
3	21.75	5.60	3.88	
		8.00		2.72
4	21.75	5.90	3.69	
		8.40		2.59
5	21.90	6.00	3.65	
		8.40		2.61
6	21.80	5.10	4.27	
		7.50		2.91
7	21.70	5.25	4.13	
		7.25		2.99

Average V_p = 3.93 km/sec

Standard deviation = 0.24 km/sec

Average V_s = 2.76 km/sec

Standard deviation = 0.16 km/sec

Comments: All velocities measured perpendicular to bedding.
Specimen length accurate to 0.10 mm.
Travel times accurate to 0.25 microseconds (V_p) and 0.50 microseconds (V_s).
Tests conducted at atmospheric pressure.

Tres Hermanos

Test Performed: Determination of V_p and V_s (ultrasonic pulse).

Lithology: Tres Hermanos Sandstone (Lower bed)

Sample #	Length (mm)	Travel Time (microsec)	V_p (km/sec)	V_s (km/sec)
1	13.37	3.10	4.31	
		4.40		3.04
4	17.67	4.00	4.42	
		6.00		2.95
5	17.51	3.90	4.49	
		5.80		3.02
6	17.49	3.90	4.48	
		6.00		2.92
9	17.32	4.00	4.33	
		5.90		2.94

Average V_p = 4.41 km/sec

Standard deviation = 0.08 km/sec

Average V_s = 2.97 km/sec

Standard deviation = 0.05 km/sec

Comments: All velocities measured perpendicular to bedding.
Specimen length accurate to 0.10 mm.
Travel times accurate to 0.25 microseconds (V_p) and 0.50 microseconds (V_s).
Tests conducted at atmospheric pressure.

Tres Hermanos

Test Performed: Tensile strength determination (Brazilian test; method of Davies and Stagg (1970).

Lithology: Tres Hermanos Sandstone (Upper bed)

Sample #	D Diameter (inches)	t Thickness (inches)	F Load (lbs)	T Tensile Strength (MPa)
1	0.76	0.82	1050	-7.40
2	0.77	0.85	1100	-7.38
3	0.65	0.80	1175	-9.92
4	0.71	0.87	960	-6.82
5	0.72	0.65	1250	-11.72
6	0.55	0.85	600	-5.63
7	0.65	0.83	1250	-10.21
8	0.70	0.71	1050	-9.27
9	0.87	0.65	575	-4.46
10	0.90	0.70	610	-4.25
11	0.60	0.83	625	-5.38

Average tensile strength = -7.50 MPa

Standard deviation = 2.50 MPa

Comments: All specimens compressed perpendicular to bedding.
Specimens generally very good.
Tensile strength values calculated according to the relation $T = 2F/Dt\pi$.

1 PSI = 6.895×10^3 Pa.

Tres Hermanos

Test Performed: Tensile strength determination (Brazilian test); method of Davies and Stagg (1970).

Lithology: Tres Hermanos Sandstone (Lower bed).

Sample #	D Diameter (inches)	t Thickness (inches)	F Load (lbs.)	T Tensile Strength (MPa)
1	0.65	0.49	950	-13.09
2	0.57	0.65	1100	-13.00
3	0.52	0.39	425	-9.20
4	0.87	0.70	1100	-7.93
5	0.87	0.52	875	-8.49
6	0.65	0.72	1262	-11.84
7	0.65	0.52	1325	-17.21
8	0.65	1.01	1213	-8.11
9	0.87	0.45	938	-10.51
10	0.87	0.71	962	-6.84
11	0.87	0.42	850	-10.21
12	0.65	0.73	1300	-12.03
13	0.65	0.83	1250	-10.17
14	0.65	0.60	655	-7.37
15	0.65	0.65	1250	-12.99
16	0.87	0.55	560	-5.14 *
17	0.64	0.93	1750	-12.91

Average tensile strength = -10.74 MPa

Standard deviation = 2.76 MPa

Comments: All specimens compressed perpendicular to bedding.
* - not included in calculations due to premature failure.
Specimens generally very good.
Tensile strength values calculated according to the relation $T = 2F/Dt\pi$.
1 PSI = 6.895×10^3 Pa.

Tres Hermanos

Test Performed: Determination of Young's modulus by uniaxial compression.

Lithology: Tres Hermanos Sandstone (Upper bed)

Sample #	Diameter (inches)	Length (in.)	Load (lbs)	Displacement (inches)	Young's Modulus (GPa)
1	0.970	2.46	675	0.00805	
			1275	0.00952	
			1800	0.01084	
			2850	0.01210	
			2950	0.01262	
			3150	0.01420	
			3900	0.01631	
			5550	0.01936	40.20
2	0.974	1.92	660	0.00552	
			1210	0.00679	
			1560	0.00737	
			1900	0.00815	
			2400	0.00894	
			3500	0.01141	
			4700	0.01326	
			5150	0.01552	41.89
3	0.970	2.35	250	0.00484	
			500	0.00657	
			1400	0.01005	
			2740	0.01452	
			2990	0.01636	23.23
4	0.970	2.34	320	0.00710	
			900	0.00963	
			1370	0.01110	
			1945	0.01257	
			2420	0.01373	
			2720	0.01473	
			3145	0.01673	
			4565	0.01983	
			5040	0.02209	31.00
5	0.975	2.45	450	0.00831	
			930	0.01041	
			1060	0.01078	
			1450	0.01189	
			1840	0.01262	
			2260	0.01357	
			2620	0.01446	
			2920	0.01588	
			3870	0.01783	36.57

Average Young's modulus = 34.58 GPa

Standard deviation = 7.59 GPa

Comments: Some variation in cementation.

1 PSI = 6.895×10^3 Pa

Tres Hermanos

Test Performed: Determination of Young's modulus by uniaxial compression.

Lithology: Tres Hermanos Sandstone (Lower bed)

Sample #	Diameter (inches)	Length (in.)	Load (lbs)	Displacement (inches)	Young's Modulus (GPa)
1	0.975	2.37	800	0.00905	
			1220	0.01015	
			1820	0.01152	
			2420	0.01273	
			2695	0.01352	
			3065	0.01457	
			4265	0.01662	
			5115	0.01799	44.55
2	0.975	2.75	940	0.00584	
			1540	0.00747	
			2140	0.00952	
			2610	0.01105	
			2930	0.01231	
			3530	0.01319	
			4230	0.01583	
			4980	0.01799	30.69
3	0.970	2.45	600	0.00679	
			1200	0.00843	
			1800	0.00927	
			3000	0.01176	
			3550	0.01290	
			4450	0.01476	
			4900	0.01568	45.13
4	0.970	2.62	770	0.00850	
			1145	0.00937	
			1775	0.01084	
			2920	0.01350	
			3770	0.01547	
			4500	0.01717	
			5110	0.01859	40.13

Average Young's modulus = 40.12 GPa

Standard deviation = 6.67 GPa

Comments: Some variation in cementation.

1 PSI = 6.895×10^3 Pa.

Tres Hermanos

Test Performed: Determination of shear strength with bevelled dies.

Lithology: Tres Hermanos Sandstone (Upper bed)

Sample #	Dimensions (inches)	Load (lbs)	Shear Strength (MPa)
1	0.81 x 0.91	1790	11.78
2	0.85 x 1.05	2400	13.02
3	0.86 x 0.83	2350	15.88
5	0.86 x 0.88	2080	13.46
6	0.85 x 0.77	2330	17.42
7	0.81 x 1.09	1630	9.00
9	0.75 x 1.08	1340	8.07
10	0.83 x 0.85	2170	15.07

Average shear strength = 12.96 MPa

Standard deviation = 3.25 MPa

Comments: Shear strength calculated from the relation
$S = F \cos\theta / A$
$\theta = 45°$, A = area, F = load

Tres Hermanos

Test Performed: Determination of shear strength with bevelled dies.

Lithology: Tres Hermanos Sandstone (Lower bed)

Sample #	Dimensions (inches)	Load (lbs)	Shear Strength (MPa)
1	1.16 x 0.80	3650	19.24
2	1.02 x 1.07	5000	22.14
3	1.16 x 1.32	7930	25.15
4	1.03 x 1.14	4575	19.02
5	1.13 x 0.82	2550	13.45
6	1.02 x 1.40	7740	26.33
7	1.02 x 0.87	3250	17.66
8	1.02 x 1.45	9900	32.52
9	1.16 x 1.25	5350	17.94
10	1.02 x 0.94	3100	15.70
11	1.16 x 1.20	6625	23.14
12	1.03 x 1.08	4450	19.43
13	1.16 x 1.15	4325	15.78
14	1.03 x 1.14	4900	20.33

Average shear strength = 20.56 MPa

Standard deviation = 4.99 MPa

Comments: Shear strength calculated from the relation
$S = F \cos\theta / A$
$\theta = 45^{\circ}$, A = area, F = load

REFERENCES

Anderson, E. M., 1951, The dynamics of faulting and dyke formation with applications to Britain: Oliver and Boyd, Edinburgh, 206 p.

Brown, E. T., 1981, Rock characterization testing and monitoring: Pergamon Press, Oxford, 211 p.

Budding, A. J., 1963, Field trip 7, Carthage area: New Mexico Geologic Society Guidebook 14, p. 74-77.

Clarkson, G. W., 1984, Implications for thermal histories of the San Juan basin and San Juan mountains since late Cretaceous time (Ph.D. thesis): Socorro, New Mexico Institute of Mining and Technology.

Englund, K. J., Sigleo, W. R., and Behum, P.T., 1983, Mineral resource potential of the Devils Fork roadless area, Scott Co., Virginia: U.S. Geological Survey Miscellaneous Field Studies Map MF-1611-C.

Griffith, A. A., 1924, Theory of rupture: Proceedings First International Congress of Applied Mechanics, Delft, p. 55-63.

Griggs, D. T. and Handin, J., 1960, Observations on fracture and an hypothesis of earthquakes: Geological Society of America Memoir 79, p. 347-364.

Haimson, B. C., 1976, Crustal stress in the continental United States as derived from hydrofracturing tests, in Heacock, J. G., ed., The earth's crust: American Geophysical Union Geophysical Monograph, no. 20, p. 576-592.

Handin, J. and Hager, R. V., Jr.,, 1957, Experimental deformation of sedimentary rocks under confining pressure: tests at room temperature on dry samples: Bulletin of the American Association of Petroleum Geologists, vol. 41, p. 1-50.

Hobbs, D. W., 1967, The formation of tension joints in sedimentary rocks: an explanation: Geological Magazine, vol. 104, no. 6, p. 550-556.

Hondros, G., 1959, The evaluation of Poisson's ratio and the modulus of materials of a low tensile resistance by the Brazilian (indirect tensile) test: Australian Journal of Applied Science, vol. 10, p. 243-264.

Jaeger, J. C., 1967, Failure of rocks under tensile conditions: International Journal of Rock Mechanics and Mining Science, vol. 4, p. 219-227.

----------, 1969, Elasticity, fracture and flow: Methuen, London, 268 p.

----------, and Cook, N. G. W., 1979, Fundamentals of rock mechanics: Chapman and Hall, London, 593 p.

Johnson, A., 1984, Physical processes in geology: Freeman, Cooper and Company, San Franciso, 590 p.

Jumikis, A. R., Rock mechanics: Clausthal, Germany, Trans Tech Publications, 356 p.

Ladeira, F. L., and Price, N. J., 1981, Relationship between fracture spacing and bed thickness: Journal of Structural Geology, vol. 3, no. 2, p. 179-183.

Lama, R. D., and Vutukuri, V. S., 1978, Handbook on mechanical properties of rocks - volume II: Trans Tech Publications, Clausthal, 481 p.

Mase, G. E., 1970, Continuum mechanics: McGraw-Hill, New York, 221 p.

Mellor, M., and Hawkes, I., 1971, Measurement of tensile strength by diametral compression of disks and annuli: Engineering Geology, vol. 5, p. 173-225.

Miller, M. S., 1974, Stratigraphy and coal beds of Upper Mississippian and Lower Pennsylvanian rocks in southwestern Virginia: Virginia Division of Mineral Resources, Bulletin 84, 211 p.

Murrell, S. A. F., 1964, The theory of the propagation of elliptical Griffith cracks under various conditions of plane strain or plane stress, Pt. 1: British Journal of Applied Physics, vol. 15, p. 1211-1223.

Ode, H., 1960, Faulting as a velocity discontinuity, in Griggs, D., and Handin, J., eds., Rock deformation: Memoirs of the Geological Society of America, vol. 79, p. 293-321.

Osburn, J. C., 1983, Coal resources of Socorro County, New Mexico: New Mexico Geologic Society Guidebook 34, p. 223-226.

Paterson, M. S., 1978, Experimental rock deformation - the brittle field: Springer-Verlag, Berlin, 254 p.

Price, N. J., 1959, Mechanics of jointing in rocks: Geological Magazine, vol. 96, no. 2, p. 149-167.

----------, 1966, Fault and joint development in brittle and semi-brittle rock: Pergamon Press, Oxford, 176 p.

Reiter, M., Eggleston, R. M., Broadwell, B. R., and Minier, J., 1986, Estimates of terrestrial heat flow from deep petroleum tests along the Rio Grande Rift in central and southern New Mexico: Journal of Geophysical Research, vol. 91, no. B6 p. 6222-6245.

----------, and Mansure, A. J., 1983, Geothermal studies in the San Juan basin and the Four Corners area of the Colorado Plateau - 1. terrestrial heat flow measurements: Tectonophysics, vol. 91, p. 233-251.

Segall, P., 1984, Formation and growth of extensional fracture sets: Geological Society of America Bulletin, vol. 95, p. 454-462.

Shoemaker, J. W., Beaumont , E. C., and Kottlowski, F. E., 1971, Strippable low-sulfur coal resources of the San Juan basin in New Mexico and Colorado: New Mexico State Bureau of Mines and Mineral Resources, Memoir 25, 189 p.

Simmons, G., and Brace, W. F., 1965, Comparison of static and dynamic measurements of compressibility of rocks: Journal of Geophysical Research, vol. 70, no. 22, p. 5649-5656.

Suppe, J., 1985, Principles of structural geology, Prentiss-Hall, Englewood Cliffs, 537 p.

Turner, F. J., and Weiss, L. E., 1963, Structural analysis of metamorphic tectonites: McGraw-Hill, New York, 545 p.

Turcotte, D. L., and Schubert, G., 1982, Geodynamics: applications of continuum physics to geological problems: John Wiley and Sons, New York, 450 p.

Vutukuri, V. S., Lama, R. D., and Saluja, S. S., 1974, Handbook on mechanical properties of rocks - volume I: Trans Tech Publications, Clausthal, 280 p.

Weissback, G., 1978, A new method for the determination of the roughness of rock joints in the laboratory: International Journal of Rock Mecahnics, Mining Science and Geomechanical Abstracts, vol. 15, p. 131-133.

Wilpolt, R. H., and Wanek, A. A., 1951, Geology of the region from Socorro and San Antonio east to Chupadera Mesa, Socorro County, New Mexico: United States Geological Survey, Oil and gas investigations Map OM - 121.

This thesis is accepted on behalf of the faculty of the Institute by the following committee:

A. J. Beddow
Advisor

John Wm. Schlueter

Allan R. Sanford

April 10, 1987
Date